**THE REPUBLIC OF TURKEY**

**BAHCESEHIR UNIVERSITY**

# DESIGN OF A PLATFORM FOR PHYSICAL PERFORMANCE TESTING OF AN AXIAL-FLOW LEFT-VENTRICULAR ASSIST DEVICE

**Master Thesis**

**İBRAHİM BAŞAR AKA**

**ISTANBUL, 2014**

**THE REPUBLIC OF TURKEY**

**BAHCESEHIR UNIVERSITY**

**THE GRADUATE SCHOOL OF NATURAL AND APPLIED SCIENCES**

**M.S. BIOENGINEERING**

# DESIGN OF A PLATFORM FOR PHYSICAL PERFORMANCE TESTING OF AN AXIAL-FLOW LEFT-VENTRICULAR ASSIST DEVICE

**Master Thesis**

**İBRAHİM BAŞAR AKA**

**Supervisor: KAMURAN KADIPAŞAOĞLU**

**ISTANBUL, 2014**

**THE REPUBLIC OF TURKEY**

**BAHCESEHIR UNIVERSITY**

**THE GRADUATE SCHOOL OF NATURAL AND APPLIED SCIENCES**

**M.S. BIOENGINEERING**

# DESIGN OF A PLATFORM FOR PHYSICAL PERFORMANCE TESTING OF AN AXIAL-FLOW LEFT-VENTRICULAR ASSIST DEVICE

**İBRAHİM BAŞAR AKA**

**08.08.2014**

The thesis has been approved by the Graduate School of Natural and Applied Sciences.

**DOÇ. DR. TUNÇ BOZBURA**
Graduate School Director

I certify that this thesis meets all the requirements as a thesis for the degree of Master of Science.

**PROF. DR. EROL SEZER**
Program Coordinator

This is to certify that we have read this thesis and we find it fully adequate in scope, quality and content, as a thesis for the degree of Master of Science.

| Examining Committee Members | Signature |
|---|---|
| Thesis Supervisor<br>**DR. KAMURAN KADIPAŞAOĞLU** | ---------- |
| Member<br>**PROF. DR. EROL SEZER** | ---------- |
| Member<br>**DOÇ. DR. SARPER ÖZHARAR** | ---------- |

## ABSTRACT

DESIGN OF A PLATFORM FOR PHYSICAL PERFORMANCE TESTING OF AN AXIAL-FLOW LEFT-VENTRICULAR ASSIST DEVICE

İBRAHİM BAŞAR AKA

Bioengineering

Thesis Supervisor: Kamuran Kadıpaşaoğlu

August, 2014, 99 Pages

Heart disease is the most frequent cause of death in developed countries. Heart Failure occurs when the heart provides insufficient blood pressure/flow for the metabolic need of the body. Due to the shortage of available donor hearts, left ventricular assist devices (LVADs) have been used to support last stage HF patients as a bridge to transplant or as destination therapy. LVADS have been produced in a few countries and the absence of domestic LVADs results in high importing costs for Türkiye. Further, scant acquisition of these devices limits academic and clinical research and restricts success in implantation and post-implantation device upkeep. Therefore, a program to produce an innovative domestic LVAD has been initiated by a researcher group in Bahçeşehir University.

Virtual design of a prototype is completed via computational fluid dynamic (CFD) optimizations. Physical testing of the prototype is required for validating the virtual results. In-vitro tests of the LVAD prototype will be conducted over a Cardiovascular Mock Circuit (CVMC), which mimics the physiology (pressure and flow characteristics) of the human cardiovascular system. Particle Image Velocimetry (PIV) will be employed for observing transition time, backflow and vortex zones. Inquiry into the inner flow passages of the device using PIV requires access of light through the opaque outer shroud which, therefore, should be constructed from transparent material. This imposes the requirement that the device be motor-less, hence an external driver mechanism be used. The design and construction of this mechanism constitutes the main objective of the present work.

3D design of the setup (called External Drive Mechanism- EDM- throughout this work), contains a DC motor, a torque sensor, a YT connector and a transparent shroud, all aligned along a straight rigid shaft. The setup is drawn and assembled via SolidWorks CAD software. Possible interruptive effects of EDM components (bearing, gaps and shaft) in LVAD flow line are evaluated by ANSYS Fluent commercial CFD package, considering head pressure, hydraulic efficiency, backflow and hemolysis characteristics. The bearing system of the EDM is designed considering hemodynamic and hemocompatibility criteria. After estimating minimum shaft diameter and motor power rating are calculated by conventional equations considering CFD data. External shaft is made of 3mm high strength Tungsten Carbide. YT-connector is the part where horizontal branch includes the shaft with plastic seal and oblique branch stands as inlet cannula.

The transparent shroud is designed and manufactured from poly-acrylic resin using Mold Casting. Main LVAD components (inducer, rotor and diffuser) are produced from Ti-Al6-V4 by Laser Sintering, in order to obtain realistic physical characteristics (inertia, surface finish). A dynamic load torque sensor with speed encoder is selected per CFD results (torque, shaft speed). CVMC, PIV accessories (LED, high-speed camera, synchronizer) and EDM are integrated and operated simultaneously via dSpace1103 data acquisition board.

EDM functions under desired physical coditions. Initial CVMC and PIV testings are achieved. EDM is capable of working up to 10krpms impeller speed, 180 mmHg head pressure and 9lt/min flow rate.

Along with EDM design, an innovative concept of blood-immersed bearing system is virtually designed and tested in ANSYS Fluent. This geometry is named bearing washing channels. Channels are placed inside stationary inducer and diffuser to provide contious washing of bearings to avoid thrombosis formation. No stasis is obeserved and minor decrease in pump geometry is estimated.

**Keywords:** Left Ventricular Assist Device, Particle Image Velocimetry, Dynamic Torque Measurement, Hydraulic Performance, Computational Fluid Dynamics

# ÖZET


EKSENEL-AKIŞLI SOL-VENTRİKÜL DESTEK CİHAZI
İÇİN FİZİKSEL PERFORMANS TESTİ DÜZENEĞİNİN TASARIMI

İBRAHİM BAŞAR AKA

Biyomühendislik

Tez Danışmanı: Dr. Kamuran Kadıpaşaoğlu

Ağustos, 2014, 99 Sayfa

Kalp Hastalıkları gelişmiş ülkelerdeki başlıca ölüm sebebidir. Kalp Yetmezliği vücudun ihtiyac duyduğu kan akışı ve basıncının kalp tarafından karşılanamaması sonucu oluşur. Mevcut donör organların yetersiz sayıda olmasından dolayı, son dönem kalp yetmezliği hastalarının tedavisinde Sol Ventrikül Destek Pompaları(SVDP) transplant yapılana kadar hastayı yaşatmak için kullanılmaktadır. SVDP'ler sadece birkaç gelişmiş ülkede üretilebilmekte ve ithalatı ülkemiz için büyük mali yük teşkil etmektedir. Ayrıca, az sayıda edinilen cihazlar akademik ve klinik araştırmaları sınırlamakta ve implantasyon ve implantasyon sonrası başarıyı azaltmaktadır. Bu nedenle, 2009 yılında Bahçeşehir Üniversitesinde bir grup araştırmacı tarafından yenilikçi bir yerli SVDP üretimi programı başlatılmıştır.

Prototipin sanal tasarımı Hesaplamalı Akışkanlar Dinamiği (HAD) optimizasyonlarıyla tamamlanmıştır. Sanal sonuçların doğrulanması için fiziksel bir prototip üretilmesi zorunludur. Fiziki performans testleri Hemodinamik Simülasyon Mekanizması(HSM) ve Parçacık Hızı Görüntüleme (PHG) teknikleri kullanılarak yapılacaktır. PHG tekniği kullanılarak akış zamanı, muhtemel geri akış ve girdap bölgeleri incelenecektir. PHG ile prototipinde iç akış bölgelerinin incelenmesi için opak dış yüzeyden ışığın geçebilmesi gereklidir. Bu nedenle dış yatak üretiminde saydam malzeme tercih edilmelidir. Bu gereklilik cihazın motorsuz olmasına sebep olmuş ve bir Dış Tahrik Mekanizması (DTM) ile sürülmesi zorunlu olmuştur. DTM in tasarımı ve üretimi bu çalışmanın ana konusudur.

DTM in 3B tasarımı SolidWorks CAD yazılımı ile çizilmiş ve imal edilmiştir. DTM elemanlarının(rulman, boşluk ve mil) SVDP akış yolundaki muhtemel engelleyici etkileri ANSYS Fluent HAD yazılımı kullanılarak incelenmiş, incelemelerde çıkış basıncı, hidromekanik verimlilik, geriakış ve hemoliz karakteristikleri göz önünde bulundurulmuştur. DTM'in rulman sistemi hemodinamik ve hemokompatibilite kriterlerine göre tasarlanmıştır. Minimum mil çapı ve motor gücü gereksinimleri HAD verileri kullanılarak standart denklemlere göre hesaplanmıştır. Harici mil 3mm Tungsten Karbür malzemeden üretilmiştir. YT-Bağlantı parçasının radyal dalı sızdırmaz keçe ile harici mili bulundurmakta ve eğimli dalı giriş kanülü olarak kullanılmaktadır.

Transparan dış yatak poliüretan malzemeden tasarlanmış ve kalıp-döküm tekniği ile üretilmiştir. SVDP ana komponentleri (inducer, rotor, diffuser) Ti-Al6-V4 malzemeden Lazer Sinterleme ile üretilmiş, bu sayede gerçekçi fiziksel özellikler (inertia, surface finish) elde edilmiştir. HAD verileri (torque, shaft speed) göz önünde bulundurularak

dinamik tork ve hız sensörü seçilmiştir. HSM, PIV komponentleri (LED, high-speed camera, synchronizer) ve DTM dSpace1103 veri toplama donanımı kullanılarak entegre edilmiş ve sürülmüştür.

DTM istenilen fiziksel koşullarda çalışmaktadır. Öncül PHG ve HSM testleri yapılmıştır. DTM 10 bin devir pervane hızına, 180 mmHg basma yüksekliğine ve 9lt/dk debiye kadar test edilmiştir.

DTM ile beraber yenilikçi bir kan ile rulman yıkama methodu sanal olarak tasarlanmış ve ANSYS Fluent üzerinde test edilmiştir. Bu tasarıma rulman yıkama kanalı adı verilmiştir. Kanallar durgun indüktör ve difüzör parçalarına açılarak rulmanların sürekli olarak yıkanması ve pıhtı oluşumunun engellenmesi amaçlanmıştır. HAD sonuçlarında durgun bölge gözlenmemiş ve pompa performansı ciddi derecede etkilenmemiştir.

**Anahtar Kelimeler:** Sol Ventrikül Destek Cihazı, Parçacık Görüntüleme, Dinamik Tork Ölçümü, Hidrolik Performans, Hesaplamalı Akışkanlar Dinamiği Analizi

## ACKNOWLEDGEMENTS

I would like to express my gratitude to my advisor, Kamuran Kadıpaşaoğlu, for his support when my visa of US was revoked and I was desperately wasting time in İstanbul. He gave me a job and a purpose. He let me experience the research of Left Ventricle Assist Devices in his laboratory. He listened my tiniest problems with patience, and always encouraged me to try new ideas throughout my graduate studies. His technical and editorial advice has taught me countless lessons and insights on the research in general. He patiently corrected my writing and spelling. Beyond all, he taught me science is not only maths but maths is basically the language of it. He is the man I admire the most who taught me Cylinder of Laplace and Cylinder of Cyrus.

I would also like to thank Professor Erol Sezer for helping me to develop some background in linear algebra and advanced calculus. He previously gave me the chance of pursuing masters degree in US as chair of the department and he solved my numerous administrative problems with patience.

I would like to thank Emir Gökberk Eken, who is a good friend always willing to help. He always supported me on any problem I have faced in last several years. I would like to thank Sina Dadgar for his helps in this project. Additionally, he patiently tried to teach me persian. It would have been a lonely lab without him. Many thanks to Çağlar Öztürk who is a friend closer than a brother. He was always there to help me.

I would also like to thank my parents and brother. They were always supporting me and encouraging me for pursuing this degree.

Finally, I appreciate the financial support from TÜBİTAK that funded the research discussed in this thesis.

**TABLE OF CONTENTS**

## LIST OF FIGURES

**1.Introduction**



**2. Materials and Methods**

**3.Results**



## List of Tables

# 1. INTRODUCTION

As a whole, this project is a part the development of an innovative Axial Flow Left Ventricle Assist Device (LVAD) in Bahçeşehir University, Turkey. LVAD is a fluid pump designed to function alike the heart. It induces unidirectional blood flow from Left Ventricle (LV) to Aorta. LVADs have been implanted as a bridge to transplant or as a destination therapy on patients with severe Heart Failure (HF) which is any defect of the heart like muscle contractility deficiencies, abnormality of beat (arrhythmia), inadequate blood flow, reduced blood pressure by inherent or later diseases[1]. Heart attacks are initiated by obstruction of coronary arteries that sustain oxygenated blood to heart muscles. Consequently, it deteriorate heart performance, particularly affecting LV which carries the load of circulation system by providing blood flow to the body.

Cardiovascular diseases are the leading reason of mortality and morbidity in the developed world. Annually, more than 5 million Europeans die due to coronary artery diseases[2]. Likewise, more than 5 million patients in USA have HF. About 600,000 people die of heart diseases in the United States annually (1 in every 4 deaths). Moreover, in 1 of every 9 deaths heart failure is a coexisting cause [3]. About half of the people who develop heart failure die in 5 years of diagnosis. Heart failure related economic burden is estimated as $32 billion annually in US[4]. Strategic Plan of Turkish Ministry of Health estimates that by 2015, 20 million people will die annually due to cardiovascular diseases[5].

A heart attack (myocardial infarction) occurs due to the insufficient blood supply to a section of the heart muscle which subsequently dies or gets injured[1]. Drug therapy or surgery is used in order to recover the fall in heart performance. However, medicine provides temporary solution and some patients are ineligible for surgery. Last stage heart failure cause permanent damage on heart muscle and it is terminal. Thus, end stage HF patients need heart transplants or Mechanical Circulatory Support System (MCSS) implantations.

Statistics in Turkey show HF is pandemic in our country as well. About a million people have HF and %20 of them reach last stage annually. Every year, approximately 3000 patients need immediate heart transplant but roughly 50 transplantations can be performed due to shortage of available donor hearts (Fig 1.1). Consequently, more than 95% of the HF patients wait up until an organ is found, yet half of these patients die in a year and most of them die in 2 years[5].

**Figure 1.1: Transplant statistics in Turkey between 2002 and 2012**

| | 2002 | 2009 | 2010 | 2011 | 2012 |
|---|---|---|---|---|---|
| Böbrek | 550 | 2.362 | 2.502 | 2.923 | 2.903 |
| Karaciğer | 159 | 592 | 695 | 904 | 1.001 |
| Kalp | 20 | 54 | 86 | 93 | 61 |
| Kalp Kapakçığı | 15 | 38 | 18 | 1 | 5 |
| Akciğer | 0 | 7 | 3 | 5 | 25 |
| Kalp-Akciğer | 0 | 0 | 0 | 0 | 2 |
| Pankreas | 0 | 18 | 29 | 26 | 6 |
| İnce Bağırsak | 1 | 1 | 3 | 1 | 5 |
| Toplam | 745 | 3.072 | 3.336 | 3.953 | 4.008 |

***Source:*Ministry of Health[5]**

The gap between number patients listed for transplant and available donors has widened in the last decade (Fig 1.2). So, almost every candidate for transplant gets mechanical support as bridge to transplant in European Union (EU) and US[6].

**Figure 1.2: Annual Distribution of Heart Transplantations vs Waiting List in Turkey**

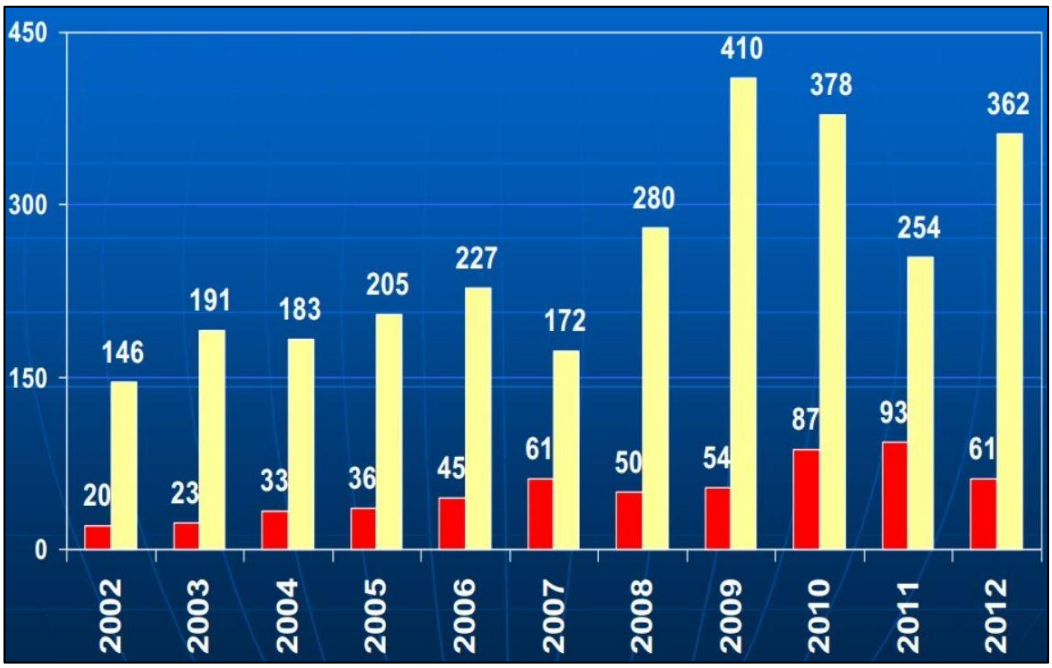


***Soruce:*** **Ministrity of Health[7]**

## 1.1. MECHANICAL CIRCULATORY SUPPORT SYSTEMS (MCSS)

Mechanical circulatory support systems (MCSS) have been designed to maintain circulatory needs of the HF patient, mostly by supporting LV, until an available organ is found. MCSS's have been implanted as destination therapy as well for certain patients who are not eligible for cardiac transplants. Most frequent type of MCSS is Left Ventricular Assist Devices (LVAD) and it implanted between LV and aorta by means of two cannulae Excessive blood load of the failing LV is taken by LVAD and propelled in to the Aorta (Fig 1.3). Hence, patient survives until an organ is found, moreover, it improves patient health before the transplantation or sometimes short-term support by LVAD can allow heart muscles to recover by itself. Since first LVAD was emerged in 60's(DeBakey)[8], sizes have been reduced from room to the palm by the advances in technology. Today LVADs are implanted inside the body and patients are mobilized during the support. Furthermore, some of these products are providing long term survival without transplant[9].

**Figure 1.3: LVAD Implanted in the Body (Left) and Internal Components (Right)**

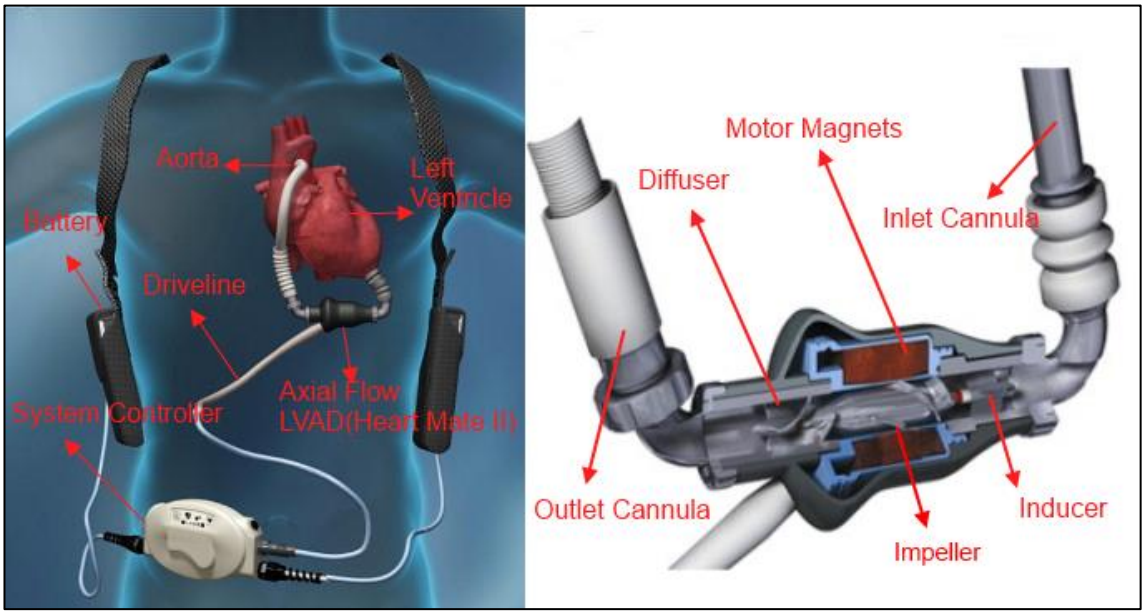


***Source:*Pagani et al.[10]**

The 2010 Registry of the International Society for Heart and Lung Transplantation indicated the percentage of adult LVAD recipients as bridge to transplant increased from 13.4 to 44.5 between two decades (1992-2001 and 2001-2009). Moreover the percentage receiving IV inotrope therapy only decreased from 55.3 to 44.5 (Fig 1.4). The superiority of LVADs over medical therapy was clearly shown even in early studies that used pulsatile LVADs[6].

**Figure 1.4: Percentage of patients received LVAD as Bridge to Transplant**

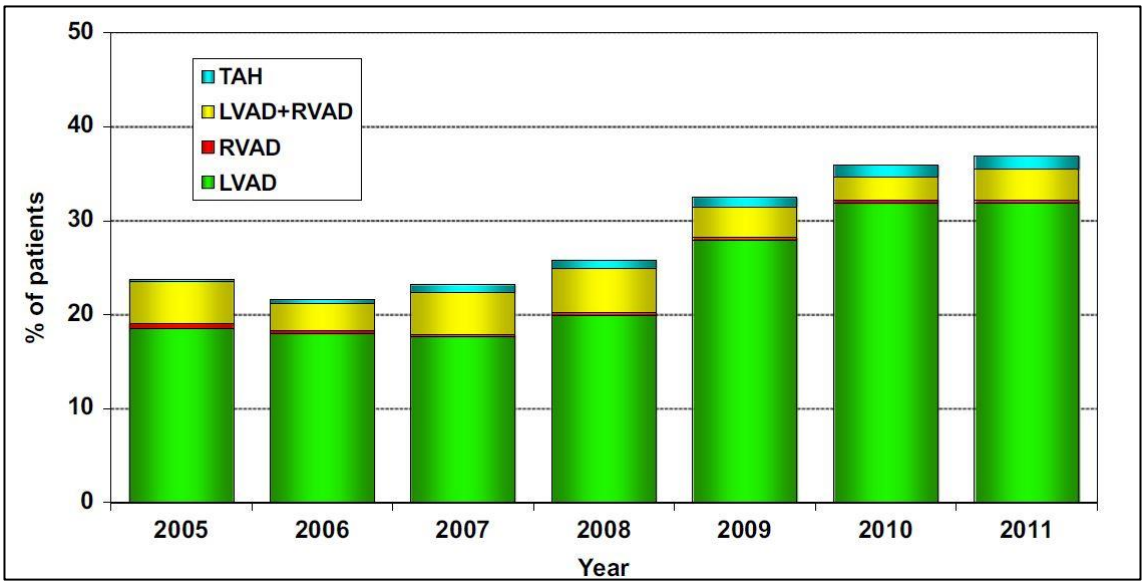


***Source:*** **International Society for Heart and Lung Transplantation[11]**

Fourth Annual Report of Interagency Registry for Mechanically Assisted Circulatory Support (INTERMACS) reveals that 12-month actuarial survival increased from 50% to 79% between 23 June 2006 and 31 December 2007. Moreover, Fifth Annual report shows survival rates as 80% for first year, 70% for second year, 59% for third year and 47% for the fourth year, among 5436 patients between June 2006 and June 2012[9].

These reports indicate a firm rise in the use of mechanical circulatory assistance for bridge to transplant therapy. Among all types of MCSDs, percentage of LVAD usage shows the most increase (Fig 1.2). In Turkey, First LVAD implantation was performed employing Jarvik-7 by Hakkı Akalın et al. in Ankara in 1989[12]. However patient died in the first month due to infection. First successful LVAD implantation was performed

on a patient in Ankara in 2002 and device of Dr. DeBakey was used by Süha Küçükaksu[13]. According to data from Turkish Society of Organ Transplantation. below shows LVAD usage until 2010 (Fig 1.5).

**Figure 1.5: LVAD experiences in Turkey 1989 to 2010**

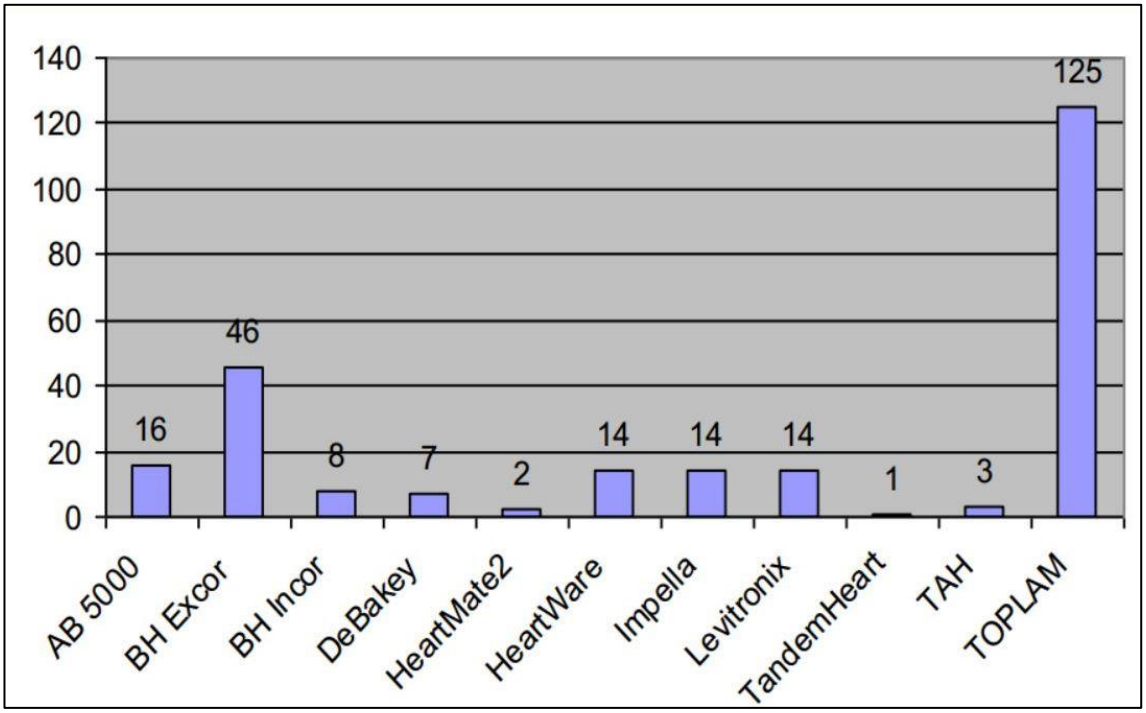


***Source:*** **Turkish Society of Organ Transplantation[14]**

### 1.1.1. Blood Pump Technology

Over the last five decades, many heart pumps were developed in order to reduce the HF effects on human circulation system by supporting blood flow. These heart pumps are categorized in two groups considering flow types (pulsatile or continuous flow) and in three generations considering preferred bearing technologies[15]. There has been a drastic transition from pulsatile pumps to continuous pumps after FDA approval of new continuous pumps. Continuous-flow left-ventricular assist devices offer certain improvements over the older pulsatile-flow devices like better fit, inaudible working, and endurance. By 2011, almost all of LVAD implants are continuous-flow devices[9].

Flow Type:

a. Pulsatile Volume-Displacement Pumps
b. Rotary Continuous Flow Pumps
    i. Axial Flow
    ii. Centrifugal (Radial)
    iii. Diagonal Flow (Mixed Flow)

Device Generations:

i. 1st generation : Reciprocating (Volume-Displacement) pumps,
ii. 2nd generation : Rotary pumps with mechanical bearings,
iii. 3rd generation : Rotary pumps with magnetic levitation or hydrodynamic bearings

**a. Types**

1st generation pumps (reciprocating-pulsatile) increase pressure in a closed chamber to create blood flow via piston like mechanical system. Increased pressure provides unidirectional blood flow through outlet valve of closed volume by overcoming aortic pressure. These types of pumps provide pulsatile blood flows as mimicking the heart. Even with a good result of a 1-year survival rate of 52% compared to medical therapy with 25%. This technology was not initially widely accepted by the medical professionals because of the large size, limited durability due to repetitive flexion and large percutaneous driveline of the pump[6].

**Figure 1.6: a)Pulsatile Pump b)Axial Flow Pump c) Centrifugal pump**

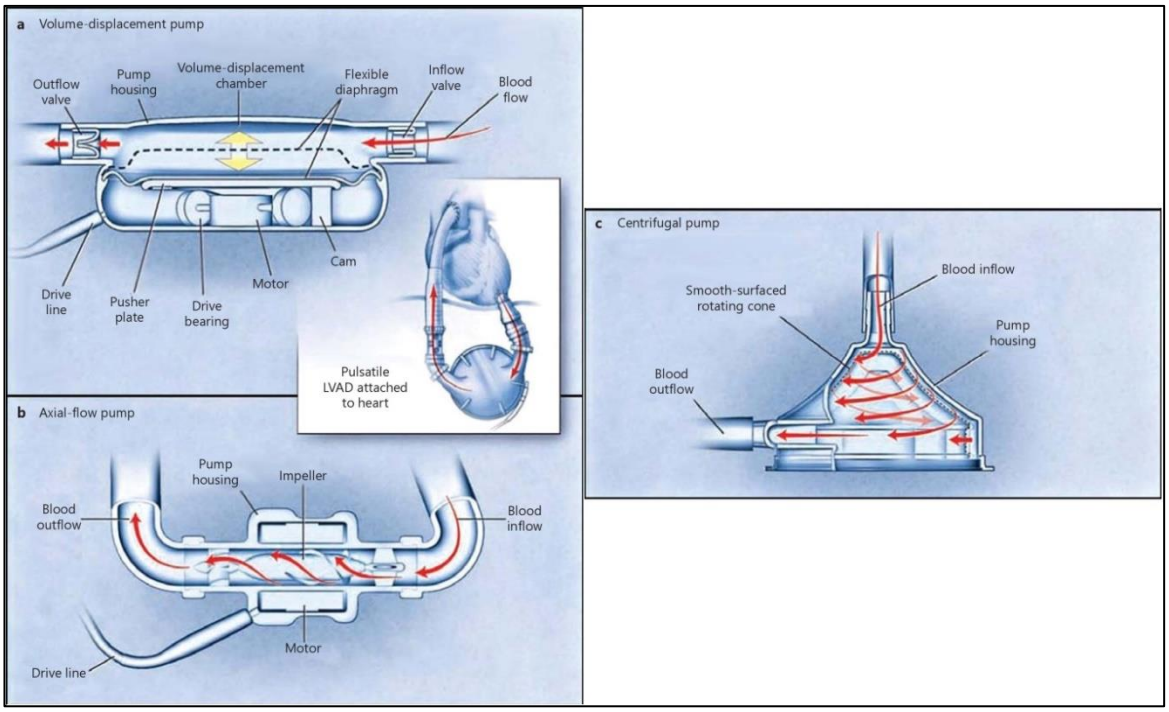


***Source:*** **Advanced HF[6]**

Further generations (2nd and 3rd) are rotary blood pumps that provide continuous blood flow by transferring mechanical energy as kinetic energy to blood via impeller, the only moving part inside of pump which allows significant size reduction and less mechanical wear (Fig 1.6). Rotary pumps provide continuous flow. Moreover, recent technology allows controlling impeller speed to create pulsatile flow[15]. 2nd generation pumps with mechanical bearings are mainly axial flow and 3rd generations are mainly centrifugal devices. Main difference of these two designs is delta P and flow indicates a clear inverse linear relationship in axial flow pumps, contrast to relatively flat pump head curve of centrifugal pumps.(Fig. 1.7)[6].

**Figure 1.7: Pump head curves of a centrifugal pump and axial flow pump**

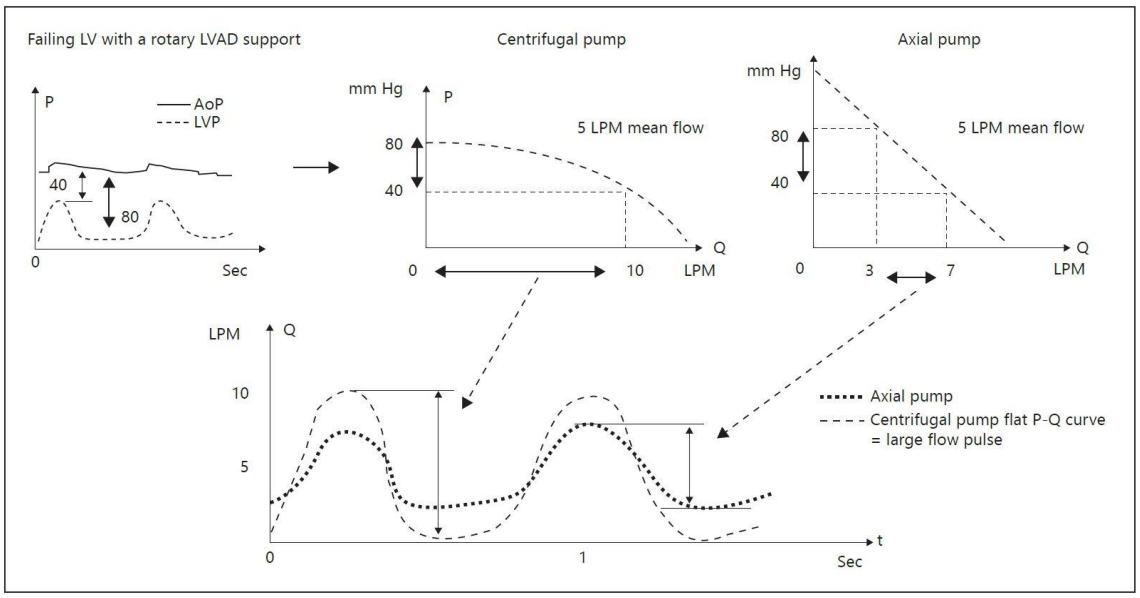


***Source:*** **Medical Physics of VADs[15]**

According to pump design theory, centrifugal pumps are capable of producing higher pressures at lower flows. On the other hand axial flow pumps provides higher flow rates at lower pressure gains. Moreover, axial flow pumps much more compact than centrifugal pumps. Thanks to their smaller size and cylinderical shape, implanting axial pumps require less time and decrease invasiveness of the operation[15].

### 1.1.2. Lvads in Literature

Considering pump generation, names, country of origins and manufacturers of some LVADs are given; (given mostly from Toptop's Thesis and H. M. Reul et al.)[16, 17]

**a. 1st Generation Pumps**

**i. HeartMate I XVE/IP (Thoratec Corporation -Pleasanton CA, USA)**

**ii. ExCor (Berlin Hertz Centrum)**

**iii. Novacor (World Heart Corporation, Novacor Corp, Oakland, CA-USA)**

iv. **Thoratec PVAD(Thoratec Corporation -Pleasanton CA, USA)**

**b. 2nd Generation Pumps**

i. **Hemopump (Medtronic Incorporation - Minneapolis, USA)**

ii. **Jarvik 2000 (Jarvik Heart Incorporation – New York, USA)**

iii. **IVAP (Sun Medical Corporation -Nagano, JAPAN)**

iv. **DeBakey VAD (MicroMED Technology Corporation)**

v. **HeartMate II (Thoratec Corporation -Pleasanton CA, USA)**

vi. **Impella (Abiomed - Aachen, GERMANY)**

vii. **Valvo Pump (Keio University & Hokkaido University -Tokyo, JAPAN)**

viii. **NIVADIII (Shangai-China)**

ix. **Heart Turcica (Koç University, 1st Centrifugal LVAD of Turkey):**
In Turkey, Prof. Dr. İsmail Lazoğlu from Koç University and Prof. Dr. Süha Küçükaksu started a program for developing a Centrifugal LVAD, namely Heart Turcica. In-vitro blood testing of Hearth Turcica is ongoing by 2014**[18]**.

**c. 3rd Generation Pumps**

i. **Streamliner (McGowan Center & Pittsburg University)**

ii. **HeartMate III (Thoratec Corporation -Pleasanton CA, USA)**

iii. **INCOR (Berlin Heart Group)**

iv. **Levitronix CentriMag (Pharos Corporation, Boston MA)**

v. **HeartWare (HeartWare Corp- Miami, Florida, USA)**

vi. **DexAide RVD, CorAide LVD-4000 (Cleveland Clinic-Cleveland, OH)**

vii. **DuraHeart (Terumo Heart, Tokyo, Japan)**

### 1.1.3. Axial Flow Lvad Technique

#### a. Main Components (Inducer, Rotor, Diffuser)

Axial flow LVADs deliver blood flow through direction of rotation axes, consist of three fundamental components where only one of them rotates. First component of axial pumps is inducer which is employed as flow straightener, located right after the inlet cannula. Main objective of this part is eliminating tangential velocity components of the flow before it reaches to the rotating part, impeller. By fluid reaches to rotary zone, unsteady flow may cause flow in reverse direction due to the motion of rotary part. Thus, inducer blades allow axial flow only by parallelizing blood flow owing to its design which is parallel to the flow channel.

Then and there, fluid enters to second component of device, named as rotor (impeller or propeller) and designed to exert kinetic energy to fluid through its blades by converting mechanical energy to hydraulic. Impeller is rotated via electromechanical motor mechanism. Then, mechanical energy (torque and angular velocity) is converted to hydraulic energy (flow and pressure change). Evidently, rotor or impeller is the main component for providing necessary energy for blood flow. High angular velocity profile of this section must be considered since it causes most of the hemolysis. Accordingly, In axial flow LVADs, impeller is also employed as the rotor of the brushless DC motor

where permanent magnets are embedded. So, along with turbomachinery calculations, electromagnetic calculations are necessary as well[16]. However, due to some experimental reasons later presented in this work, to conduct physical experimentation, an external driver will be used to drive impeller instead of embedding DC motor to the prototype.

While flow passing through rotor/impeller, it gains high tangential velocity or kinetic energy. Third component of axial flow pump, diffuser is employed to decelerate tangential velocity that is stationary component of device, and is designed to decelerate tangential velocity of the flow and lead it parallel to rotation axis to avoid circulative flow at pump outlet[16]. Consequently, this geometry causes conversion of kinetic energy to static pressure gain. Furthermore, inducer and diffuser components include rotor shaft pins and bearing systems.

**b. Bearings**

Bearing selection is an important criterion for ensuring hemocompatibility. Major hemolysis takes place around bearings due to high local stresses. Pump generations are categorized considering the bearing system which defines amount of hemolysis and therefore, conceivable support period[19].

In the 1$^{st}$ generation pumps, bearings are located outside of the diaphragm which reciprocates into the chamber. However, this plastic cover raptures in time due to fatigue. Subsequently, possible dispersion of bearing lubricant into the blood limits usage period of displacement pumps. Then, rotary pumps with lubricant free mechanical bearings (2$^{nd}$ generation pumps) were developed to support heart for longer durations. However, blood itself serves as lubricant in 2$^{nd}$ generation pumps which causes high hemolysis around bearings. Then, hydro-dynamic bearings were introduced in some of the 3$^{rd}$ generation pumps to support impeller with high precision clearances for allowing hemoglobin free blood plasma only to support the impeller in vertical direction[19, 20].

Finally, magnetic levitation of impeller was advanced in some 3$^{rd}$ generation pumps by embedding two isopolar magnets in impeller and pump housing. Magnetic force of these magnets holds impeller in position without any contact which eliminates bearing

induced hemolysis. Coagulation is also reduced due to simpler structure where mechanical bearings are removed which causes stagnant flow. However, extra magnets are increasing mass and size of the device. Moreover, energy consumption of magnetic levitation control reduces battery life and causes heating due to eddy currents[19].

Initially, our pump is designed to be $2^{nd}$ generation with mechanical bearings. However, geometric shape allows us to embed extra magnets into the rotor for magnetic levitation in future.

## 1.2. PROCESS TO DEVELOP A LVAD

LVAD is a pump that provides flow and pressure rise by consuming electrical energy. Brushless DC motor is used to convert electrical energy to mechanical energy as torque and angular velocity to rotate impeller. Rotary component (impeller) converts mechanical energy to hydraulic energy as head pressure and flow. Pump design to satisfy hemodynamic performance requirements and hemocompatibility. Computational performance testing results of the pump geometry determines power rating of the dc motor, minimum shaft diameter and several other mechanical constrains to be considered for designing the physical test setup, namely External Drive Mechanism (EDM).

**Figure 1.8:Design steps of a LVAD**

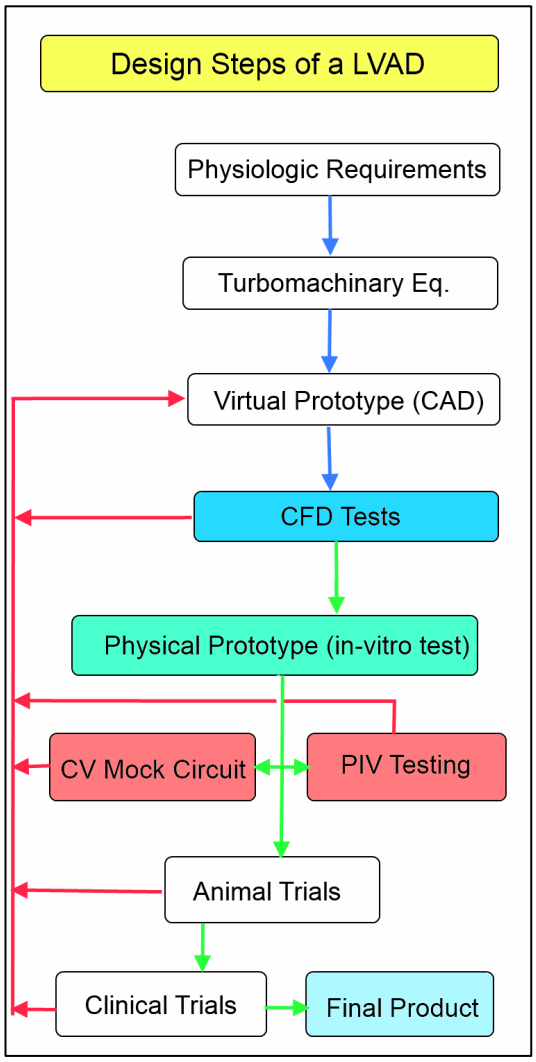


***Source:*** **Made by I.B. Aka**

Design of a virtual prototype is the first step through manufacturing the commercial product . Initially, geometric parameters (hub and tip diameters, cross sectional area, blade attack and trail angles etc.) were calculated by conventional turbomachinery equations to reagarding human physiological needs[16, 21]. Secondly, 3D model of the pump was generated by computer aided design (CAD) tools. Later, 3D model was virtually tested via computational fluid dynamic (CFD) softwares. CFD analysis and iterative modification process had continued until having perfect dimensions statisfying all hemodynamic and hemocompatibility criteria., FP1 of K. Toptop was the best design to be manufactured for physical testing[16].

Then now, a physical prototype is produced namely the External Drive Mechanism, to simulate its performance under realistic physical conditions. After conducting Particle Image Velocimetry (PIV) and Cardiovascular Mock Circuit (CVMC) testing, prototype FP1 will either be validated or invalidated. If the physical prototype of FP1 gets validated by further testing, an implantable version will be manufactured for animal testing. Otherwise, virtual prototype will be reviewed and tested through same steps until a successful protoype is found (Fig 1.8).

### 1.2.1 PIV Testing

Primarily, particle image velocimetry (PIV) method is applied to physical prototype to validate CFD results of boundary layer separation, flow field visuals, stagnation and high velocity gradient regions. Outsized variances between computational and physical test results require the adjustment of the virtual prototype to satisfy the design criteria. Then, optimization on pump geometry continues until CFD and PIV tests results meets to adequate physiological needs[15].

PIV is a technique which visually measures 2D flow field of a flow. A powerful light source illuminates a layer of the flow field while a synchronized high speed camera takes two consequative images of field of interest to calculate the velocity by image processing. Motion of the particles are easily observable by human (Fig 1.9). 3D

reconstruction of the flow through complete pump geometry will be done as the next step of this project.

**Figure 1.9: PIV Application illustration**

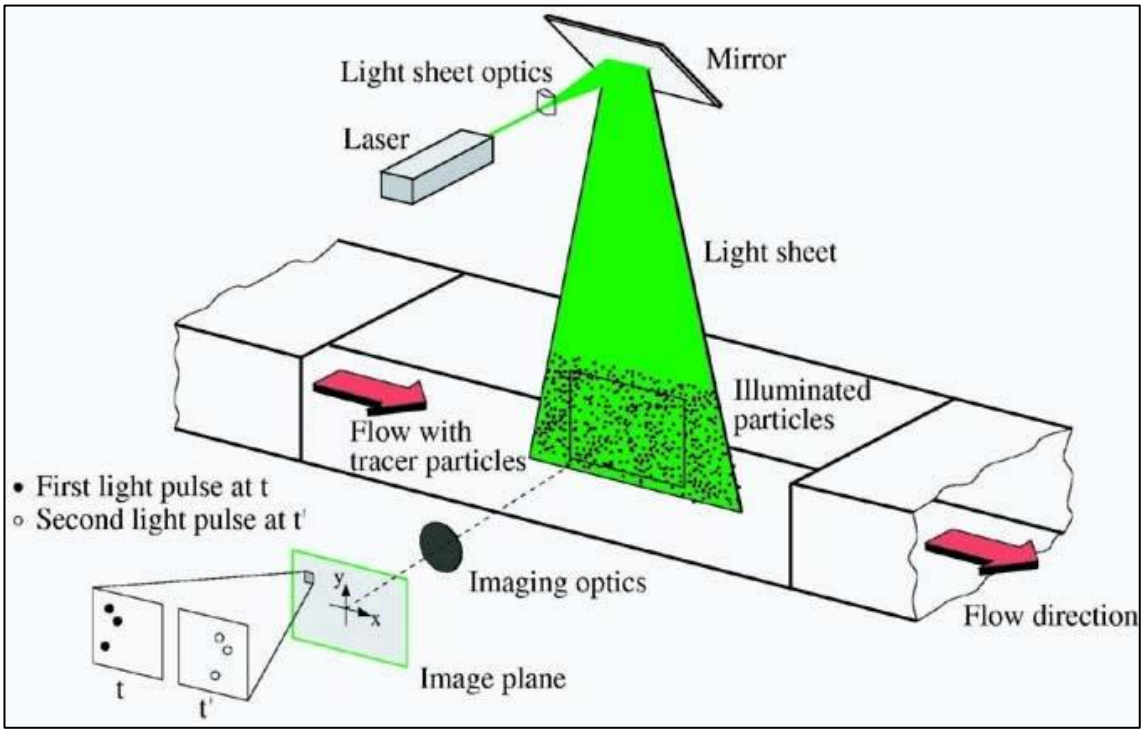


***Source:*** **IAS[22]**

### 1.2.2 CVMC Testing

Along with PIV tests, mock circuit (Dynamic simulation mechanism of circulatory system) tests will be conducted to observe physiological effects of device by repeating the physiology of a failing heart and supporting it (CVMC) with the LVAD. Moreover, mock circuit test is also necessary to develop a controller algorithm for manipulating the device to sustain an adaptation between pump operation and physiologic demands. According to pump hydraulic characteristic determined by CFD and physical performance tests, necessary rotational velocity and torque demands will be known and motor power rating will be calculated for the final product needed for next stage, animal testing. After observing acceptable hemocompatibility on animal physiology, the LVAD can be tried on human subjects in clinical trials as last step for design.

Novel design of our CVMC system uses a compressor for air pressure to create pulses like a real ventricle in the chamber. One way valves function like human cardiac valves. Pressures and pulses of the ventricular and atrial chambers are controlled by check valves and a computational control system. Consequently, CVMC mimics the flows and pressures of a human cardiovascular system (Fig 1.10). Physical setup of FP1 driven with variable velocity will be tested over CVMC to support ventricle without losing pulsatility as the next step of this project[23].

**Figure 1.10: CVMC Setup**


***Source:*** **Emir Eken's Thesis[23]**

## 1.3 LITERATURE REVIEW AND GAP

As described before, annually less than 5% of the HF patients receive heart transplant in Turkey. Rest of the patients needs mechanically circulatory support systems, mostly LVADs to live. Since most LVADs are manufactured by corporations from US, Germany or Japan; other countries have to import from these countries to recover patient needs[17]. However LVAD prices and maintenance costs bring significant economic burden. Moreover, countries with limited research on the field, cannot proficiently implant LVADs on patients, as these devices must be used by experienced personal. So, training technicians through physical and clinical testing process will help doctors to sustain patients for long. Therefore, producing domestic LVADs is essential for removing economic burdens and for covering patients' needs in other countries as well.

This goal can be achieved by designing numerous devices and training proficient technical personal on the field. In Turkey, another research group in Koc University has completed a centrifugal pump prototype based computational simulations and conducting in-vitro blood tests by 2014[18]. There are two different domestic efforts to develop LVADs, however there are many steps to follow yet for completing a prototype, such as physical performance testing (PIV and CVMC tests) and later in-vivo testing (animal and clinic tests).

Physical testing of the virtual prototype is a significant step of developing a LVAD before manufacturing a total prototype for in-vivo tests. Meeting hemodynamic needs of human body is necessary for evaluating the performance of the LVAD. Moreover, before starting hemolysis tests, many researchers use Laser Doppler Velocimetry (LDV) or Particle Image Velocimetry (PIV) for visualizing flow profiles in the pump. High velocity gradients can cause hemolysis while stagnant regions can cause thrombosis[15].

By employing PIV in LVAD design process, optimization of hemolysis and thrombosis characteristics is possible before animal tests. Therefore, a transparent and motorless

prototype must be manufactured. Some of the physical test setups of LVADs in literature for PIV testing is presented below. However, there are some inadequate methods applied in literature for manufacturing the in-vitro test setup of an LVAD for PIV tests. Moreover, some of the methods used to produce these setups are not clearly expressed.

Optical clearness of the transparent housing is an important factor affecting the qualitiy of the PIV testing along with the amount of refraction. All setups in literature are using machined acrylic blocks for shroud. However, machining diminishes transparency of the acrylic. Therefore, hand polishing is applied over the part for improving transparency. However, hand polishing causes different transparencies through the geometry and is not exactly a repeatable procedure. Moreover, assembly, data acquisiton and transparency of the physical prototype and manufacturing methos are not clearly stated in majority of the literature. In this work, details of all procedures are explained and a repeatable method for manufacturing a transparent shroud is offered for physical performance tests for LVAD design.

### 1.3.1 Physical Test Setups In Literature

PIV measurements are used for LVAD design for more than a decade now. Several different test setups are used for employing PIV on LVADs with respect to the tested LVAD generation with one obligatory similarity, transparent housing for the pump. Along with PIV measurements, there must be a mock circuit for providing chambers to receive and pump blood with desired head pressure, flow rate and rotational velocity. Different from our complicated Cardio Vascular Mock Circuit, these circuits are mostly simple high pressure- low pressure chambers. Several physical testing setups are presented in detail below in pump generation and chronologic order (1 pulsatile, 1 centrifugal and 2 axial test setups);

### 1.3.1.1 Pulsatile flow pumps

**PIV on Spiral Vortex Pulsatile Pump[24]**

In this study, PIV measurements were conducted on a spiral vortex (SV) pulsatile pump. A multiplane scanning Stereo-PIV (MS-SPIV) system was desgined for three-dimensional volume mapping of liquid flows enclosed by complex geometries since its clear that due to large displacement of diaphragm of pulsatile pumps complex flow fields are created that can not be investigated by Laser Doppler Velocimetry or 2D-PIV.

**Figure 1.11: Transparent pump body**

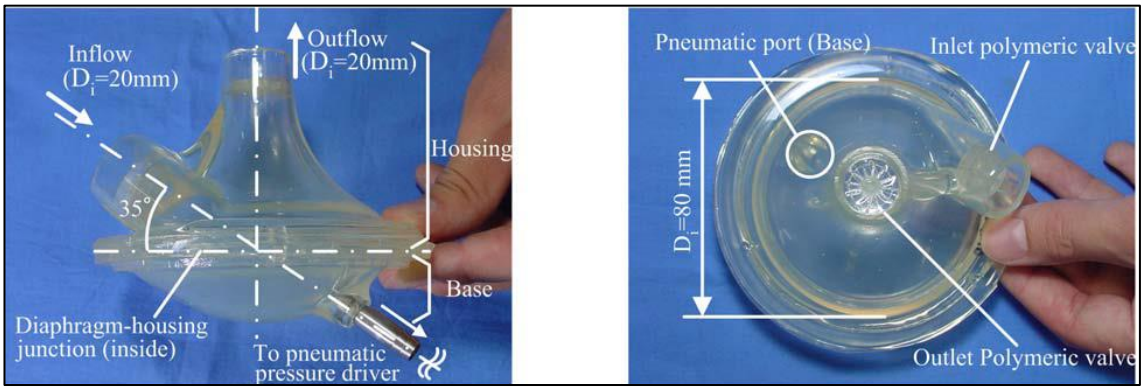


***Source:*** **PIV on Spiral Vortex Pulsatile Pump[23]**

The optical system was constructed on a motorized sliding scanning stage. Housing and pumps base is machined from Perpex blocks and assembled with a polyurethane diaphragm (Fig 1.11). The real-scale pneumaticly compelled Perspex model of the SV pump was used in an in vitro cardiovascular flow simulator (Mock Circuit) with nominal physiologic conditions as heart rate of 72 beats/min, flow rate of 5.0 L/min. Pressures are measured with conduit-type transducers and pulse timing is given byan external pulsation unit. Newtonian blood analog fluid with similar to Perpex refractive index is used(mixture of saturated aqueous sodium iodide 79%, glycerol 20% and distilled water 1%). Seeding particles used were novel fluorescent particles (D=18 μm, ρ=1500 Kg/m3). PIV setup consisted of two 12-bit CCD cameras (1280×1024 pixels, PCO SensiCam, PCO, Germany) and a two double-pulse lasers (Solo PIV, New Wave Research, Inc., CA, U.S.A.) of nominal 120 mJ (Fig 1.12).

**Figure 1.12: Diagram of the rig**

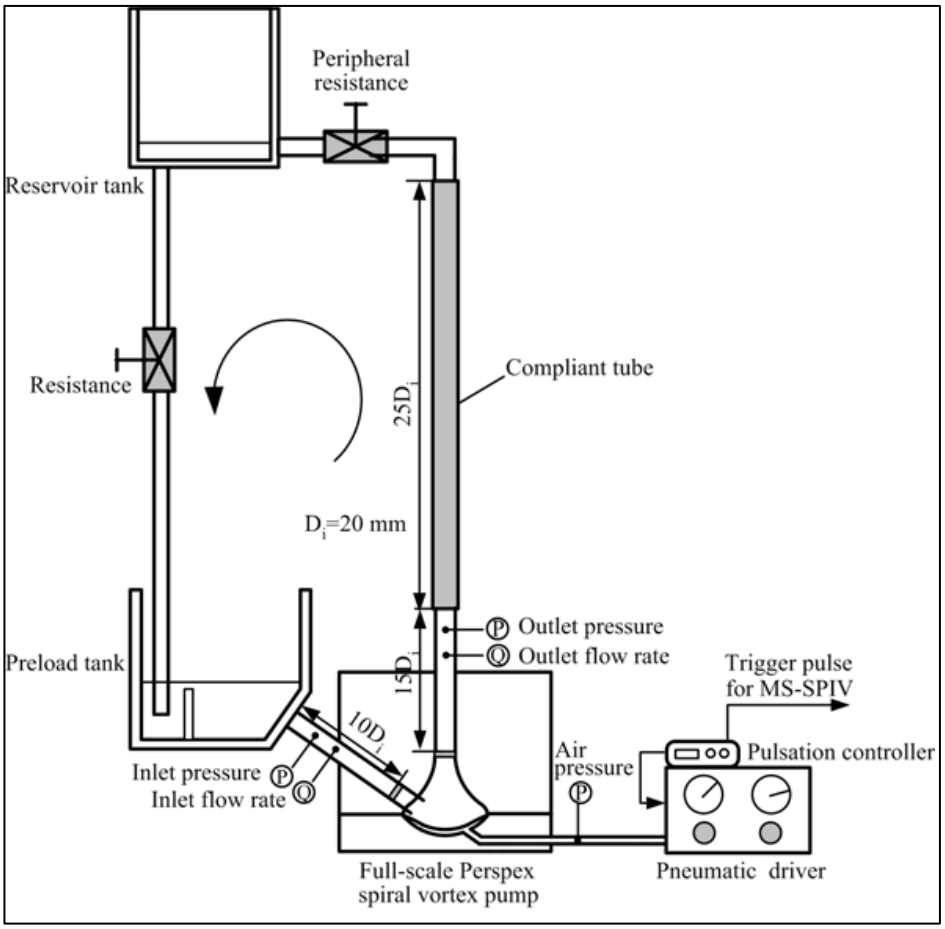


***Source:*** **PIV on Spiral Vortex Pulsatile Pump[23]**

A commercial PIV software (VidPIV 4.6, Intelligent Laser Application Gmbh, Germany) was used for post processing. A 3D calibration plate is sensitively placed with a micrometer to relate pixels to mm in PIV results. The scanning positions were set at seven verticle planes (Fig 1.13). Phase-locked measurements were taken during different phses of crdic cycyle (mid diastole, systole onset, mid systole and end systole) to observe the complex behaviour of the unsteady vortex. The velocity vectors were averaged over 600 pulsatile cycles.

**Figure 1.13: Diagram of the complete setup**

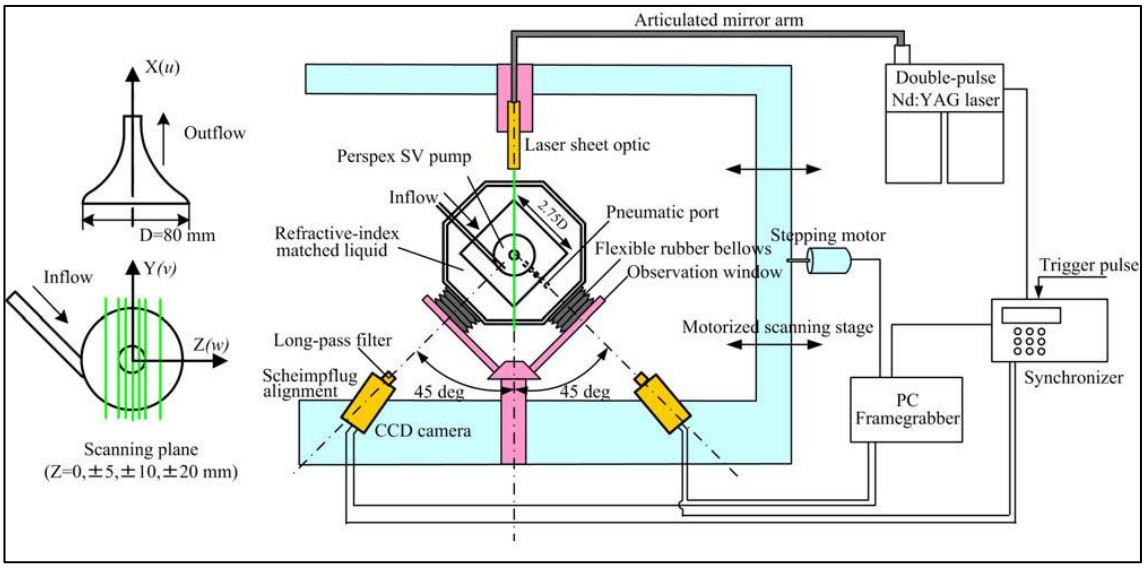


***Source:*** **PIV on Spiral Vortex Pulsatile Pump[23]**

The results demonstrated that an initial vortex configuration advanced during diastoly was a major reason of determining a near-wall whirling and instant velocity rise during systole. Among various involving factors, it was shown that the inlet flow inside a chamber revealed an important diffusivity in the direction of a pump apex (Fig 1.14).

**Figure 1.14: PIV vectors of different layers**

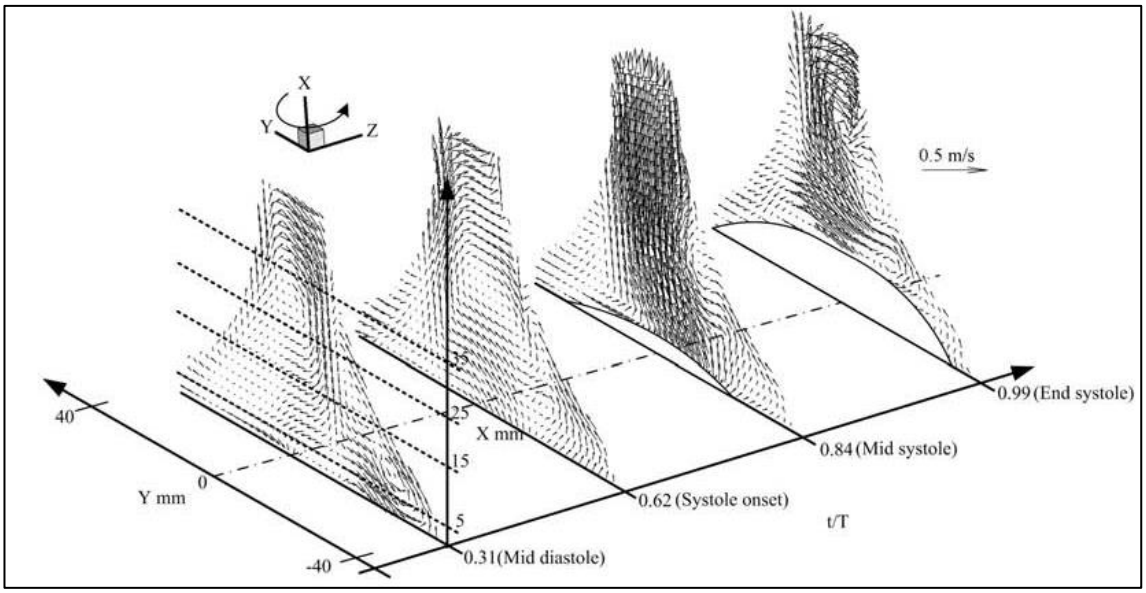


***Source:*** **PIV on Spiral Vortex Pulsatile Pump[23]**

### 1.3.1.2 Continuous flow pumps

#### a. Centrifugal Pumps

**PIV on CFVAD3, a Continuous Flow Magneticly Levitated Pump[25]**

The third prototype of a continuous flow ventricular assist device (CFVAD3) is being developed and tested. The blood flows through a four-bladed impeller (supported by magnetic bearings) and small clearance region on either side of the impeller enclosed completely by a shroud (Fig 1.15). Measurements of velocities PIV of a fluid similar viscosity of blood was made with two different speeds in one of these clearance regions between shroud and impeller. Measurements are compared with computational results.

**Figure 1.15: PIV compatible shroud**

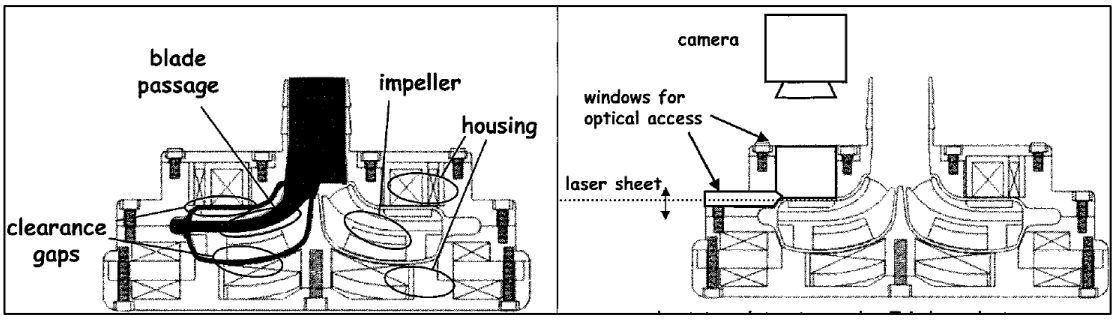


***Source:*** **PIV on CFVA[25]**

A prototype CFVAD3 pump was manufactured and assembled with a transparent opening for a laser sheet entering to the CFVAD3. Then light scattered from tracing particles to be observed over a second window perpendicular to laser sheet by a camera. The pump has a single moving part, a magneticly levitated impeller. Clearance between impeller and shroud is approximately 0.75 mm. The transparent openings are made of clear quartz and polished for gaining superior transparency. The laser sheet is formed from the 8 mm round beam exiting the laser and through a combination of lenses, focuses to target with a thickness of approximately 75 microns.

The pump is mounted on a translation stage for sliding laser sheet position by 1micron increments to evalute complete region of the gap. Gap size requires 10 different layers of measurement. Three dimensional velocities are calculated by 10 layers and compared with CFD results (Fig 1.16).

A commercially available PIV system is used. The laser and camera are synchronized. A Software completes image analysis required to define velocities. A pulsed laser at 532 nm illuminates tracer particles that are added to the fluid. The particles have zero buoyancy. These particles have 10 microns diameter. A digital camera collects the images.

**Figure 1.16: Velocity profiles of CFD and PIV results are compared**

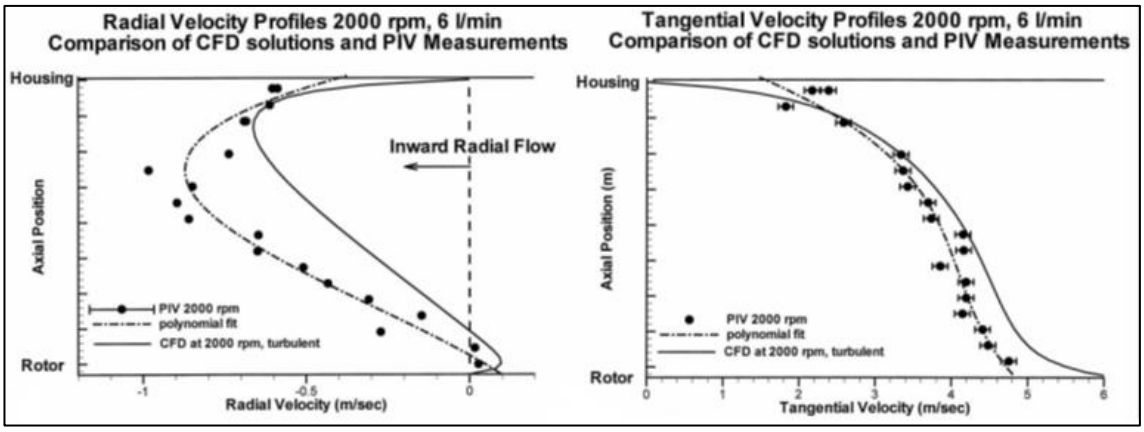


***Source:*** **PIV on CFVA[25]**

### b. Axial Pumps

**PIV Test on LEV-VAD,a Magneticly Levitated Axial LVAD [26]**

LEV-VAD has an unobstructed flow pathway and no secondary flow regions unlike many other pumps. It generates significantly less stagnant flow. The pump design is completed by computational fluid dynamics (CFD) modeling for calculating pressure-flow curves, hydromechanic efficiencies, fluid shear stress and exposure times to shear stresses. Axial fluid forces acting on the impeller is estimated for the magnetic suspension design. Physical performance testing was done on a plastic made prototype of the LEV-VAD for evaluation of the CFD predictions. The LEV-VAD creates 6 l/min and 100 mm Hg at 6300 rpms. The CFD results commonly approve the experimental measurements with apprximately 10% difference over the entire range of rotational speeds tested. A plastic prototype pump, specifically for fluid dynamic measurements, was designed and built as seen in Figure 1.17.

**Figure 1.17: Transparent rotor, shroud and test setup**

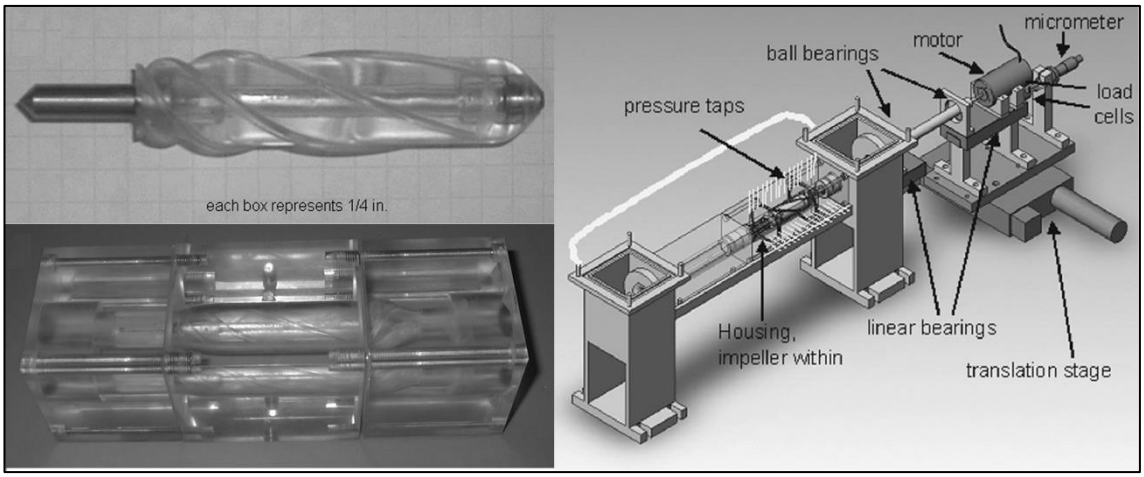


***Source:*** **PIV on LEV-VAD[26]**

The physical pump has the same flow pathway as the CFD model. However, the impeller is driven by a shaft that permits accurate location of the impeller and allows direct measurement of the axial force acting on the impeller. The pump housing was machined from a monoblock acrylic. Pump parts (inducer, diffuser and impeller) was made from urethane casting. The final pieces were hand polished to have accurate dimensions. Finally, brass pieces were inserted into the urethane to provide a metallic mark for an inductance type position sensor. Pressure gain, flow rate, and axial force were measured over different rotational speeds. The test setup contains an inlet and outlet reservoir, entrance pipe, drive motor, translation platforms for locating the impelle, pressure sensors and load cell. The test fluid in the setup was a 40% by volume aqueous solution of glycerin for equivalent viscous properties in the CFD calculations. The plastic pump's impeller was driven over a stainless steel shaft that passes through the outlet tank inside a custom shaft seal made from graphite impregnated Teflon. The main shaft has a diameter of 12.7 mm, thinning to 3 mm within the pump's exit pipe in order to reduce flow obstruction. The shaft was supported by two ball bearings and driven by a high-speed DC stepping motor. The rotational speed was continuously monitored and controlled. The platform containing rotary ball bearings and the motor was fixed on linear bearings to allow sliding axial direction. The axial force induced from expelled fluid on the impeller was transferred through the shaft and measured with the load cell. Flow rates were measured by an ultrasonic flow meter. Pressures were measured from both tanks with a diaphragm pressure transducer. A noncontacting

position sensor (Kaman, Inc., Colorado Springs, CO) was installed in the plastic pump's housing and used to measure the position of the impeller by the brass inserts. LabView program (National Instruments, Austin, TX), was used data acquisition. Measurements are compared with CFD results (Fig 1.18).

**Figure 1.18: Head pressure, axial loads are compared for CFD, Physical testing**

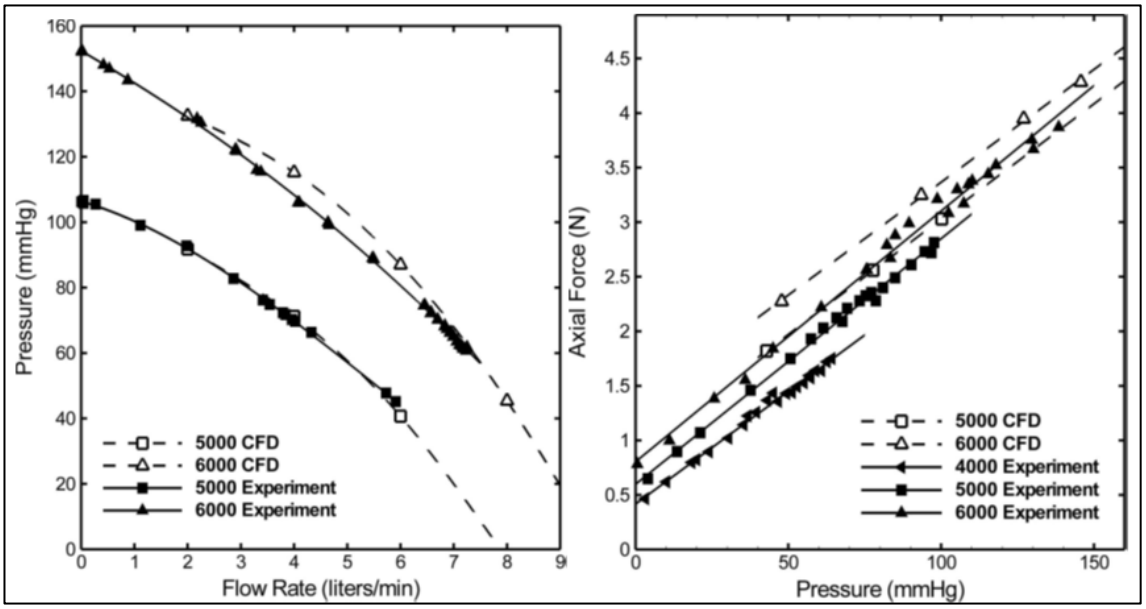


***Source:*** **PIV on LEV-VAD[26]**

**PIV Test on a Magneticly Levitated Axial LVAD [27]**

Experimental evaluation of a magnetically suspended axial flow blood pump is explained in the article. The pump consist of a three-blade straightener, a two-blade impeller, a permanent magnet-embedded cylinder shrouding the impeller and a three-blade diffuser. The internal flow fields were evaluated formerly by CFD and the pump characteristic curves were calculated. Particle image velocimetry (PIV) measurement of the pysical pump model was conducted to confirm the CFD results. To provide optical access, an acrylic prototype was manufactured with the impeller driven by a servomotor instead of embedded magnets since it is opaque. Then, a fluid mixture with similar viscosity as blood and with the refractive index close to the acrylic was used to avoid refraction. According to the CFD results, the axial flow blood pump could generate satisfactory pressure head at the rotating speed of 9500 rpm and flow rate of 5 L/min. PIV measurements were conducted under sama flow conditions. Experiments indicated

that the physical results were close to CFD results Therefore the CFD model is validated.

The axial blood pump consist of a three-blade straightener, an enclosed twoblade impeller, and a three-blade diffuser. Its axial length is 60mm and outer diameter is 19 mm. The impeller was driven by the Lorentz force as the only moving part. There was a clearance between the rotor cylinder and the pump housing. The diffuser has three blades for the simplicity of PIV measurement.

**Figure 1.19: Diagram of the PIV setup**

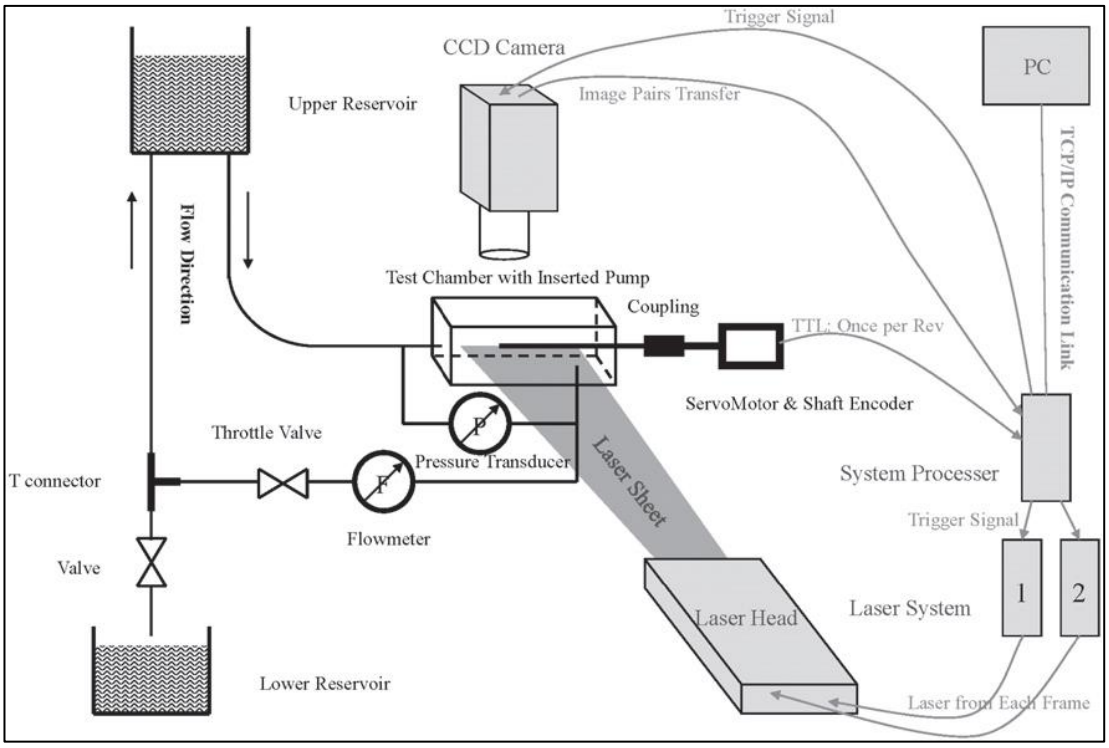


***Source:*** **PIV Test on a Magneticly Levitated Axial LVAD[27]**

Figure 1.19 shows the diagram of the constructed experimental test setup. The pump model maufactured has the exact dimensions of the prototype. During pump operation, the flow rate is controlled by the throttle valve, and the pressure head across and the flow rate is obtained from the pressure transducer and the flowmeter. There are magnets on the shroud of a LVAD. However, it is impossible to execute PIV testing through the opaque magnets. Thus, the impeller is compelled by a servomotor through a shaft. The test model is partially build from acrylic to allow illumination of the laser. In order to

minimize the vibration of the functioning impeller, a bearing holder was placed. The straightener, impeller, and diffuser are all made of acrylic and glued together to the impeller. The impeller is driven by a steel shaft, which is implanted through the bearings and bearing holder (Fig 1.20). The PIV system used in this study was the Dantec FlowMap PIV system (Dantec Dynamics A/S, Skovlunde, Denmark). The Gemini PIV 200-15 (NewWave Research, Fremont,CA, USA), a doublecavity pulsed neodymium yttrium aluminum garnet laser system, was employed as the illumination soruce.

**Figure 1.20: Exploded view of setup components**

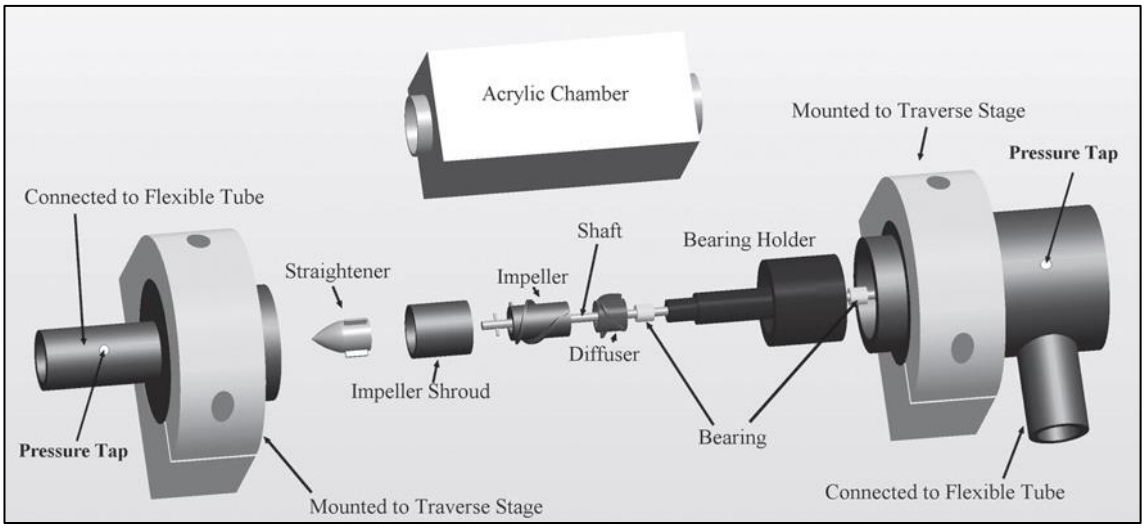


***Source:*** **PIV Test on a Magneticly Levitated Axial LVAD[27]**

Computational fluid dynamics was previously applied to evaluate the flow field of the axial flow blood pump.The experimental test presented that the CFD simulation could predict the pump characteristic curves with comparable fashions. Additionally, the PIV measurement was conducted for the validation at various flow and rotation conditions. Commonly, the CFD results complemented fairly well with the PIV results (Fig 1.21).

**Figure 1.21: CFD and Physical head curves are compared**

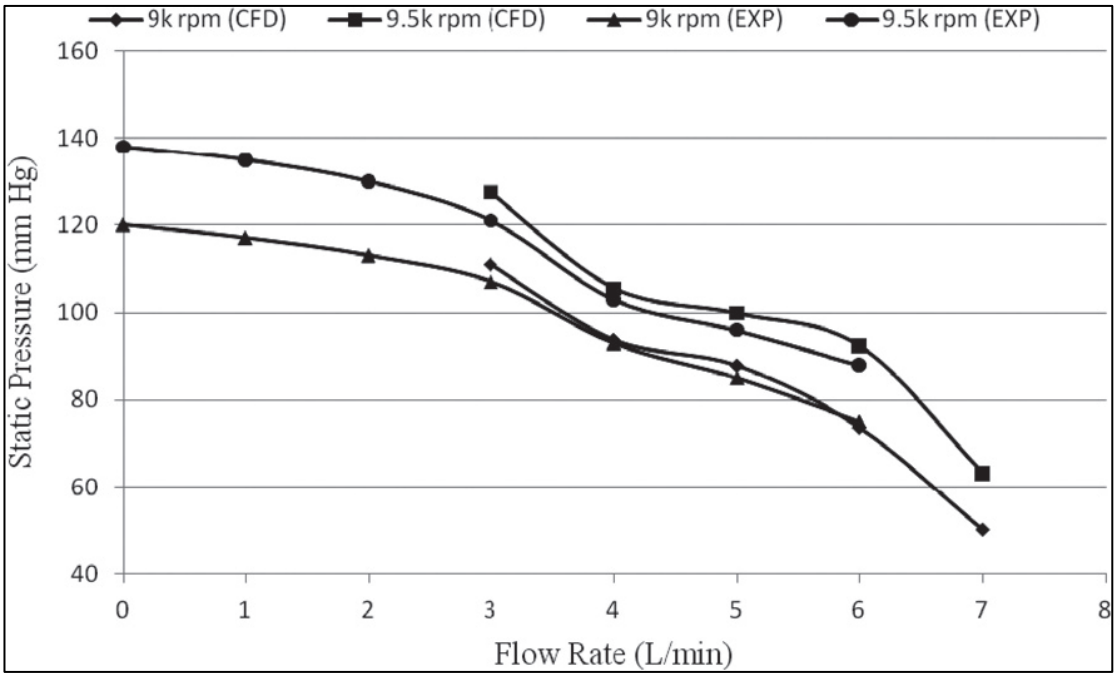


***Source:*** **PIV Test on a Magneticly Levitated Axial LVAD[27]**

## 1.4 PROJECT FIELD

A research group from Bahçeşehir University started a program to develop axial flow LVAD in 2009 to fill these missing steps in Turkey and obtain a commercially used product. This program includes all steps in Figure 1.8, until now a virtual prototype is designed by CFD optimizations[16, 21]. Also a novel Cardiovascular Mock Circuit is designed, manufactured and tested[23]. PIV test setup is acquired and preliminary test are conducted. The present Master Thesis is a dual object project of axial flow LVAD development program and starts from manufacturing of a physical prototype of the first virtual prototype to results of the initial PIV and Mock Circuit tests. Moreover, an innovative and experimental metod for bearing washing for 2$^{nd}$ generation axial pumps is presented and virtual prototype is investigated in CFD tests. This double-objective project includes;

**a. Design and Construction of the Physical Test Setup EDM**

i. Literature search on current devices and physical test setups,
ii. Theoretical design of a bench-top physical test setup for LVAD (EDM)
iii. Initial 3D design via SolidWorks (CAD tool),
iv. Computational fluid dynamic analysis of the prototype via ANSYS Fluent
v. Manufacturing of the transparent prototype
vi. Assembly, application and simultaneous data acquisition with PIV and CVMC

**b. An Innovative Method for Washing Bearings of 2$^{nd}$ Generation Axial flow LVADs**

i. Virtual design of the novel bearing washing channels for LVAD
ii. Initial 3D design via SolidWorks (CAD tool),
iii. Computational fluid dynamic analysis of the washing channels via ANSYS Fluent

Major objective of this project is to design and manufacture a physical prototype for PIV testing of the final prototype of Toptop, namely FP1 which achieved all hemodynamic and hemocompatibility criteria on computer based performance results (CFD tests). This project covers R&D process of LVAD from Virtual Prototype to construction of a physical prototype functioning adequately for PIV performance testing and Cardiovascular Mock Circuit testing to validate computer based performance results and initial results of PIV and CVMC tests.

Furthermore, as the minor objective, a innovative bearing washing concept is presented and investigated by CFD tests. Thus, remaining sections of this thesis are divided in two separate sections according to these two different objectives. After satisfactory results of physical testing, there are other significant design steps to complete the LVAD for commerical use. These further steps will be discussed in future work section.

### 1.4.1. Design Criteria

Concisely, all prototypes were developed to accomplish the same objective, validating virtual prototypes by creating similar pressure heads and flows under similar conditions, eventhough all of them have different geometries, materials and working procedures. Additionally, accomplishing manufacturing the functionıng prototype is not the final step before in-vivo testing, correspondingly setup must be compatible with physiology which will be revealed by further testing of the setup by PIV method and CVMC testing with realistic cardiac dynamics. To be brief, physical testing setup must be designed to satisfy hemodynamic performance as well as hemocompatibiliy.

#### 1.4.1.1 Physical setup

Initially, physical setup must be identical to the virtual setup in the terms of physical features for accurate validation. Wide range of parameters must tested and evaluated. Setup must endure high speeds, pressures and flows with low wear and vibrations. Transparency must be ensured for appropriate PIV testing. Operating conditions estimated from CFD results are given as;

**a. Mechanical Performance**

*i. Bearings : 10000rpm*

*ii. Shaft : 0.5N axial load and 5mNm Torque @ 10000rpm*

*iii. Shroud : Visually clear ~1.3 refractive index*

*iv. Pump Parts : Titanium and Exact Dimensions Of FP1*

*v. Base(Mount) : Aligned and Stainless*

**b. Hemodynamic Performance**

*i. Head pressure (ΔP) : 80 < ΔP < 120 mmHg*

*ii. Blood Flow (Q) : 3 < Q < 8 L/min*

*iii. Angular Velocity (w) : 8 < W < 11 krpms*

*iv. Torque Load (T) : 3 < T < 5 m.Nm*

*v. Efficiency (%) : 22 < n < 32*

### 1.4.1.2 Innovative Washing Channels

As stated before, most hemolysis occurs around bearing regions of the 2nd generation pumps. Also, continuous washing of all surfaces contacting blood is key for eliminating thrombosis formation. Therefore, a new concept of bearing washing for 2nd generation axial flow LVADs are offered. State of the art technology is magnetic suspension of the impeller (rotor) region of the pump[19]. However, physical setup must be transparent and therefore motorless for PIV tests. An external motor and drive shaft is employed for positioning and driving the impeller. Morevoer, this shaft is used for direct measurement of hydraulic torque load acting on the impeller. FP1 functions between 8 to 10 krpms. This high rotation creates significant shear force on red blood cells (RBCs) and cause hemolysis. Moreover, complex structures of bearings cause most stasis. Stasis or stagnation causes thrombosis (coagulation) which can not be tolerated[16].

Hereby, a new concept of bearing washing for 2nd generation axial pumps is suggested and investigated by our research group. Bearing washing channels are opened through the inducer and diffuser parts of the pump to allow continuous blood flow as the pump functions. Length of the parts were kept same while the diameter of the channels are

changed and optimized regarding initial CFD data. Bearing washing channels must provide continuous flow of blood over bearings without losing significant amount of hydraulic energy or efficiency of the standard model.

.

**Hemodynamic Performance**

i. *Head pressure (ΔP)* : *~100mmHg*
ii. *Blood Flow (Q)* : *~5 L/min*
iii. Stagnation : Not Tolerated

# 2. MATERIALS AND METHODS

As known from the literature search and illustrated before, design process of all of the heart pumps (LVAD, RVAD, BiVAD or TAH) are gone through physical testing (in-vitro testing). Laser Doppler Velocimetry or PIV are two quantitative methods for evaluating hemodynamic and hemocompatibility characteristics of a heart pump. Hemodynamic characteristics of the pump must be evaluated over CVMC while it mimics failing physiology of LV, for wide range of realistic results. In this work, initial testing is conducted on a simple High Pressure-Low Pressure dual chamber system. However, all necessary connetions and control software for CVMC testing is prepared for future work. Bearing system is designed considering hemocompatibility and mechanical needs with respect to the CFD results. High transparency is assured by mold casting method rather than hand polishing of machined acrylic blocks. Assembly is designed in CAD and presicion mating of the parts assured by high tolerance manufacturing dimensions. As stated before, Materials and Methods section will follow in two sections as External Drive Mechanism and Bearing Washing Channels.

## 2.1 EXTERNAL DRIVE MECHANISM

External Drive Mechanism consists of titanium machined pump components (Inducer, Rotor, Diffuser), transparent shroud, drive shaft, YT connection part, custom made viton oil seal, couplings, dynamic torque sensor with encoder, L-shape motor holder, DC motor and machine aluminum base for assembling all. Complete system is designed to function simultaneously for PIV and CVMC tests. DC motor is controlled over dSPACE data acquisition system. Also the same system measures and calculates desired parameters of pump performance.

Rigidity of the rig is important for hemodynamic tests. Setup must be leakage proof and shaft alignment must be precise for avoiding vibration at higher speeds (~9000 rpm nominal). Moreover, PIV technique requires high transparency through target for visualizing flow field. Therefore, housing of the pump is made of transparent cast resin with a better than glass refractive index of 1.48. However, Ti6Al4V material is used for

manufacturing pump parts to have realistic physical features like inertia, power rating of future motor design, etc. Transparency through internal components were not necessary since observing one quadrant of the rotor was enough due to radial symmetry of the pump design (Fig 2.1).

**Figure 2.1: Radial symmetry of impeller blades**

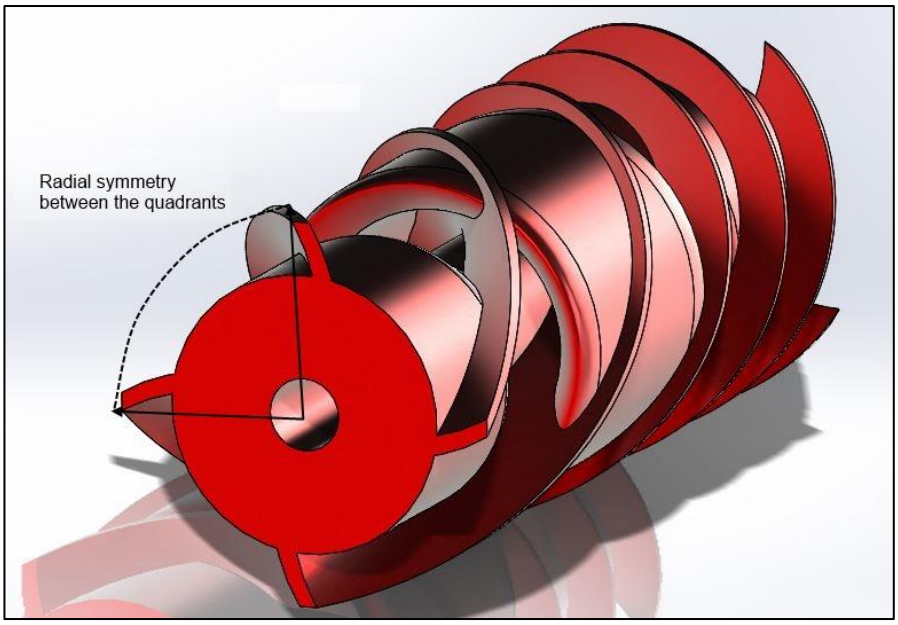


***Source:*** **Made by I.B. Aka**

### 2.1.1 Virtual Design

#### 2.1.1.1 Pump components (Inducer, Diffuser, Rotor)

Complex geometry of rotor of FP1, due to innovative magnet carrier circle and secondary blood pathway, prevents standart monoblock machining even with a 5-Axis CNC. Therefore, these components must be manufactured by 3D printing or Laser sintering, either of which being layer-by-layer manufacturing methods which allow the most complex geometries. H9 or H6 engineering tolerances are given for fixing shaft into the rotor and bearings placed inside of the stationary parts (inducer and diffuser) respectively. Rotor hub and tip diameters, attack and trail angles of all rotary or stationary blades are modelled identical to CFD results of FP1 of Toptop (Fig 2.2).

**Figure 2.2: Magnetic cylinder and central flow channel**

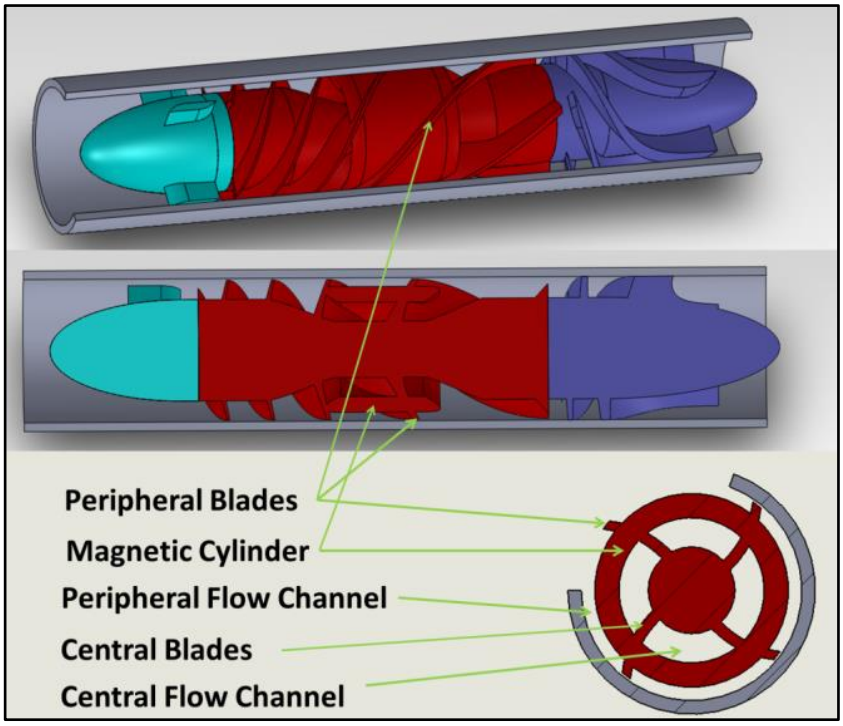


***Source:*** **Toptop's thesis[16]**

Physical Gap between stationary parts and rotary part is included as well as 3x8mm bearing hole. Since the physical setup must driven with and external shaft, inlet side is chosen for transferring rotary motion to the pump. Therefore, a shaft hole is included through inducer part from the beginning to the bearing hole (Fig 2.3).

**Figure 2.3: Pump Parts (Inducer,Rotor,Diffuser) with gaps**

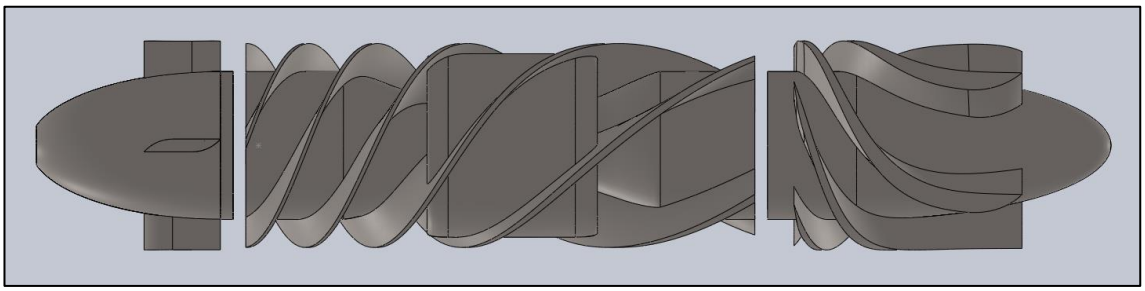

***Source:*** **Made by I.B. Aka**

### 2.1.1.2 Bearings

As mention before, bearing system of a heart pump is vital. It defines hemocompetibilty and pump performance in all means. Eventhough, magneticly levitated pumps (3rd generation) are proven to give better hemolysis results, even though control units are bigger and battery lives are shorter[28]. Our LVAD (FP1) is designed to be build with mechanical bearings (2nd generation). However, hub diameter is large enough for implementing magnets for magnetic suspension later through the project.

Even though mechanical bearings cause some hemolysis, they are energy effective. Particularly ceramic bearings are durable, hemocompatible and corrosion resistant. For instance, custom made ceramic bearings of Jarvik2000 were put on accelerated tests equivalent more than 10 years and proven to be durable[29]. Longest supported patient lived over 8 years by 2013. Rotor component of  axial pumps are self-aligning in rotary axis by its own momentum. Thus, pivot bearings are enough for axial pumps. Polyethylene, Alumina Oxide, Zirconia Oxide, Silicone Nitride ,Silicone Carbide are some materials used for LVADs with pivot bearings. Male ceramic – female polyethylene pivot bearing formation shows 10 year durability with accelerated tests [30].

**Figure 2.4: View of shaft and bearings inside transparent virtual model of FP1**

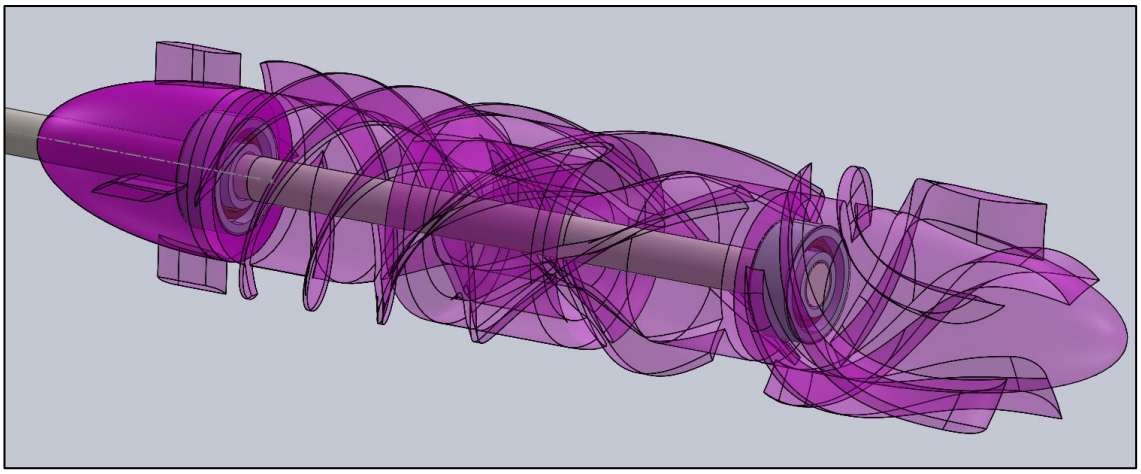

***Source:*** **Made by I.B. Aka**

Moreover, ceramic materials are non-ferromagnetic which reduces energy losts due to eddy currents. Therefore, employing ceramic bearings prolonge DC motor efficiency and increase patient mobility due to increased battery life. Moreover, standart mechanical bearings need lubricant to function which may damage blood in case of a leakage. Contrary to that, ceramic bearings can function even without any lubricant due to their high heat and corrosion resistant material[31]. For instance, Silicone Nitride has 50% higher modulus of elasticity compared to steel. Therefore, Ceramic bearings can handle 40% higher speeds than standart bearings. Moreover, ceramic balls have smoother surface finish than steel which reduces spindle deflection and vibration. Only drawback of ceramic compared to steel is price. Machining of ceramic is much harder and expensive than steel. However, these costs are exponentially decaying in the last years.

Outer diameter of the bearings must fit into the hub of diffuser and inducer components by design (Fig 2.4). Inner diameter of the bearing is determined by shaft calculations later shown in this thesis. Outer diameter is dictated by commercial product that is decided to be used later (Fig 2.5).

**Figure 2.5: Bearing holes and bearing fit inside stationary inducer and diffuser**

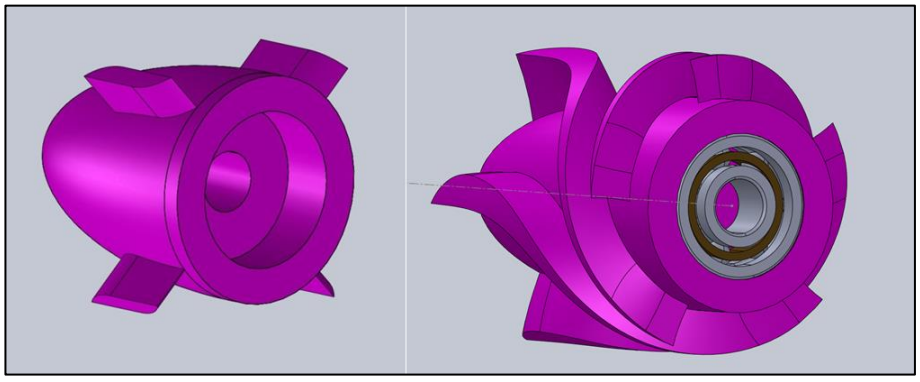

***Source:*** **Made by I.B. Aka**

ABEC (American Bearing Manufacturers Association) class of a bearing defines the clearance between balls and walls of the bearing. Bearings under the abec system are typically called "precision bearings", and they are rated with a number from 1 to 9. Higher number defines more precise clearances. ABEC 1 bearings have 7.5 $\mu$m where

ABCE 9 bearings have 1.2 $\mu$m clearances[32]. Red blood cells (RBCs) have approximately 7.5 $\mu$m diameter[33]. So smaller clearances contacting blood can avoid intrusion and destruction of RBCs. Therefore, our bearing should be at least ABEC 3 to avoid hemolysis inside the bearing zone.

#### 2.1.1.3 Shaft

Initial design of the shaft is calculated by conventional shaft design equations by estimated loads of CFD results. Shaft is the most curical part for transmitting rotary motion along with bearings. Along with mechanical design criteria, shaft diameter effects hydrodynamic characteristics of the pump as well. Shaft diamater must be as small as possible to avoid excessive obstruction of blood pathway. Minimum shaft diameter determined by calculations and shaft is modelled by CAD and tested in CFD for evaluating possible obstruction of flow and pump performance which mentioned later in this work.

To design a durable and stable shaft, material choice, manufacturing method and working environment are as important as the mechanical and geometric design. Axial loads are generally very small where bending or torsion dominates. There are no significant radial load in our design except gravitational force acting on impeller body. Therefore, axial and radial loads are neglected for diamater calculation[34]. However, possible shaft buckling and critical speed were studied later considering our initial shaft diameter. Stress analysis for fatigue highly depend on load consentration which depends on size specifications which is unknown for initial design of the shaft. Therefore, size dependent parameters are selected as conservative as possible for initial design. DE-Goodman criterion is suitable for initial design which is simple and conservative according to the Shigley's Mechanical Designs' 7$^{th}$ Chapter. Since alternating and midrange stresses of bending and torsion are dimension dependend(2.1), safety factor `n` is substituted instead of these (2.2). Combination of all leads to equation (2.3) with assuming shaft is round and filled according to von Mises stresses[34].

$$\sigma = K_f \frac{Mc}{I} \, , \tau = K_{fs} \frac{Tc}{J} \qquad \text{Eq 2.1}$$

$$\frac{1}{n} = \frac{\grave{\sigma_a}}{S_e} + \frac{\grave{\sigma_m}}{S_{ut}} \qquad \text{Eq 2.2}$$

$$d = \left(\frac{16n}{\pi}\left\{\frac{1}{S_e}\left[4\left(K_f M_a\right)^2 + 3\left(K_{fs} T_a\right)^2\right]^{\frac{1}{2}} + \frac{1}{S_{ut}}\left[4\left(K_f M_m\right)^2 + 3\left(K_{fs} T_a\right)^2\right]^{\frac{1}{2}}\right\}\right)^{\frac{1}{3}} \qquad \text{Eq 2.3}$$

For a rotating shaft with constant bending and torsion, terms can be simplified by assuming midrange bending moment and alternating torsion are equal to 0.

Then equation is simplified to;

$$d = \left(\frac{16n}{\pi}\left\{\frac{2\left(K_f M_a\right)}{S_e} + \frac{\left[3\left(K_{fs} T_m\right)^2\right]^{\frac{1}{2}}}{S_{ut}}\right\}\right)^{\frac{1}{3}} \qquad \text{Eq 2.4}$$

Torque distribution over impeller blades at nominal speed is estimated as 0.0042 Nm from CFD results. Shaft material is assumed to be Ti6Al4V as other parts. $K_f$ and $K_{fs}$ are fatique consentration factors for bending and torsion and $S_{ut}$ and $S_e$ are minimum tensile strength and endurance strength of the rotary shaft. $K_f$ and $K_{fs}$ are assumed 1.5 for safety and $S_e$ is assumed as half of minimum tensile strength for conservative results. ($S_{ut} = 950MPa$ for Ti6Al4V and Ma=0.0025Nm by 0.02kg impeller placed after a125mm long shaft). Safety factor `n` is taken 1.5.

**Figure 2.6: External shaft fits inside the bearings embedded in stationary inducer and diffuser**

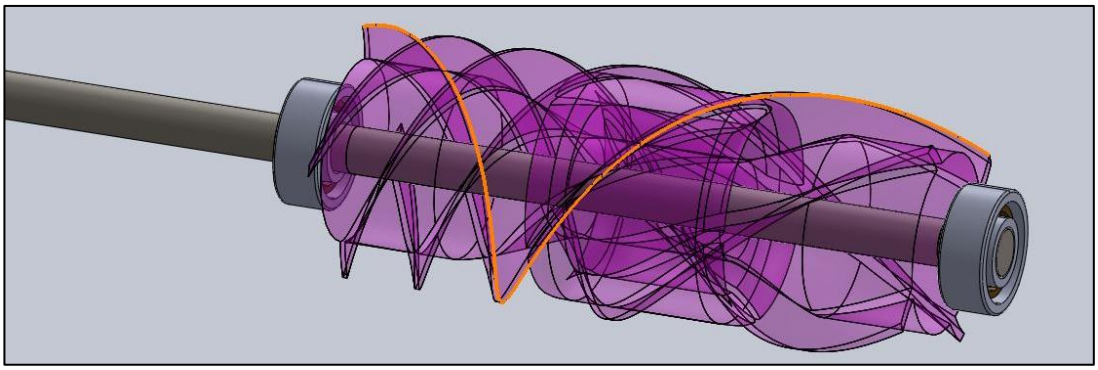

***Source:*** **Made by I.B. Aka**

Minimum shaft diamater is found 0.5mm according to these most conservative assumptions. However there is significant axial force acting through the blades, so shaft buckling must be evaluated as well. Buckling equation gives allowable load which must be higher than 0.46 N which is found by CFD analysis.

$$P = \frac{\pi^2 EI}{l} \qquad \text{Eq 2.5}$$

Result shows that 175cm long Ti6Al4V shaft with 0.5mm diameter can handle 30N axial load without buckling.( Ix = 0. $477x10^{-8}kgm^2$ and E=113.8 GPa)

Critical speed is another parameter for assuring stable functioning of the EDM. At particular higher speeds, shafts vibrate even with perfect alignment. This is called critical speed of the shaft. The Smaller the diameter and the longer it is, the shaft will reach critical speeds at lower rpms (Critical Speed is low).

$$N_c = F_a \frac{60\lambda^2}{2\pi l^2}\sqrt{\frac{EI}{\gamma A}}\ (Rpm) \qquad \text{Eq 2.6}$$

where $l$ is the distance between supports, F is safety factor (taken 2), I is the minimum secondary moment of shaft crossection. $\gamma$ is specific gravity. $\lambda$ is determined with respect to supports of the shaft (3.9 for Fixed-Supported) and A is cross-sectional area of the shaft.

**Figure 2.7: Cross-section view of the shaft and bearings inside FP1**

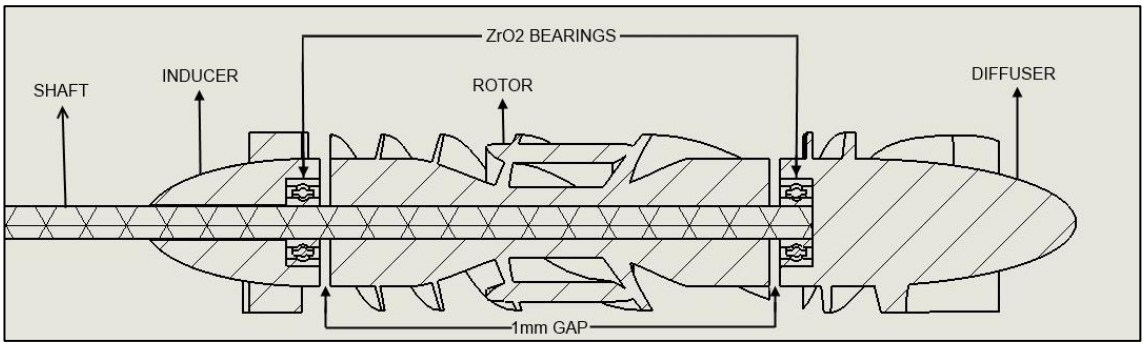


***Source:*** **Made by I.B. Aka**

Here first critical speed of the shaft with a safety factor of 2 is found 3650 rpm which is very short of our needs. Therefore we decided to use 3mm diameter shaft which gives the first critical speed at 22000 rpms. Finally, 3mm diameter and 175mm long shaft is determined to be used for  EDM (Fig 2.6 and 2.7).

#### 2.1.1.4 Housing (Shroud)

Shroud of commercial heart pumps is generally made of stainless steel or titanium. Some recent products use ceramic material for shroud as well to reduce magnetic losses. As explained before, this prototype must have transparent shroud for allowing LED lightsheet. Shroud also needs to avoid absorbing water for enduring prolong tests (Fig 2.8).

**Figure 2.8: Side view of the FP1 inside inital circular shroud**

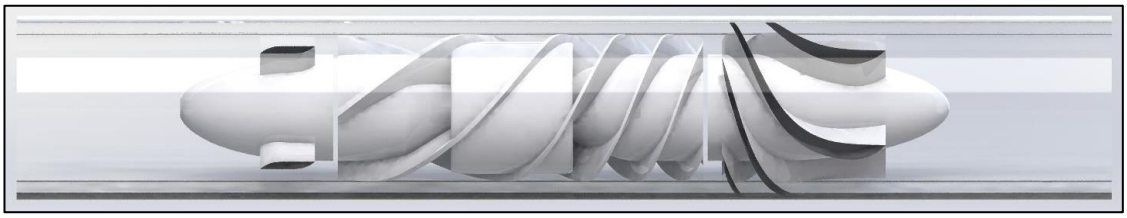

***Source:*** **Made by I.B. Aka**

PIV testing method employed in this project is 2D so many sublayers of the pump geometry must be tested and computational methods are used for 3D reconstruction of streamlines. Thus, camera and LED must slide in the radial direction of the pump. While LED slides through the pump, circular shape of shroud causes different rates and angles of refraction and reflection (Fig 2.9).

**Figure 2.9: Circular Shroud of FP1**

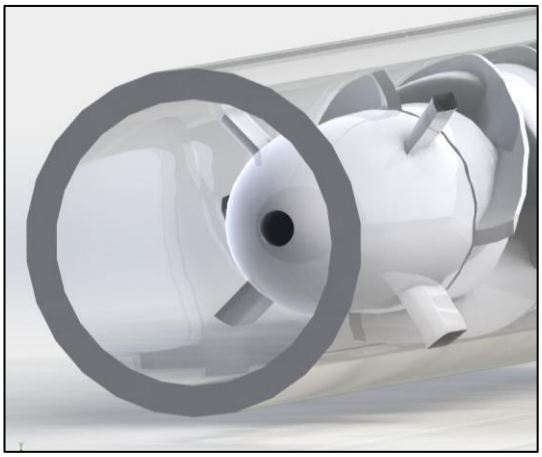

***Source:*** **Made by I.B. Aka**

Therefore, rectangular shape is employed for housing. Rectangular shroud meets LED sheet with 90°s for all layers. However, rectangular shape brings extra thickness and therefore more refraction of light. For avoiding this, flow pathway of the shroud is centered as close as possible to the side. By this design, there is enough room left on the other side of the housing for mounting screws and sensors.

Fixing stationary parts on shroud is another problem for EDM design. Most axial pumps are constructed with tight fitting of stationary parts. However, this causes scratches over the surface of the transparent material which reduces transparency. Using adhesives cause terminal fixation of the parts and this eliminates modularity for further geometry iterations and can cause misalignment depending on size tolerance of stationary parts and shroud. Therefore, a group of setscrews are placed around the shroud to hold and align stationary inducer and diffuser which holds bearings. Consequently, well alignment of all these parts is important for stable functioning of the shaft and the pump (Fig 2.10).

**Figure 2.10: Final (Rectangular) design of the shroud**

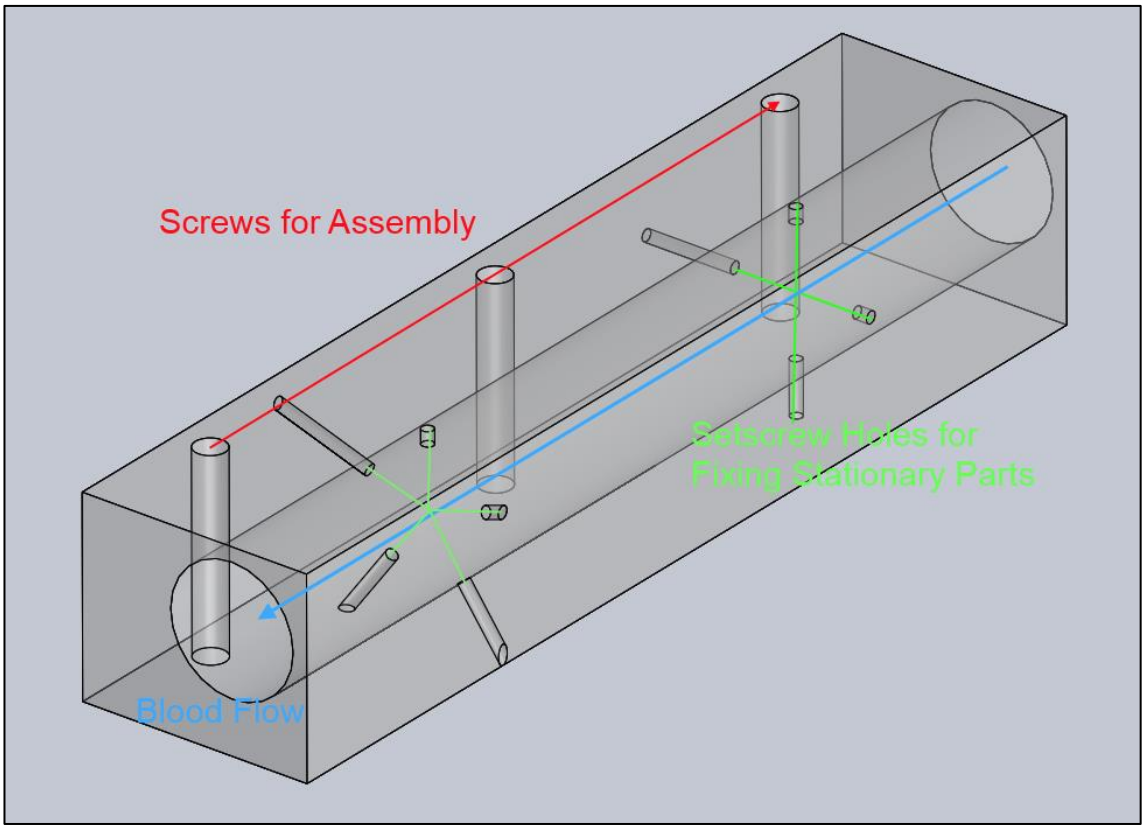


***Source:*** **Made by I.B. Aka**

Given the geometry, material choice and manufacturing methods are important as well. Most of the physical test setups in the literature uses machining of an acrylic block for housings. However, this method requires hand polishing for perfect transparency which can not be done exactly same for everytime. Therefore, we have decided to use mold casting for superior transparency for PIV tests.

#### 2.1.1.5 YT connection

External shaft meets water inside the pump. Therefore, a special inlet canula must be designed for transmitting water and rotary motion together without leakage. To solve this problem, a custom part is desgined (YT Connection) (Figure 2.11). Y branch of the YT serves as the inlet canula of the pump where axial branch carries the shaft sealed with an oil seal to prevent possible leakages. YT part designed to shrink fit into the housing to prevent leakages in between (Fig 2.11).

**Figure 2.11: YT Connection**

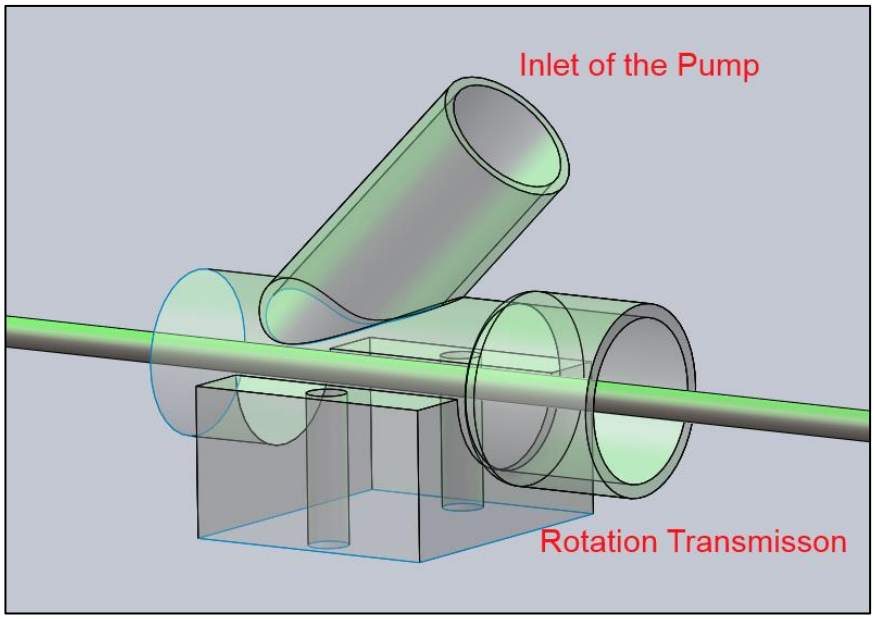


***Source:*** **Made by I.B. Aka**

### 2.1.1.7 Sensors

Various sensors to evaluate different characteristics of the prototype is required. Pressure gain, rotation speed, torque load over the impeller are the three most important parameters for evaluating pump performance. Vibration of the shaft is another parameter to be evaluated and minimized. However, most vibration measurement devices on the market have too large probes making the measurement impossible without obstracting blood flow. Vibration measurement will be tackled in the subsequent steps of this project.

For measuring pressure rise by the pump, two different types of sensors are employed. Millar pressure catheters(Millar, TX, USA) can be implemented anywhere through the shroud (housing) by punching holes without interfering bloodflow however they are too costly. In this project, SICK PBT-RB1(SICK, Waldkirch, Germany) pressure transducers are mounted at the bottom of the CVMC chambers to measure inlet and outlet pressures of the pump (Fig 2.12).

**Figure 2.12: SICK PBT-RB1**


***Source:*** **SICK Sensors[35]**

Dynamic measurement of volumetric flow rate is conducted by a Transonic TS410 ultrasonic flowmeter(Transonic Inc, USA) clipped over the outlet cannula of EDM (Fig 2.13).

**Figure 2.13: Transonic pipe clamp sensor and measurement unit**


***Source:*** **Artisan Technology (Transonic Sensors distributer)[36]**

Dynamic torque load measurement is necessary for evauating pump hydromechanic efficiency which is the ratio of hydraulic energy outcome to the given mechanical energy as;

$$\eta = \frac{\Delta P.Q}{T.\omega} \qquad \text{Eq 2.6}$$

Therefore, a dynamic torque sensor with desired measurement range is selected from Burster, Germany (Fig 2.14). This sensor has an embedded encoder for velocity measurement as well. Then, assembly was designed considering and including these.

**Figure 2.14: Burster dynamic torque sensor**

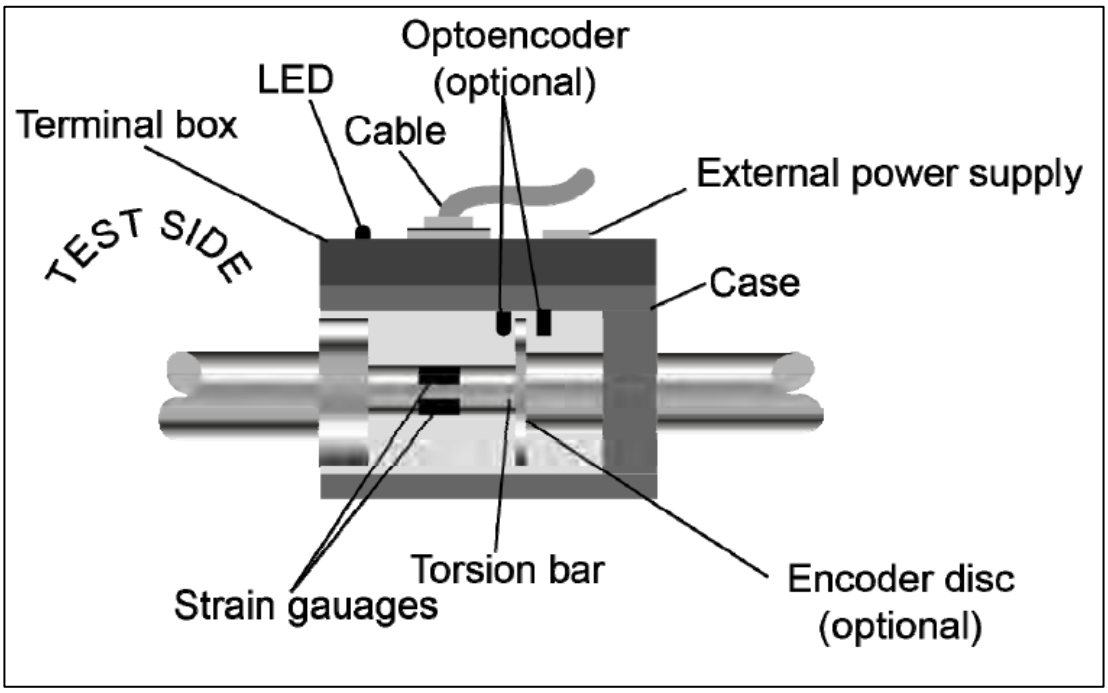


***Source:*** **Burster 8661 Data sheet[37]**

### 2.1.1.6 External DC motor

Power rating of the external driver is determined considering CFD results. Either a DC motor or a stepper motor could be employed. However, DC motors are cost effective. Therefore, approximate size of the DC motor is determined from the DC motors in market. A L shaped mount for the motor is designed to be assembled to the EDM base (Fig 2.15).

**Figure 2.15: DC motor with L-connetion**

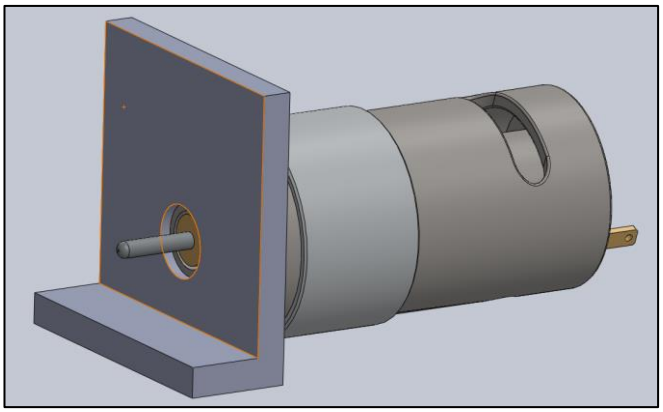

***Source:*** **Made by I.B. Aka**

Other than DC motors, high speed stepper motors are used in physical testing of heart pumps. Stepper motors are easier to control and precise in motion. However they are extremely expensive compared to standard DC motors. It is possible to control DC motor at desired speeds by reading encoder data and employing a proportional controller in our control card (dSPACE, Germany). This method is cost effective and as efficient as an expensive high speed stepper motor. This project includes a proportional controller for motor speed. However, PID controller can be implemented simply by software manipultion in dSPACE.

### 2.1.1.7 Assembly

Finally virtual design of the assembly was done mainly with respect to the shaft alignment. Height of the shafts of the dynamic load torque sensor is determined as the standard for assembly. Therefore, housing is designed with the same height to match shafts of the pump and the sensor placed on a flat surface. A metal mounting block is designed as the base of the complete setup. Screwholes on the base are desgined for mounting to the PIV setup. Flexible couplings are used to connect DC motor to sensor and sensor to pump (Fig 2.16 and 2.17).

**Figure 2.16: Side view diagram of the EDM**

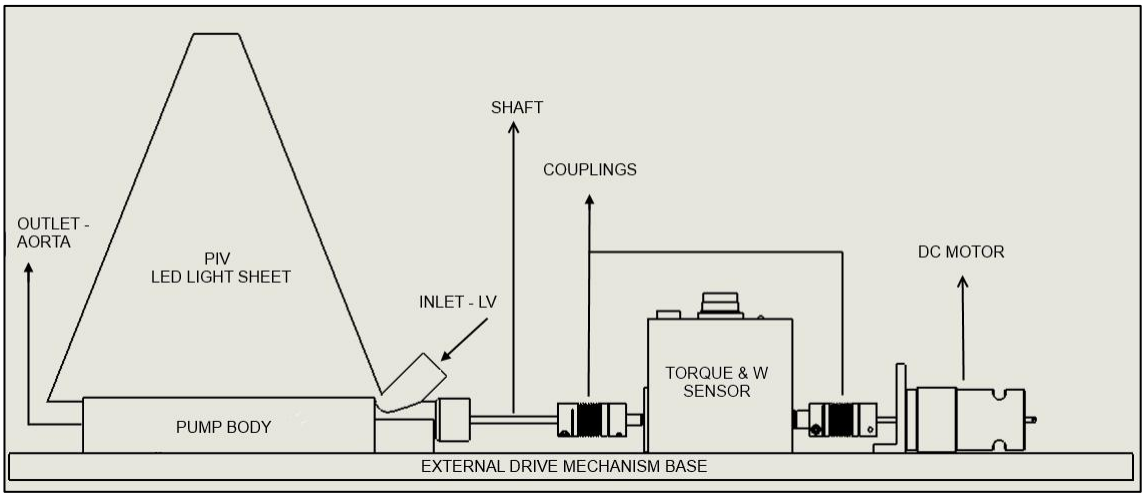


***Source:*** **Made by I.B. Aka**

**Figure 2.17: Final EDM render by SolidWorks**

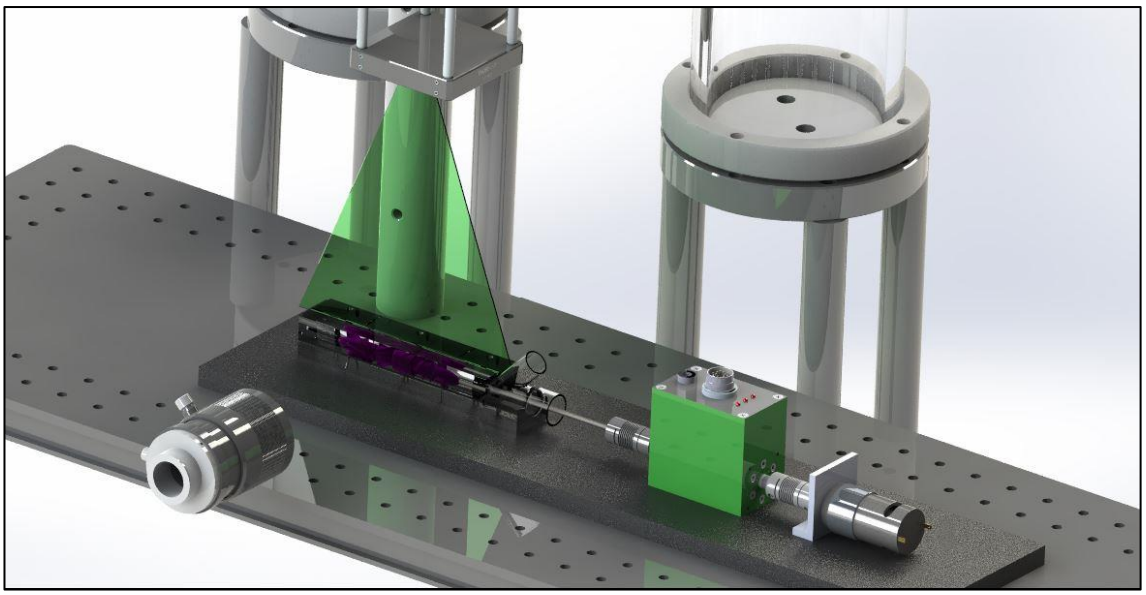

***Source:*** **Made by I.B. Aka**

### 2.1.1.8 Virtual Testing (CFD) of the Assembly Before Production

As stated previously, there are numerous components interfering with the blood pathway of the physical prototype which were not present in virtual prototype. Effects of these componenets were unknown before including them in virtual model and CFD testing. The external shaft is required for driving the motorless impeller. The shaft is placed inside the blood pathway through the complete length of the prototype.

Additionally, gaps between the impeller and stationary parts (inducer and diffuser) were not modeled in CFD optimizations before. Bearing system of the final prototype is not defined yet. However, physical test setup must have mechanical suspension of the external shaft for normal operation. All of these components must be included in the virtual model to observe possible effects on pump performance with respect to hemodynamics and hemocompatibility. Therefore, before producing the External Drive Mechanism, a virtual model of the exact design is tested by CFD.

**a. Virtual assembly**

3D virtual design of the EDM geometry was created to conduct CFD analysis before physical system is constructed. By CFD solver model, virtual geometry of device should be specified. ANSYS Fluent need the fluid volume domain (complement of the solid impeller geometry inside shroud) to function. These solution domains should be designed 3D by CAD softwares. CFD packages include CAD tool as many other commercial CAD packages. In this work, SolidWorks 2013 (Donated by Tekyaz, Istanbul) software was used to model EDM in terms of parameters that was specified according to FP1 and EDM designed mentioned before (Fig 2.18 and 2.19).

**Figure 2.18: 3D drawing of EDM fluid domain**

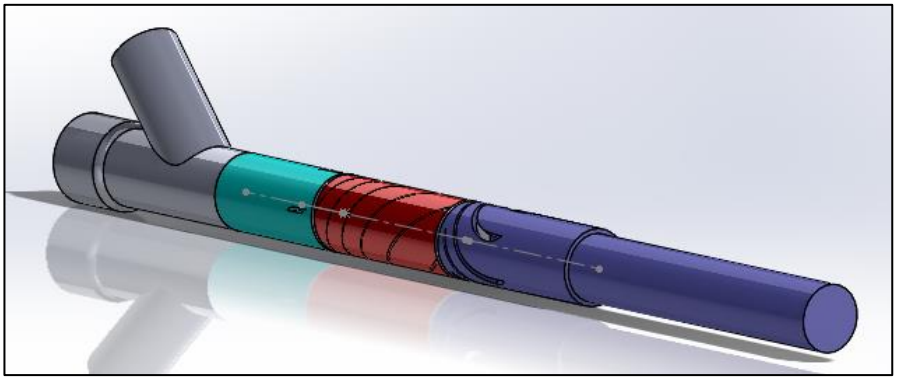

***Source:*** **Made by I.B. Aka**

Included parts are inducer, rotor and diffuser. Moreover, there are gaps and bearings embedded inside stationary parts to suspend the external part. The YT connection and the external drive shaft is also included. Some of these detailed parts are simplified for

ease of CFD calcualtions. So, all parts have independent design characteristics depending on their roles.

**Figure 2.19: Cross-section of the EDM fluid domain (bearings and gaps are shown)**

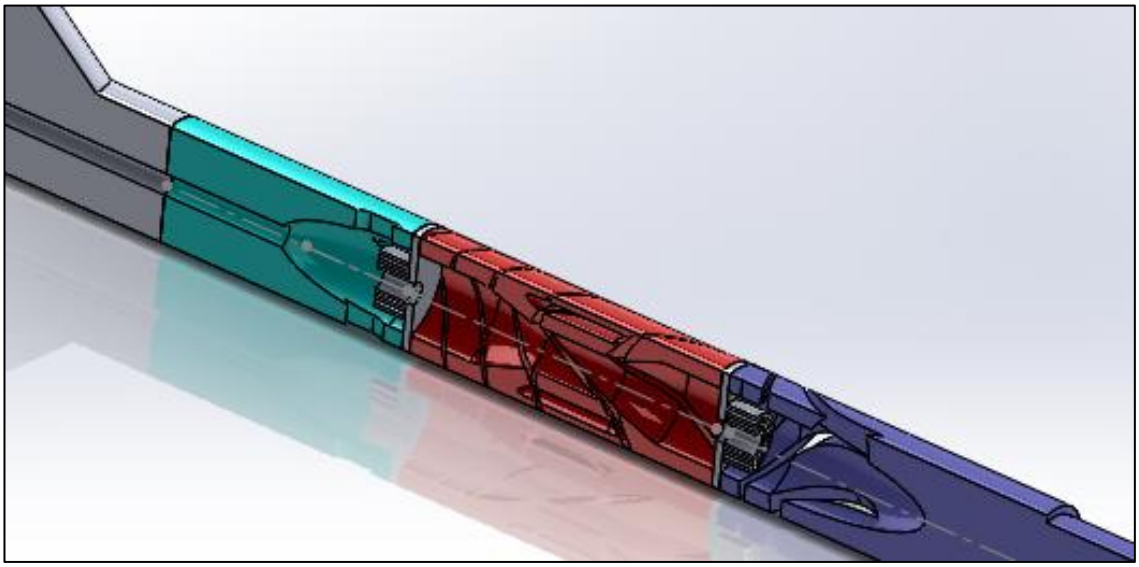

***Source:*** **Made by I.B. Aka**

**b. Computational Fluid Dynamics Study of the External Drive Mechanism**

2D turbomachinary calculations and simplified 3D virtual testing is not enough to evaluate complete performance of the EDM. Additional components of EDM (YT connection, drive shaft, bearings and gaps) affects flow field and therefore should be evaluated by detailed CFD analysis. Fluid dynamics is purely based on Continuity, Momentum , Energy and Reynolds Averaged Navier Stokes (RANS) equations[16, 38]. In general, CFD is a numerical approximation of flow simulation based on these equations. Moreover, CFD analysis is capable of employing dynamic results for further analysis of heat transfer. Virtual performance testing of complete 3D virtual geometry of EDM completed on ANSYS Fluent software is explained in this section. After completion of CFD analysis, boundary layer separation, turbulence results, vortices and dynamic and static pressure levels through complete pump geometry are numerically calculated and visually viewed.

CFD software primarily split fluid domain into small cells and solves equations related to the given model for every cell. Network of these small cells is called mesh or discrete

solution domain. Particularly fine cell sizes can be required for accuracy in certain solutions such as, turbulence models. Flow model should be evaluated by including other desired equations along with Continuity and Momentum equations. These extra flow modeling equations allows defining dynamics of fluid under distinctive conditions such as turbulence, heat transfer or acoustics. At that point, boundary conditions are given to software for identifying physical conditions in virtual environment like wall motion or heat exchange.

After obtaining solution of every cells in the fluid domain, CFD software considers previous results as the input for following iteration and solves the same equations with these new parameters for every cell repeatedly. These iterations last until the difference between results of two iterations become too small. This is called convergence of the solution. Consequently, flow dynamics of the pump is estimated for evaluation of he desired conditions.

**c. Turbulence Model**

Blood flow in the impeller part of a pump has high tangential velocity gradient caused by rotational motion. Reynolds Number (Re) defines flow characteristics as laminar or turbulent with respect to the velocity of the flow. High flow speeds with Re>2500 starts to show turbulent characteristics and above 10000, flow characteristic turn out to be completely turbulent. Fluid in high velocity gradient areas such as inducer and diffuser gaps (before and after the impeller) in the pump shows fully turbulent characteristics as it suddenly accelerates and decelerates. So, turbulence model must be applied along with the governing equations[26].

Turbulence models are vary consistent with application and in general heart pumps in literature are simulated by Standard k-ε or k-ω Turbulence Models because of the high velocity gradient[39]. k stands for kinetic energy , ε for dissipation rate and ω for frequency. Both models have their own advantages and limitations on accuracy of flow dynamics results. Standard k-ε turbulence model of ANSYS Fluent is extensively used to model flow turbulence in heart pumps. k and ε factors are adjustable, yet default values are preffered for our tests[16].

Flow turbulence varies at central and near wall regions of the domain. Employing the turbulence model simply estimates turbulence in general flow domain. However, to estimate realistic flow features near wall region, various turbulence types from wall to center are grouped into three layers depending to distance from boundary (wall surface) as shown in Fig 2.20.

The flow around viscous sublayer is practically laminar due to the no slip condition and the molecular viscosity plays a governing role in momentum. Second region namely buffer zone shows transition between laminar and turbulent flow characteristics. The most exterior layer is considered fully turbulent. These dimensions of these layers are defined by a distance factor $y^+$ (Fig 2.20) [16].

$$\frac{y}{y^+} = \frac{\mu}{\sqrt{\sigma_{ss}\rho}} \qquad \text{Eq 2.7}$$

y is the distance from surface to boundary , $\mu$ is the fluid viscosity, $\rho$ is the density and $\sigma$ is wall-shear stress.

**Figure 2.20: Mesh structure over boundary for turbulence model selection**

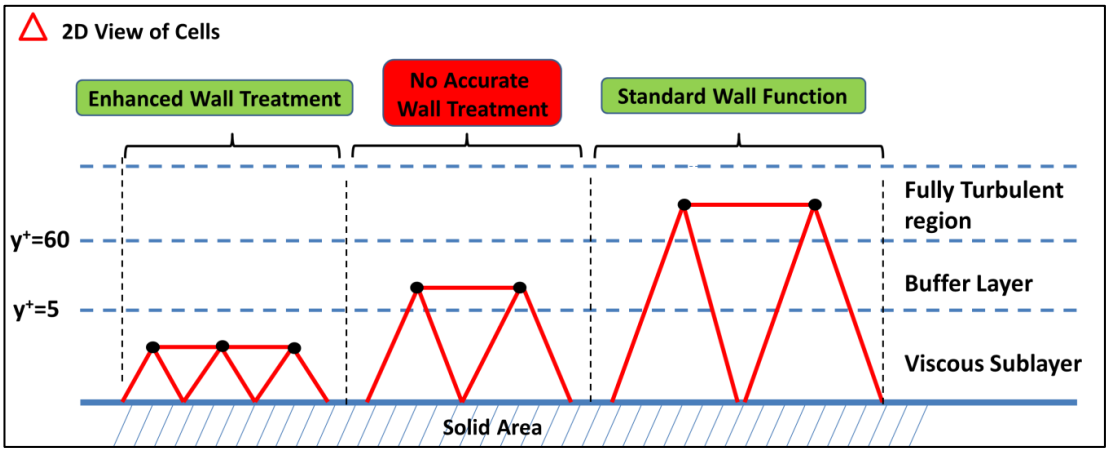


***Source:*** **Toptop's thesis [16]**

Flow characteristics can be modeled for viscous sublayer with Enhanced Wall Treatment and for fully turbulent layer with Standard Wall Function. However the flow inside the Buffer Zone can not be precisely modelled. Therefore, first node closest

to surface should be placed inside viscous sublayer or fully turbulent region. Wall treatment method must be choosen considering the first node.

FP1 has small clearances between blade tip and shroud (0.2mm) and the first node is placed in in "viscous sublayer" ($y^+$<5) by fine meshing and Enhanced Wall Treatment is used for this calculation[16].

**d. Finite Element Methods (Mesh)**

Discretization of fluid volume into smaller volumes is called meshing. Meshes can be triangular or rectangular in 2D and pyramid, tetrahedral or hexahedral elements. Than CFD solver runs governing and additional model equations on every cell to estimate flow characteristics[16, 27]. Meshing operation is vital for having realistic results by having fine network of cells and correct geometric shapes. However, excessive meshing causes prolonged solution without significant differnce in result. Thus, finer mesh structure must be created for critical areas showing diverse flow characteristics instead of the complete domain[26].

Critical areas where flow has high velocity and shear stress mostly occur at rotor and diffuser blades entrance where fluid instantly accelerates and decelerates[21]. Additionally, bearings are modelled with finer mesh structure as they have small gaps and high velocity. Non-smooth contact of arriving flow to blade creates backflow mostly occuring between part transitions[16]. Therefore, rotor-inducer and rotor-diffuser clearances are included and modelled with fine meshes (Fig 2.21).

**Figure 2.21: Cross-section of EDM mesh**

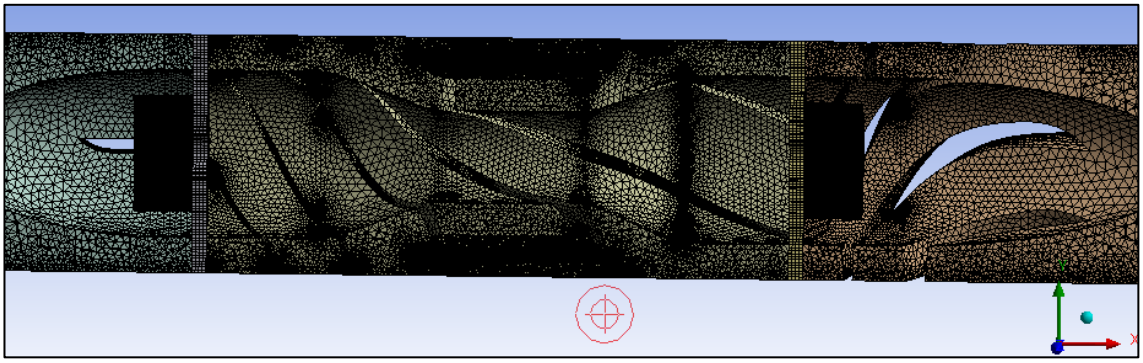

***Source:*** **Made by I.B. Aka**

Fine mesh sizes at boundary layer ensured the first node position inside viscous sublayer (Fig 2.22). Therefore, enhanced wall function was used to estimate flow dynamics at boundary layer. This choice can later be validated with $y^+$<5 contour at post processing by observing the distance of first cells from the blade boundary[16].

**Figure 2.22: Finer mesh structure around clearances**

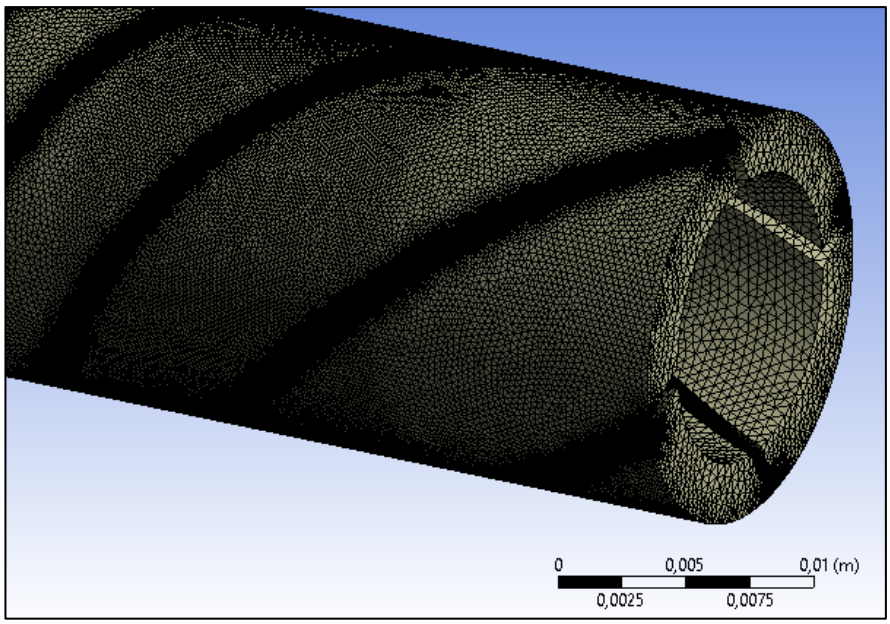


***Source:*** **Made by I.B. Aka**

**e. Physical Conditions of CFD**

Our fluid domain material blood is a non-Newtonian fluid. Density and viscosity values are taken 1050 kg/m$^3$ and 0.0035 Pa.s respectively from literature[16, 26]. Other physical condition of the simulation is the movement of particular walls (impeller, shaft and bearing walls). Particular conditions are set by defining separate groups (surfaces and volumes) in the domain. Unlike other stationary components, impeller, bearing and shaft components were defined with frame rotation at given shaft velocity.

In this project, inlet and outlet of EDM were defined as mass flow inlet and pressure outlet. Simulations were performed at given mass flow rate and pump hemody namic performance as numerically evaluated as mass-flow averaged static pressure at pump inlet. Backflow between parts typically arises as a result of incidence angle between

attacking flow and blade attack angle. However, these angles have been optimized until FP1 is desgined by Toptop et al. [21] and further optimization would be considered after PIV testing ongoing on EMD.

### f. Analysis Procedure & Results

As stated before, FLUENT runs governing equations along with turbulence model formula over each cell for each iteration. After every iteration, deviation between results of two consecutive iterations gets closer to zero. When results of any parameter between two consecutive iterations are negligibly small ($\Delta<10^{-4}$), solution converges. Thus, it is not a proof of accuracy of the model. Mesh sizing and turbulence model are two important factor for realistic estimations as mention previously. Moreover, higher orders of the differential momentum and turbulence equations provides further accuracy of results by cost of computational time[16, 26].

Simulation can be initialized with approximate velocity values to acquire quicker convergence of simulation. CFD tests of EDM are run with FP1 results which are approximately same. For EDM testing, fluid domain was divided into 10-15.000.000 meshes and run in DELL Workstation which has 32 GB RAM and 12 processors with 2.66 GHz. Solution was converged within 2.250-2.700 iterations during 12-18 computation hours. Finer meshing of bearings, gaps and blade tips ensures accuracy at a cost of extra solution time.

**Figure 2.23: Streamlines of velocity inside EDM**

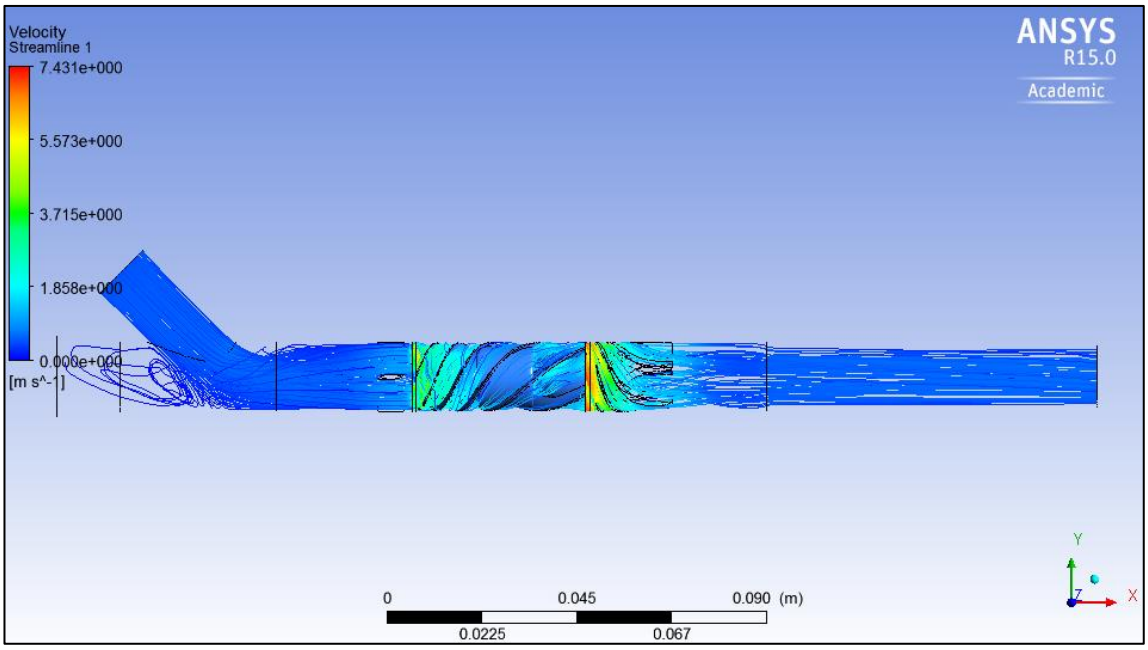


***Source:*** **Made by I.B. Aka**

As the result of the CFD testing of EDM, added components such as external drive shaft, YT connection, gaps and bearings showed insignificant difference from FP1 results (Fig 2.23). Therefore, we have decided to manufacture EDM as it is. Other previous virtual models are tested before they are optimized to EDM but not included in this thesis. The table below shows the comparison of EDM and FP1 at 927 rad/s. Circular shape of the outlet cannula was forming an obstruction to flow, however no secondary flow formations are observed in streamlines.

**Table 1: EDM vs FP1 CFD results**

| Model | Flow Rate(L/min) | Pressure Head (mmHg) | Torque(mNm) | Efficiency |
|---|---|---|---|---|
| **FP1** | **5** | **104.4** | **4.2** | **29.67%** |
| **EDM** | **5** | **93.05** | **3.97** | **28.03%** |

### 2.1.2 Manifacturing the External Drive Mechanism

Design of the EDM is evaluated with CFD tests. No secondary flow regions, stasis for vorticies are observed from the streamlines generated at post processing of the cfd results. EDM structure is physically manufactured with approximately same geometry. In this section of the thesis, manufacturing, assembly and operation procedures of EDM are explained in detail.

#### 2.1.2.1 Pump components (Inducer, Diffuser, Rotor)

As stated before, complex geometry of the impeller component enforces the use of 3D printing method which is also called additive layer manufacturing[40]. Central flow channel and magnet cylinder creates inner gaps which can not be machined from single block by CNC. Thus, Laser Sintering of Ti6Al4V is used for production of inducer, rotor and diffuser. Commercial version of the pump will most probably be made of titanium as well. So using this material allowed us to observe realistic physical features through the testing of the prototype. Moreover, surface finish of the laser sintered parts is better than 3D printed plastic parts which shows rectangular corners around the circular hub.

Principle of laser sintering is based on addition of micron-thick layers of material over a surface and fixing every layer to the previous layer by employing the heat of the laser. This method allows manufacturing of almost any complex geometry, layer by layer. To produce physical prototype of FP1, an EOS M280 (EOS GmbH, Munich, Germny) is employed in CAD/CAM Center of Süleyman Demirel University, Isparta. With a construction volume of 250 x 250 x 325 mm, the EOS M 280 consents fast and flexible manufacturing of multifaceted metal parts straight from CAD data (Fig 2.24).

**Figure 2.24: Construction volume after production**

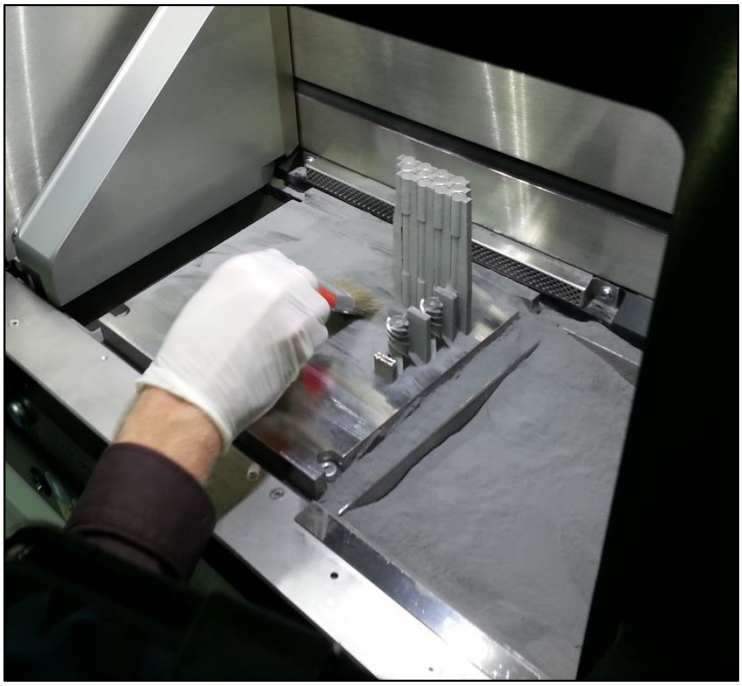

***Source:*** **Made by I.B. Aka**

EOS Titanium Ti64, a Ti6Al4V alloy, which was used for inducer, impeller and diffuser parts. This alloy is regarded as having outstanding mechanical properties and corrosion resistance combined with low specific weight and biocompatibility. Typical achievable part accuracy is given ± 50 µm for this material by producer. Minimum wall thickness is given approximtely 0.3 – 0.4 mm where our thinnest impeller blades are 0.6mm thick. Surface roughness average, as built, is stated as 9 to12 µm.

Accuracy of the parts is important to repeat CFD tests physically. Moreover, having right engineering tolerances for tight fitting of shaft and bearings in to pump parts is important for assembly. To assure high accuracy, several trial parts are produced with various hole sizes, until acceptable tolerances are found (Fig 2.25). H6 tolerance is applied for thight fitting of bearings. Even though the blade thickness of the impeller (0.6 mm) is in range of EOS M 280, faulty blades were manufactured with faults several times due machine-related reasons. Finally, correct geometry with acceptable tolerances is manufactured. However, part dimensions are slightly different than desired parts.

**Table 2: Desired and Actual part diameters after manufacturing**

| Part | Inducer | Rotor | Diffuser |
|---|---|---|---|
| Desired | 16,40mm | 16mm | 16,40mm |
| Actual | 16,359mm | 15,892mm | 16,350mm |

**Figure 2.25: Trial particels for determining fitting tolerances**

***Source:*** **Made by I.B. Aka**

EOS M280 places a 30µm layer of Ti6l4V dust and melts the layer down within the verticle crossection of the given CAD drawing. Support structures are build considering geometric shape to avoid bending of unsupported crossections like magnetic cylinder. However, cleaning these supports cause extra roughness around the joint (Fig 2.26).

**Figure 2.26: Support structure of the impeller**

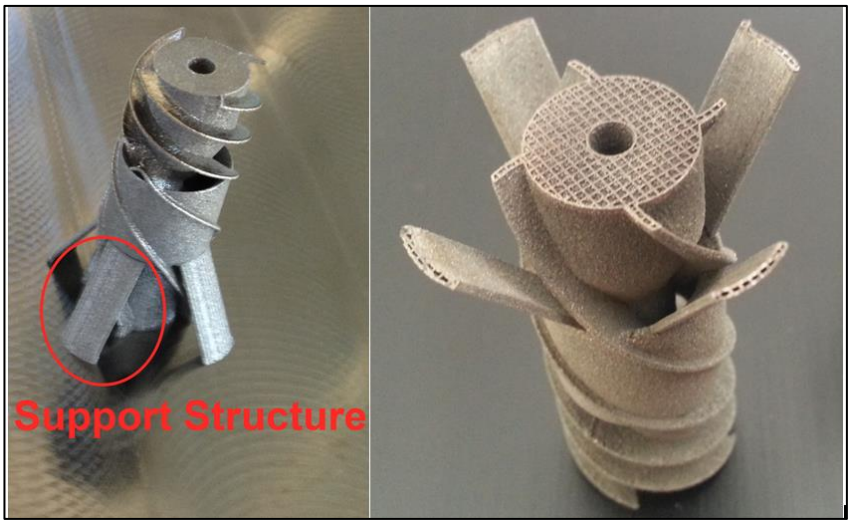


***Source:*** **Made by I.B. Aka**

Even though, initial testing of the pump will be completed with PIV tests by using water as the fluid, in-vitro blood tests must be conducted over EDM as well. Surface roughness of laser sintering is not acceptable for blood. Moreover, titanium surfaces are shiny which is undesired for PIV due to poor signal to noise ratio of images. Therefore, sand blasting is applied to the pieces by hand after production (Fig 2.27).

**Figure 2. 27: Final parts Inducer, Diffuser, Rotor**

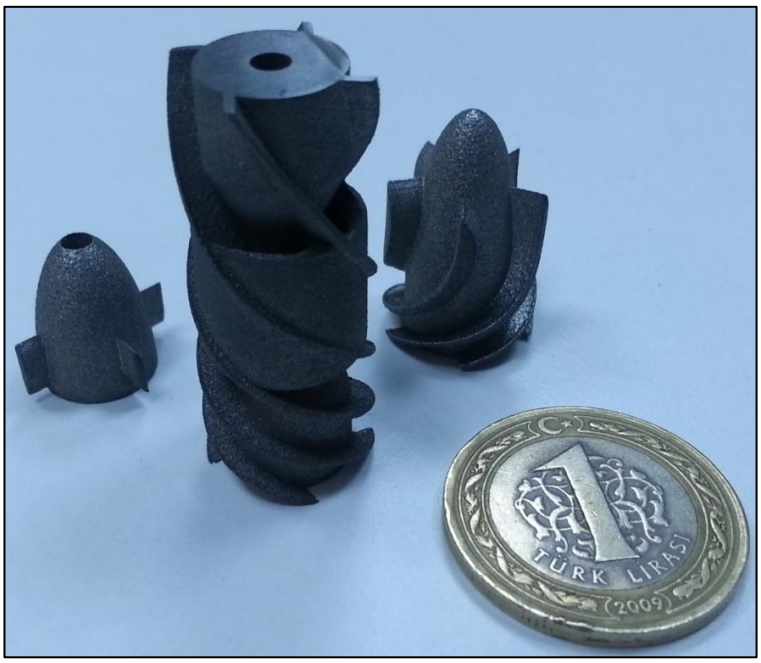


***Source:*** **Made by I.B. Aka**

Illumination system of our PIV setup is a LED based light source at 532nm, which corresponds to the green region of the visible spectrum. To reduce reflection and to improve signal to noise ratio, sand blasted final parts are dyed with magenta color which is the complementary color of green. Thigh fitting of the shaft into the rotor (impeller) is achieved by 5mm incremental pushes by hand while it is mounted on a turning machine. Smooth fitting of the shaft into the bearings embedded inside inducer and diffuser was done by hand and the gap between parts are set with a high presicion compass with respect to the FP1 Dimensions (Fig 2.28).

**Figure 2.28: painted EDM parts are assembled with presicion compass**


***Source:*** **Made by I.B. Aka**

### 2.1.2.2 Bearings

Considering bearing needs defined in previous section of the thesis, a material and market research is conducted. Outer diameter of the bearings must be smaller than the hub size of the pump and inner diameter must fit to the previously calculated shaft size (Fig 2.29).

An acceptable bearing size with Zirconia Oxide (ZrO2) material is found from VXB Bearings, CA, USA with dimensions of 3x8x3 mm as inner diameter, outer diameter and thickness, respectively. Unfortunately, ABEC 3 bearings were not present in their

stocks. Thus, ABEC 1 bearings were to be used until blood tests. These bearings are capable of running over 25 krpms up to 180C°.

**Figure 2. 29: Bearings are thight fitted into inducer and diffuser**

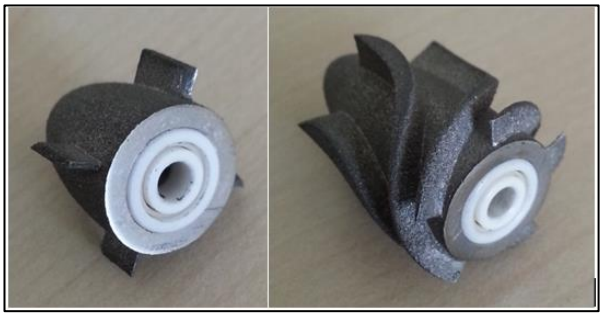

***Source:*** **Made by I.B. Aka**

### 2.1.2.3 Shaft

Miniature drive shafts are not available on Turkish market. However, 316L stainless steel 3mm rods are available for different purposes. Initally, 316L shafts were used for EDM. However, their elastic modulus was not good enough for operating conditions of EDM. Later, 3mm Tungsten-Carbide HB44UF rods were found from Böhler Maden, Kocaeli normally used for manufacturing milling tools.

Shaft diameter equations are completed according to Ti6Al4V material with elastic modulus of 113.8 GPa but Tungsten-Carbide material has even higher elastic modulus of approximately 550 GPa. It can only be machined with materials of superior hardness such as cubic boron nitride and diamond. Therefore previous shaft diameter equations become even more conservative due to higher elastic modulus. 330mm long 3mm diameter rod is cut as 175mm according to the theoretical shaft design. It is tight fit into to impeller with 0.01mm tolerance.

### 2.1.2.4 Housing (Shroud)

Housing or shroud is the most important component of EDM to allow PIV measurement. Various models and manufacturing methods are given in the literature section of this thesis. Unlike others, housing of the pump was manufactured by resin casting rather than monoblock acrylic machining by the cost of presicion (Fig 2.30).

Monoblock acrylic machining is precise in dimensions due to CNC machining but procedure reduces transparency of the acrylic. Therefore, hand polishing is applied over the outer surface and inside the inner circle (blood pathway) which is not a repeatable process. For every production, different amount of material will be removed and transparency is not homogenic through the piece.

Tranparent mold casting is a method where a prepared mixture of chemicals are poured into a mold under vacuum. Depending on the product, transparency of the cast resin parts are more transparent than machined parts.

**Figure 2. 30: Final version of the shroud**

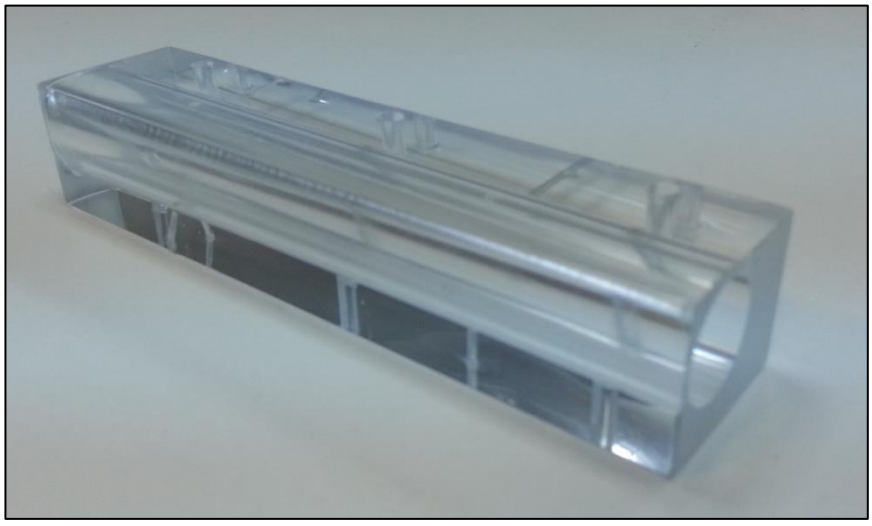

***Source:*** **Made by I.B. Aka**

**Figure 2. 31: Manudacturing process of casted transparent shroud**

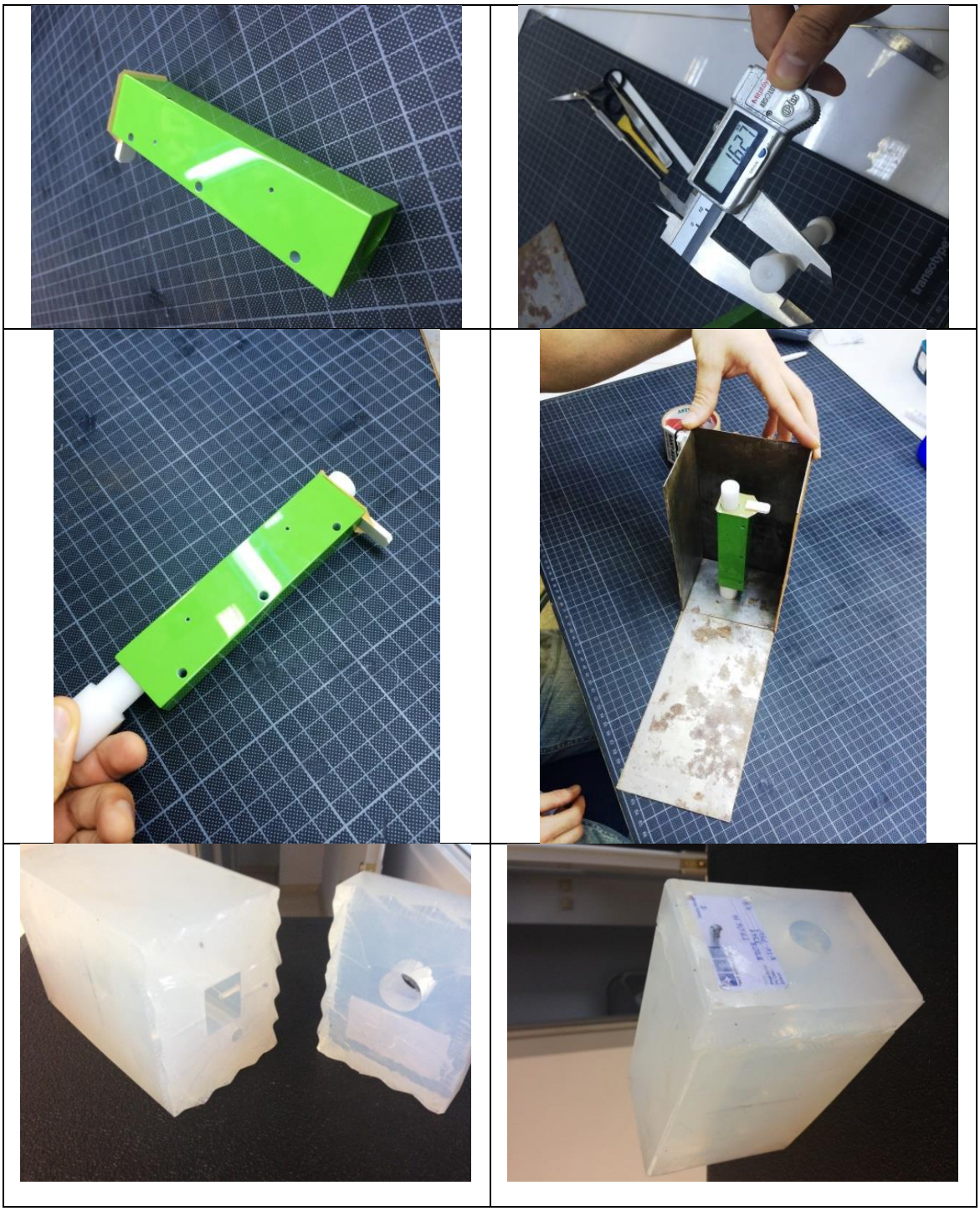

***Source:*** **Made by I.B. Aka**

The silicone mold of the pump housing was taken from two pieces of masters as a PTFE cylinder and a rectanglular ABS plastic profile. Pump housing (shroud) is designed rectangular for providing equal refraction of sliding LED light along the region of interest (Fig 2.31).

Initially, master models of the outer shell is produced by POLYJET technology by OBJET Connex 500(Stratasys, USA) with 16 micron tolerance using opaque photopolymer resin (Verowhite, USA). Surface of the mold is covered with micron thick dye to enhance surface quality and maximize the transparency of the part(shroud). Master model of the circular blood pathway is manufactured by a CNC turning machine with tolerance of +/- 0,05 mm from PTFE. Surface finish of this master is enhanced by polishing (Fig 2.31).

Two of these master models (PTFE cylinder and 3D printed rentanguler piece) are combined concentric inside each other in a rectangular frame to allow casting the silicone mold material VTV750 (Renishaw, England) which later become the mold of the transparent model. Silicone mold is cured for 24 hours. Finally, transparent polyurethane resin material Alchemix VC 3341 (Alchemie, England) is casted into the silicone mold under vacuum by gravitational force. Transparent resin model is cured in 15 minutes (Fig 2.31).

Undesired remaining chips are cleared and polished. Contrary to machining of a mono-block acrylic, cast resin is more transparent and accurate in dimensions due to avoiding any hand polish on the final part.

### 2.1.2.5 Assembly

Assembly of these parts is vital for efficient and safe testing. Impeller of EMD rotates up to 10 krpms. Therefore, precise alignment of the shaft is important to avoid excessive vibration which can damage torque sensor. Moreover, misalignment of the shaft reduces lifetime of components by increasing wear and fatique.(shigley's)

Micrometers are used for aligning small diameter shafts in literature (untario). Laser alignment is another method which is not commercially provided for miniature shafts in Turkey. Unfortunately, alignment of EDM shaft only lies on presicion manufacturing of the components. Therefore, base mount of the assembly is manufactured by CNC machine with sub micrometer presicion. 500x120x18 mm aluminum plate is machined for ensuring surface is flat and holes are given from CAD drawing for ensure presicion assembly of parts (Fig 2.32).

**Figure 2.32: Drilling of the base on 3 axis CNC machine.**

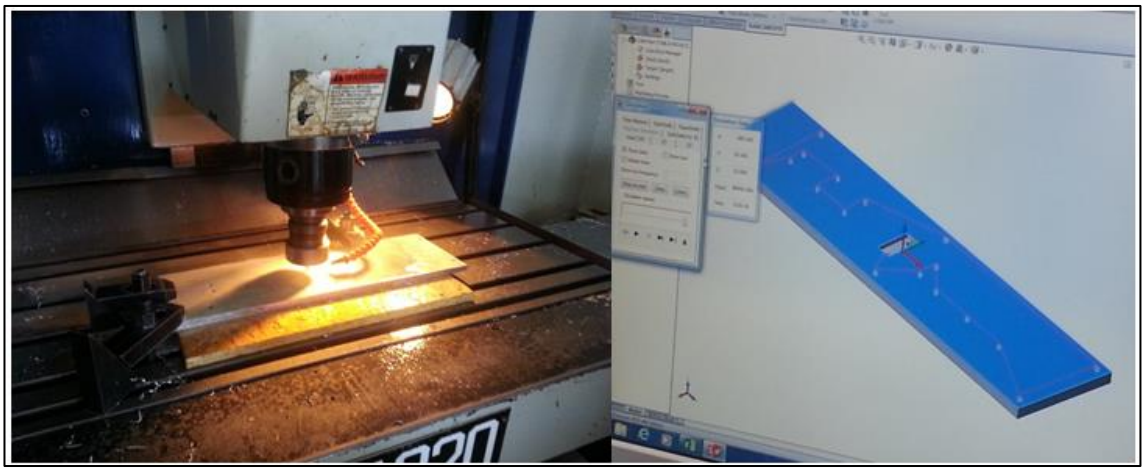

***Source:*** **Made by I.B. Aka**

SICK PBT-RB1 pressure transducers are embedded in the bottom of our inlet and outlet reservoirs (low pressure-high pressure reservoirs) and Transonic flowmeter is clamped on the outlet cannula of EDM. Power supply of pressure transducers are provided from a power supply where transonic has its own internal power source (Fig 2.33).

**Figure 2.33: SICK pressure transducer and Transonic flow meter**

***Source:*** **Made by I.B. Aka**

Pump parts are thight fit into the shroud and stationary parts (inducer and diffuser) are stabilized by miniature setscrews (2mm). Shroud is mounted to the base by two metric 4 screws. Torque sensor (Burster 8661) is mounted to the base by its factory made metric 3 screw from the bottom. An L-shaped mount is machined for fixing DC motor on correct position. Two flexible Toolflex 9 couplings (KTR Couplings, Germany) are employed to transfer rotation from DC motor to trque sensor and torque sensor to impeller (Fig 2.34).

**Figure 2.34: Virtual diagram of EDM (Top) and physical prototype (Bottom)**

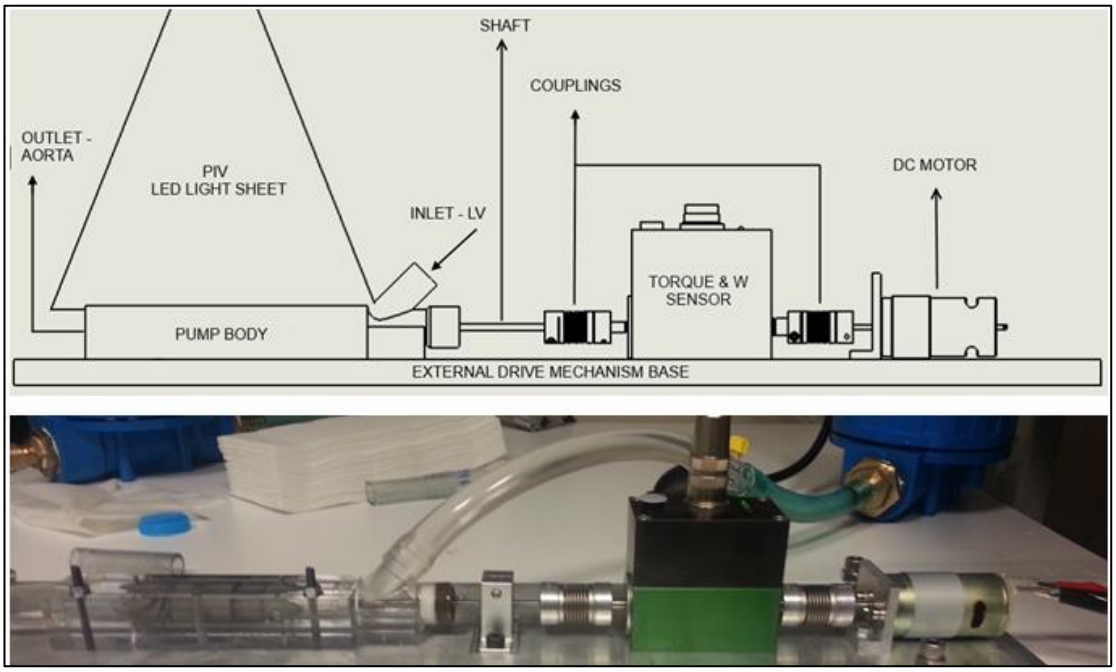


***Source:*** **Made by I.B. Aka**

### 2.1.2.6 Initial Tests and Computer Interface

After assembling EDM components, dSPACE RTI1103 (dSPACE GmbH, Munchen,Germany) board is used for data acquisition (DAQ). Moreover, dSPACE board is used as the controller of DC motor as well. Simulink (Matlab,USA) software with embedded dSPACE package is used for DAQ and signal processing (Fig 2.35).

**Figure 2.35: Simulink diagram of EDM measurement and control interface**

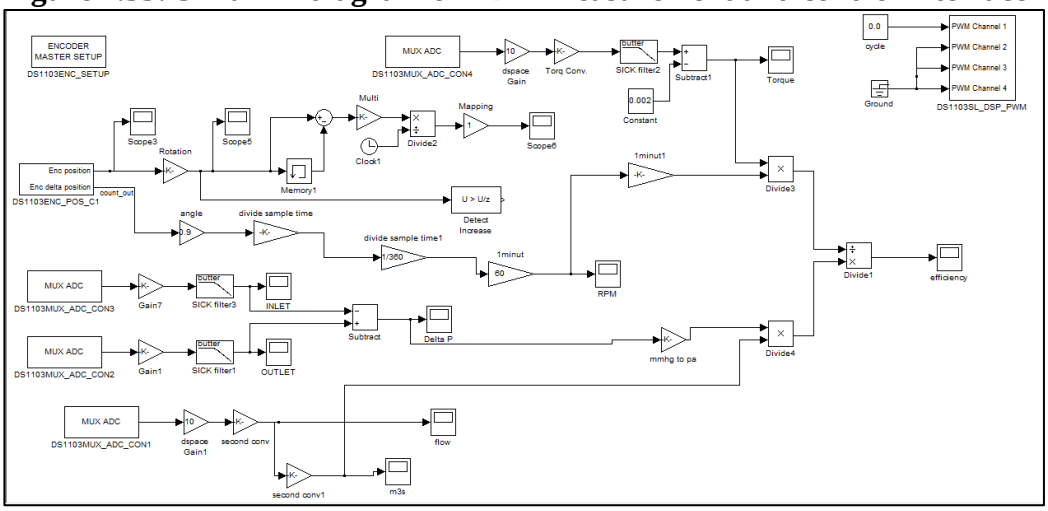


***Source:*** **Made by I.B. Aka**

Second order butterworth filters of Simulink are used for noise cancelling. Dynamic calculation of hydromechanic efficiency is done on simulink. Voltage to unit measurements of each sensor is completed with respect to the calibration sheets given from the manufacturer. Real time recording and observation of each signal is achieved by a dSPACE ControlDesk 3.7.3 user interface. Fig 2.36 shows EMD functions at 8400 rpms, 106mmHg pressure and 5lt/min flow rate

**Figure 2.36: Dspace interface while EDM functions at steady state**

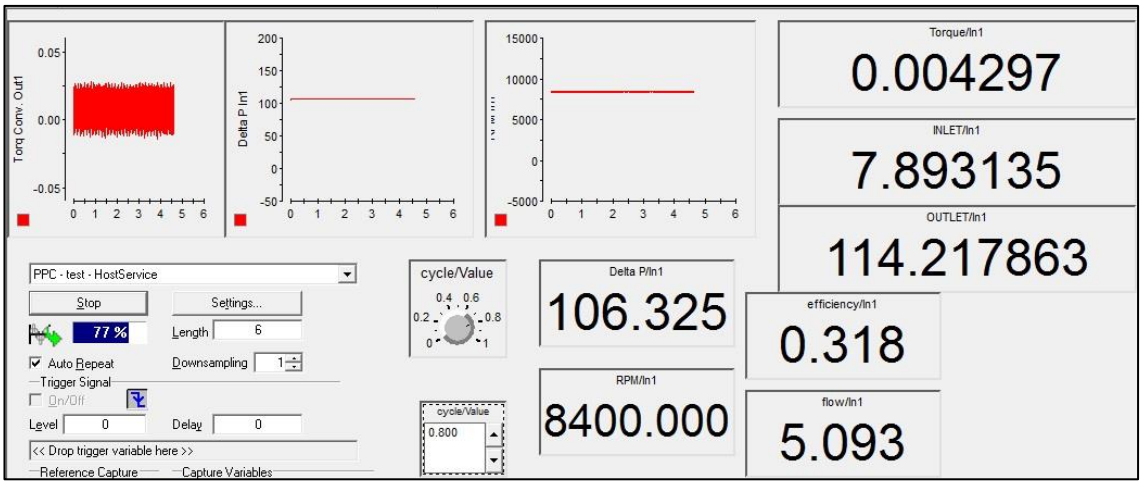


***Source:*** **Made by I.B. Aka**

DC motor is driven over dSPACE as well. A Pulse-width modulation (PWM) signal is generated. Duty cycle of the signal is proportional to the voltage supply to the drain which is proportional to angular velocity of DC motors. Therefore, PWM signal acts like a proportional controller where fixed voltage of the source causes 10 krpms when PWM sends 100% duty cycle (0.8 gives approximately 8 krpms). PWM signal is used to trigger DC motor over a MOSFET integrated power transistor IRFZ48N with 250hz frquency. IRFZ48N (IR World, USA) channels source voltage to drain (DC motor) with respect to the duration determined by duty cycle. A diode (1N4003) is used between positive and negative inputs of DC motor to eliminate back electromotive force (Fig 2.37). H-bridge formation of diodes were not necessary since the motor is driven unidirectionally.

**Figure 2.37: IRFZ48N casing, block diagram and electrial specs**

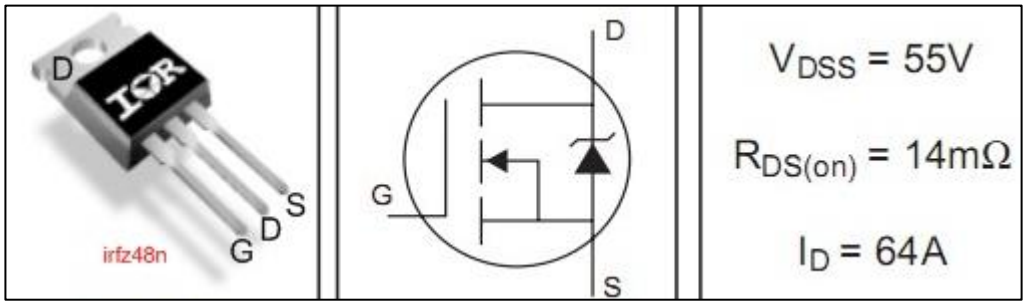


***Source:*** **IR World Datasheet[41]**

Motor speed is read from internal encoder of Brüster 8661 torque sensor. Encoder has 400 increments(0.9 degrees/increment). Motor speed is used to generate a TTL signal over PWM channels of dSPACE for synchronization of PIV system with EDM. Synchronization of these two systems are crucial to conduct PIV experiments over the moving region of the pump (impeller). Rotating impeller creates different angles and shapes during PIV readings without synchronization. Therefore, a TTL signal with certain frequency given from impeller speed ensures that each of the image pairs are taken at the same position of the impeller. Complete setup is shown in Figure 2.38.

Initial PID test are ongoing with tuning of parameters Kp, Ki, Kd for optimizing rise time, settling time and stability which are presented in results section of the thesis.

**Figure 2.38: EDM Test setup with high and low pressure reservoirs**

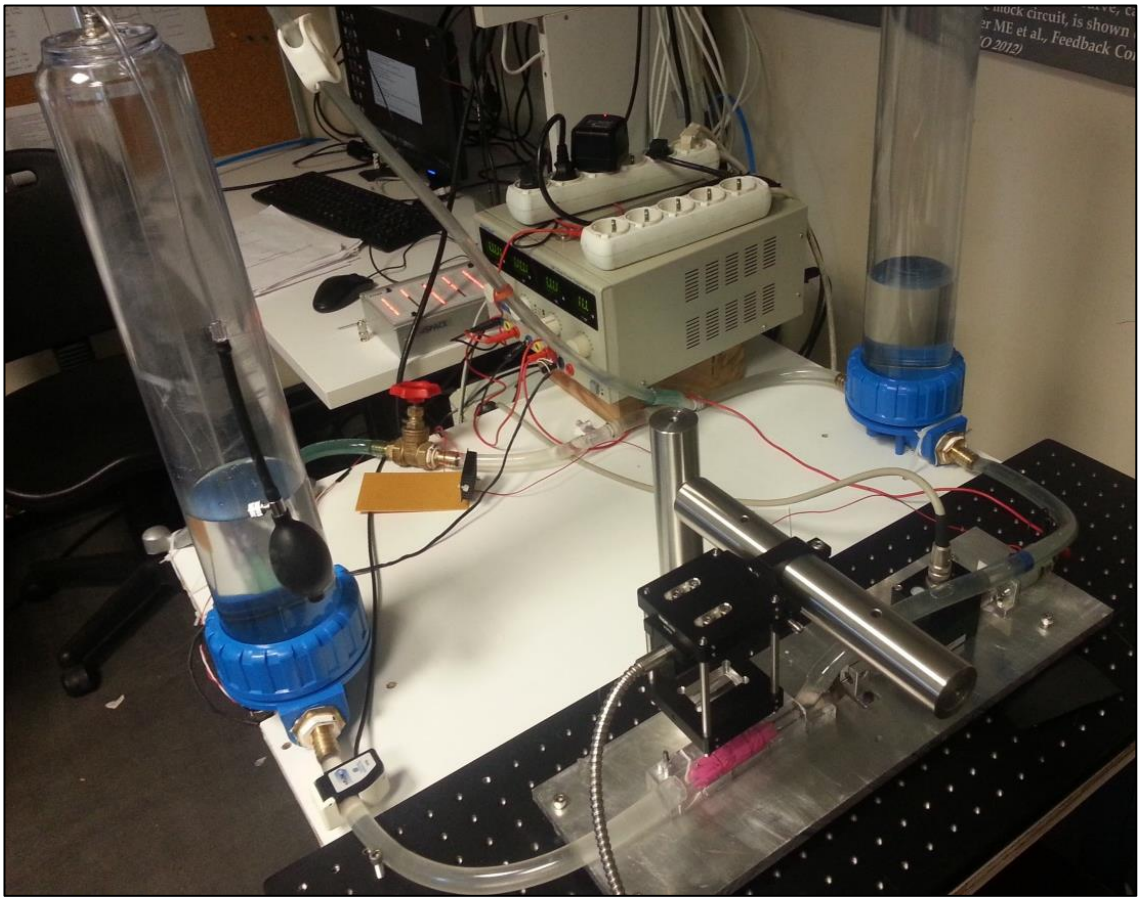

***Source:*** **Made by I.B. Aka**

## 2.2 BEARING WASHING CHANNELS CFD

### 2.2.1 Washing Channel Concept (for 2nd Generation Axial-Flow Pumps)

As stated before, most hemolysis and thrombosis occur around bearing regions of the 2nd generation pumps. Continuous washing of all surfaces contacting blood is key for eliminating thrombosis formation. Therefore, a new concept of bearing washing 2nd generation axial flow LVADs are offered. State of the art technology is magnetic suspension of the impeller (rotor) region of the pump. However, physical setup must be transparent and therefore motorless for PIV tests. An external motor and shaft are employed for positioning and driving the impeller. Morevoer, this shaft is used for direct measruement of hydraulic torque load acting on the impeller. FP1 functions between 8 to 10 krpms. This high rotation creates significant shear force on red blood cells (RBCs) and cause hemolysis. Moreover, complex structures of bearings cause most stasis. Stasis or stagnation causes thrombosis (coagulation) which can not be tolerated.

Accordingly, a new concept of bearing washing for 2nd generation axial pumps is suggested and investigated by CFD. Bearing washing channels are opened through the inducer and diffuser parts of the pump to allow continuous blood flow as the pump functions. Length of the parts were kept same while the diameter of the channels are changed and optimized regarding initial CFD data. Bearing washing channels must provide continuous flow of blood over bearings without losing significant amount of hydraulic energy of the standard model.

Innitially, 2mm diameter channels are used but this big of a diameter caused reduction of the flow rate up to 10%. Therefore, 1mm channels are tested and only this work is presented in this thesis.

### 2.2.2 3D Virtual Design of Bearings and Washing Channels

This part of thesis consists of 3D virtual design of bearings and a novel concept of washing channels over the standard geometry of FP1 to conduct CFD analysis as fluid volume (complement of solids between parts and shroud) as a feature of ANSYS Fluent which is mentioned in the CFD testing of EDM in this thesis before (Fig 2.39).

**Figure 2.39: 3D virtual cross-section view of FP1 with washing channels**

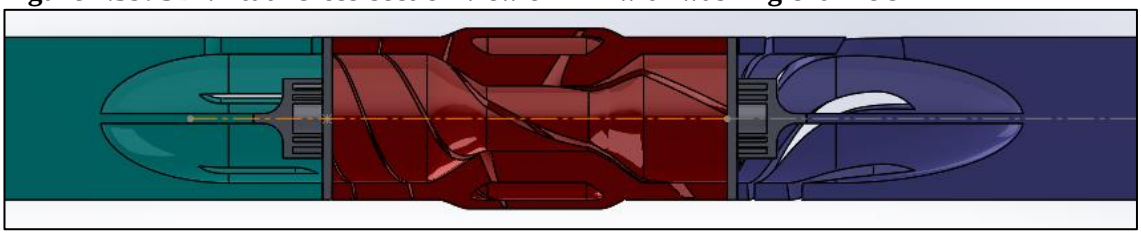

***Source:*** **Made by I.B. Aka**

Axial flow heart pumps include three blade stages called inducer, rotor and diffuser. As mentioned previously, inducer eliminates tangential components of fluid flow at rotor inlet, impeller exerts kinetic energy to fluid and diffuser converts this kinetic energy to potential energy or in other words velocity to pressure.

Bearings are not usually studied in CFD testing of 2$^{nd}$ generation axial flow LVADs in literature. However, they have great effect on hemocompatibility. Therefore, an approximate geometry of bearings are studied (Fig 2.40). Exact dimensions of bearings can not be evaluated by CFD software due to geometric constrains. Small clearances are difficult for creating enough amount of meshes and hyperbolic geometries (circular shapes contacting planar shapes like radial clearance of bearings) cause numerical errors in CFD solvers.

**Figure 2.40: 3D Virtual bearing model**

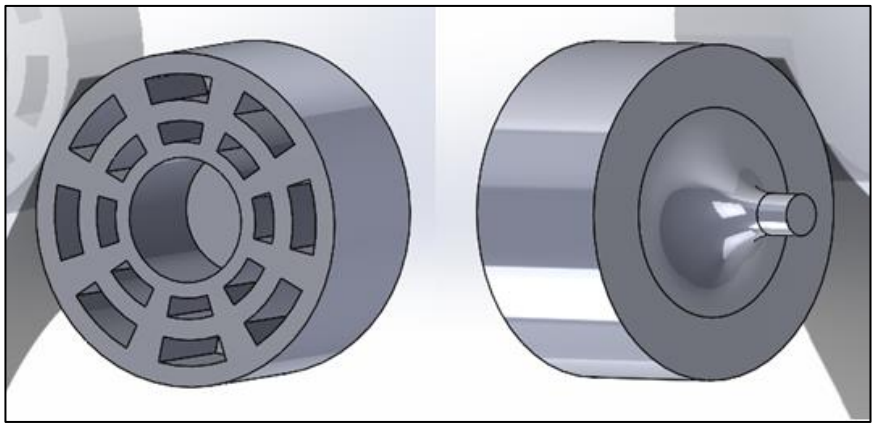

***Source:*** **Made by I.B. Aka**

### 2.2.3 Meshing and Solution Models

Meshing structure and turbulence model were applied for CFD tesing is explained in detail before in ‘2.1.1.8 Virtual testing of EDM’ section of this thesis. Finer mesh structure is provided for washing channels and bearings as these regions are region of interest of this study and CFD performance of standard FP1is already investigated for comparison of the results of the model including these channels and bearings (Fig 2.41). Further investigation of these channels will be investigated physically on EDM as the next stage of this project.

**Figure 2. 41: Close view of mesh structer in washing channels and bearings**

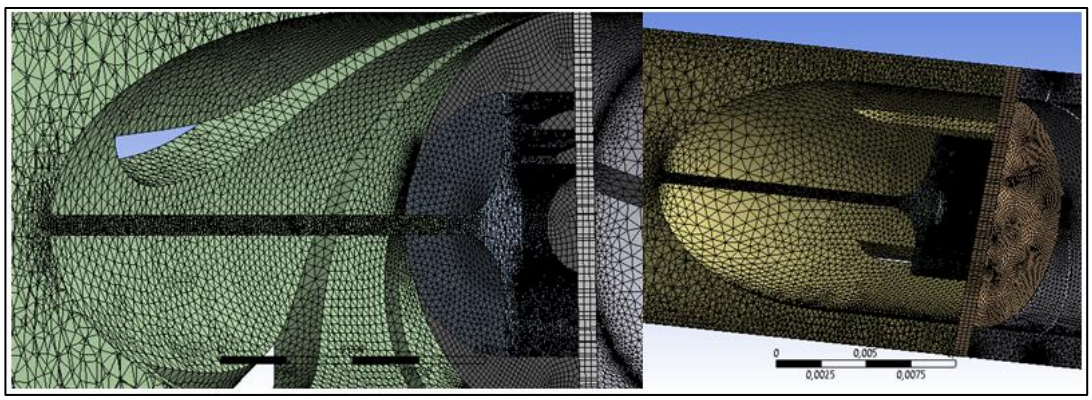


***Source:*** **Made by I.B. Aka**

# 3. RESULTS

## 3.1 EDM RESULTS

Design and Manufacturing of the physical test setup compatible with PIV and CVMC of prototype FP1 is accomplished (Fig 3.1). EDM is tested under various physical conditions and initial PIV testing is completed. Tansparency of the shroud is applicable for PIV tests. EDM functions without leakage. Vibration is minimum at high speeds by inspection (up to 10krpms). Real time control and data acquisition is achieved. Initial measurements are close to CFD estimations. Initial tests are conducted with proportional control of EDM with ± 10rpms accuracy (Fig 3.2). However, PID controller is implemented and tuning process is ongoing.

**Figure 3.1: Close view of EDM shroud while PIV test is ongoing**

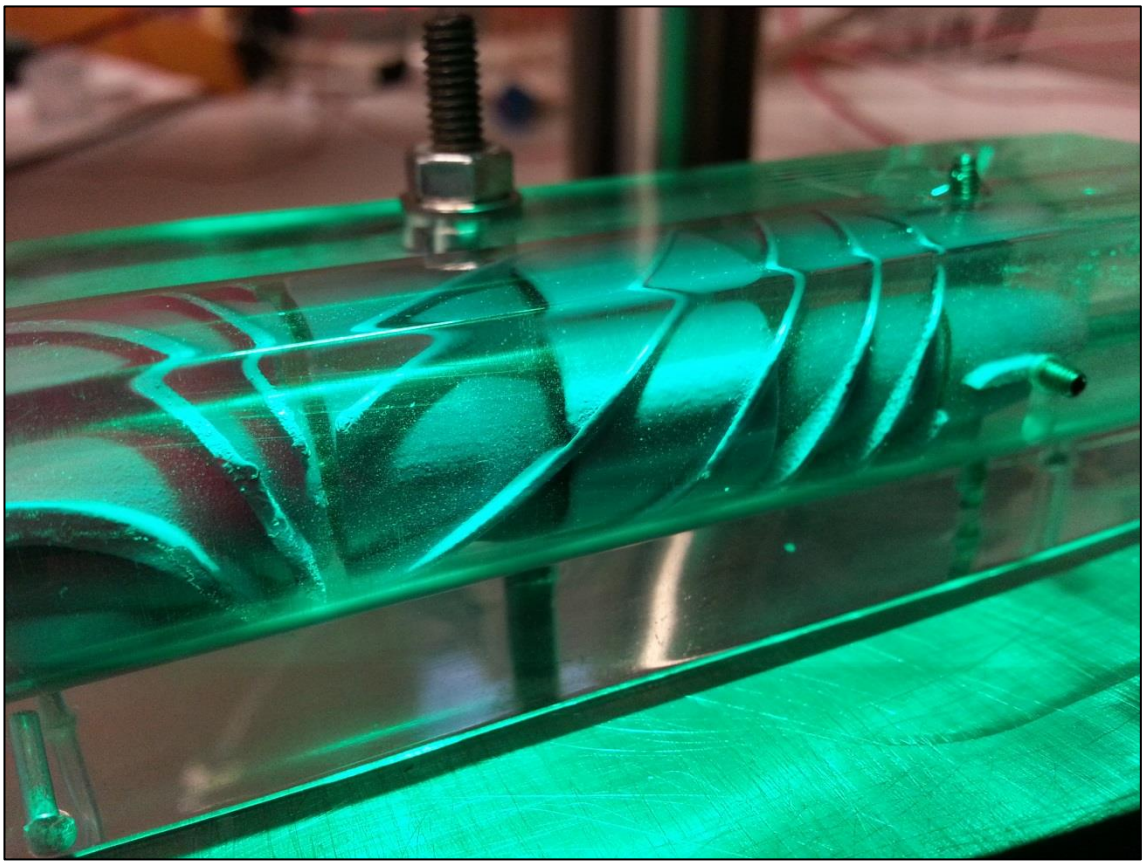

***Source:*** **Made by I.B. Aka**

**Figure 3.2: Unit step response of EDM (Torque, Head pressure, speed curves)**

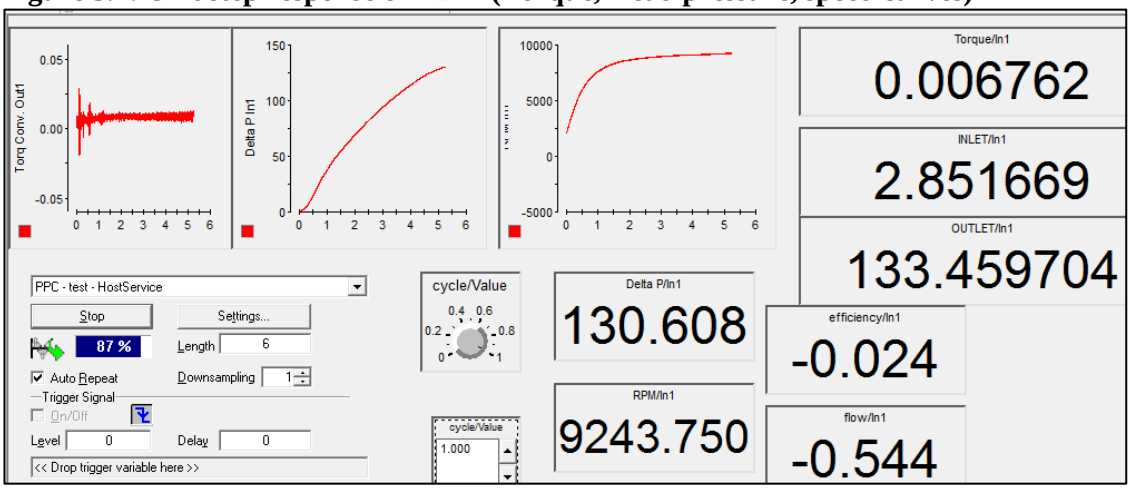


***Source:*** **Made by I.B. Aka**

### 3.1.1 Hemodynamic Results

EDM is tested under various conditions considering physiological limits. Initial hydrodynamic results are presented below;

**Table 3: Head pressures at different speeds and flow rates**

| Flow Rate (lt/min) | Pressure @ 8600rpms (mmHg) | Pressure @ 8800rpms (mmHg) | Pressure @ 9000rpms (mmHg) |
|---|---|---|---|
| 3 | 138 | 142 | 150 |
| 4 | 124 | 132 | 141 |
| 5 | 114 | 121 | 128 |
| 6 | 94 | 103 | 111 |
| 7 | 74 | 83 | 86 |
| 8 | 55 | 64 | 65 |

**Figure 3.3: Head curves of EDM at 8600,8800 and 9000 rpms.**

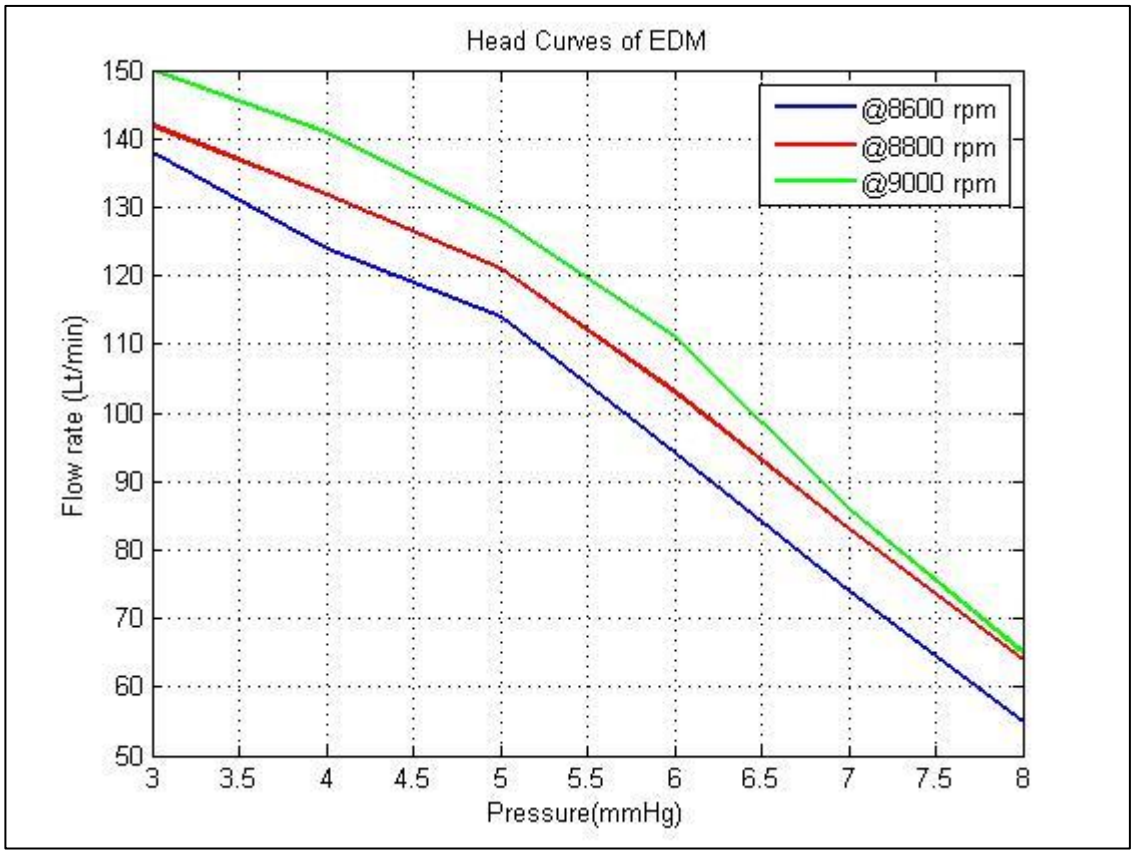


***Source:*** **Made by I.B. Aka**

Virtual FP1s' CFD results of Toptop was compared with physical EDM results. There is a characteristic increase of pressure of EDM at lower flow rates. Head curves show resemblance at different speeds (Fig 3.3). Moreover, angle of head curves of EDM is higher than virtual head curves of FP1. On the other hand, FP1 CFD tests are achieved with respect to the material properties of blood. Initial EDM testing is achieved with water. Comparison plots are given;

**Figure 3.4: Head curves at 8600 rpms**

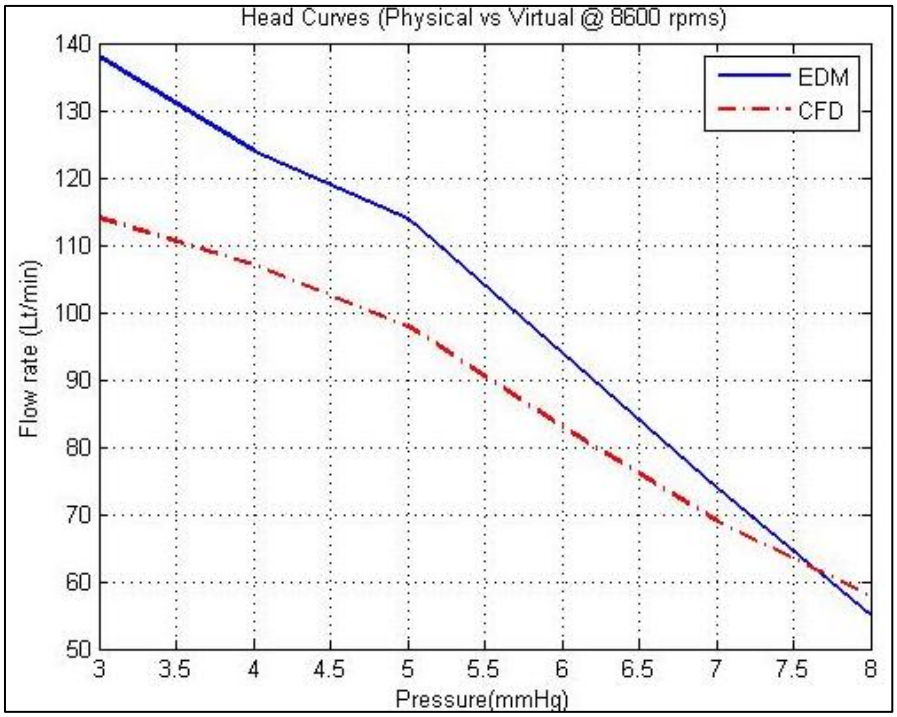


***Source:*** **Made by I.B. Aka**

**Figure 3.5: Head curves at 8800 rpms**

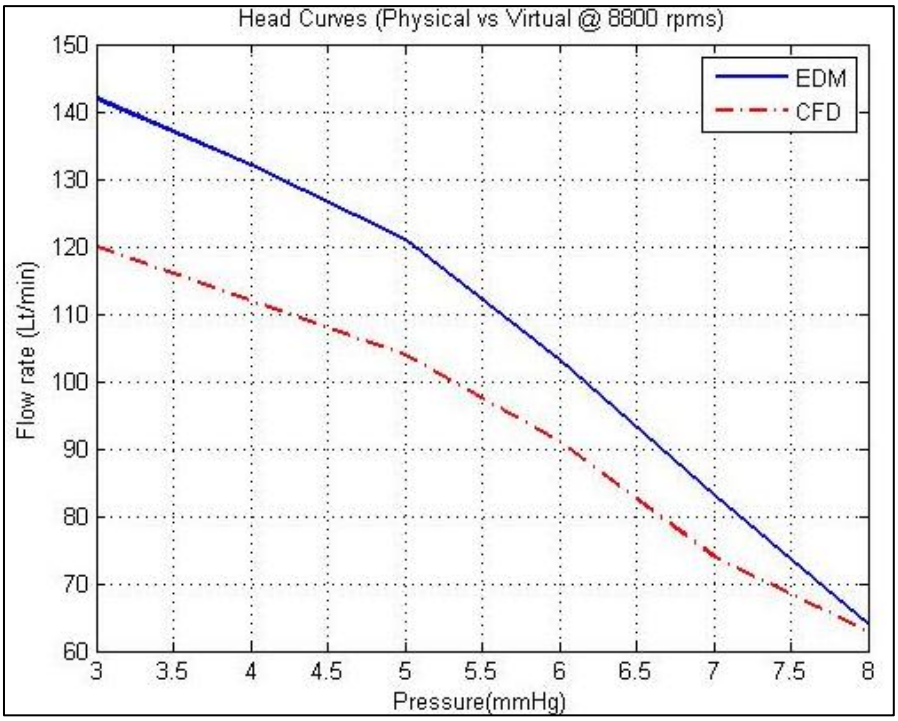


***Source:*** **Made by I.B. Aka**

**Figure 3.6: Head curves at 9000 rpms**

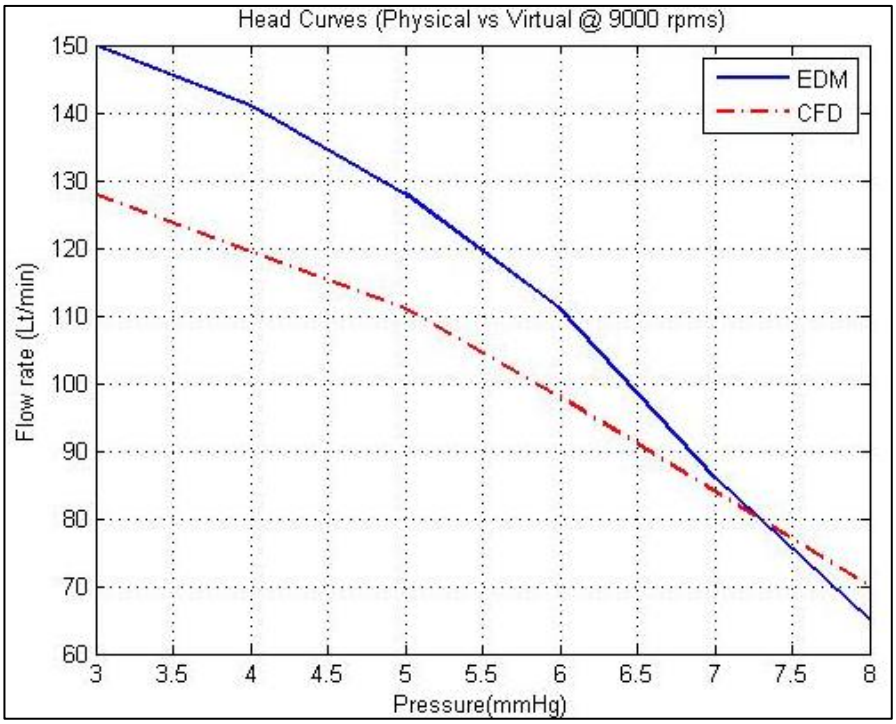


***Source:*** **Made by I.B. Aka**

Implementation of PID controller for speed control is ongoing. Parameters have been changed to improve rise time, settling time and stability (Fig 3.7 and 3.8).

**Figure 3.7: PID controller section of EDM interface**

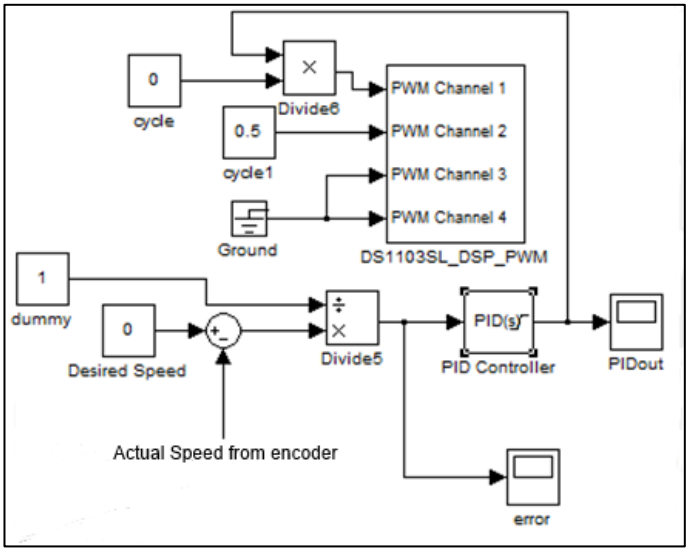


***Source:*** **Made by I.B. Aka**

**Figure 3.8: PID tuning at 6000 rpms**

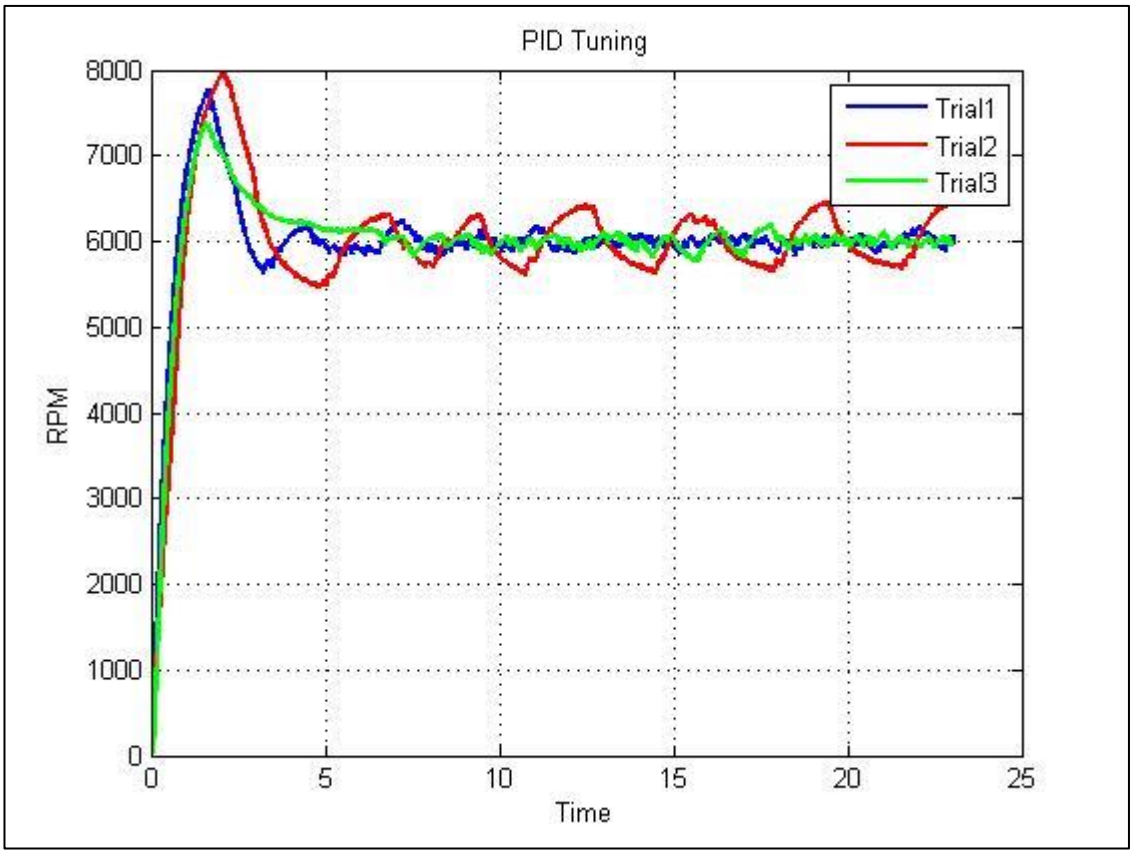


***Source:*** **Made by I.B. Aka**

### 3.1.2 PIV Results

Initial PIV testing is ongoing. Transparency of the shroud is enough for PIV measurements. Particles are clearly seen inside the shroud. EDM control interface is generating a trigger signal successfully for PIV system for taking images at given position of the rotary impeller. Some results of inducer part is given;

**Figure 3.9: Two consecutive images for calculating motion of particles**

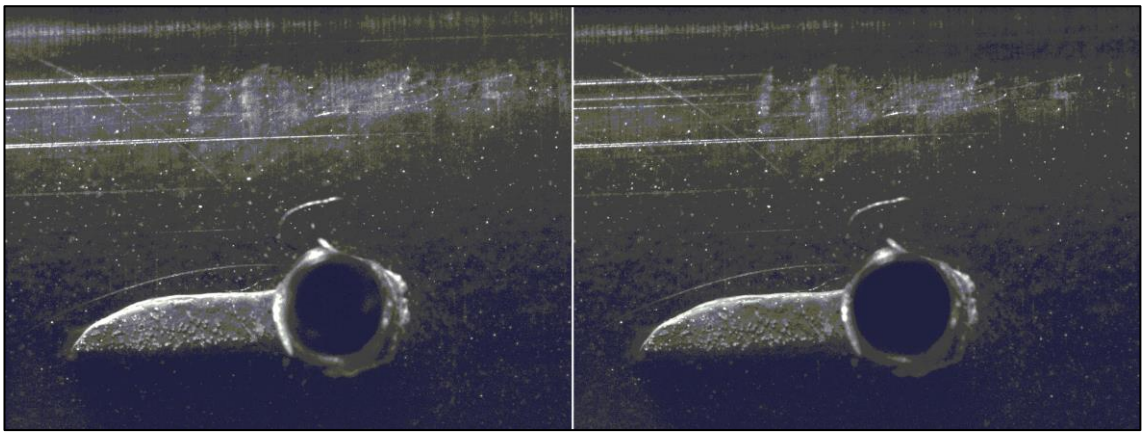

***Source:*** **Made by I.B. Aka**

**Figure 3.10: PIV results with respect to the images above**

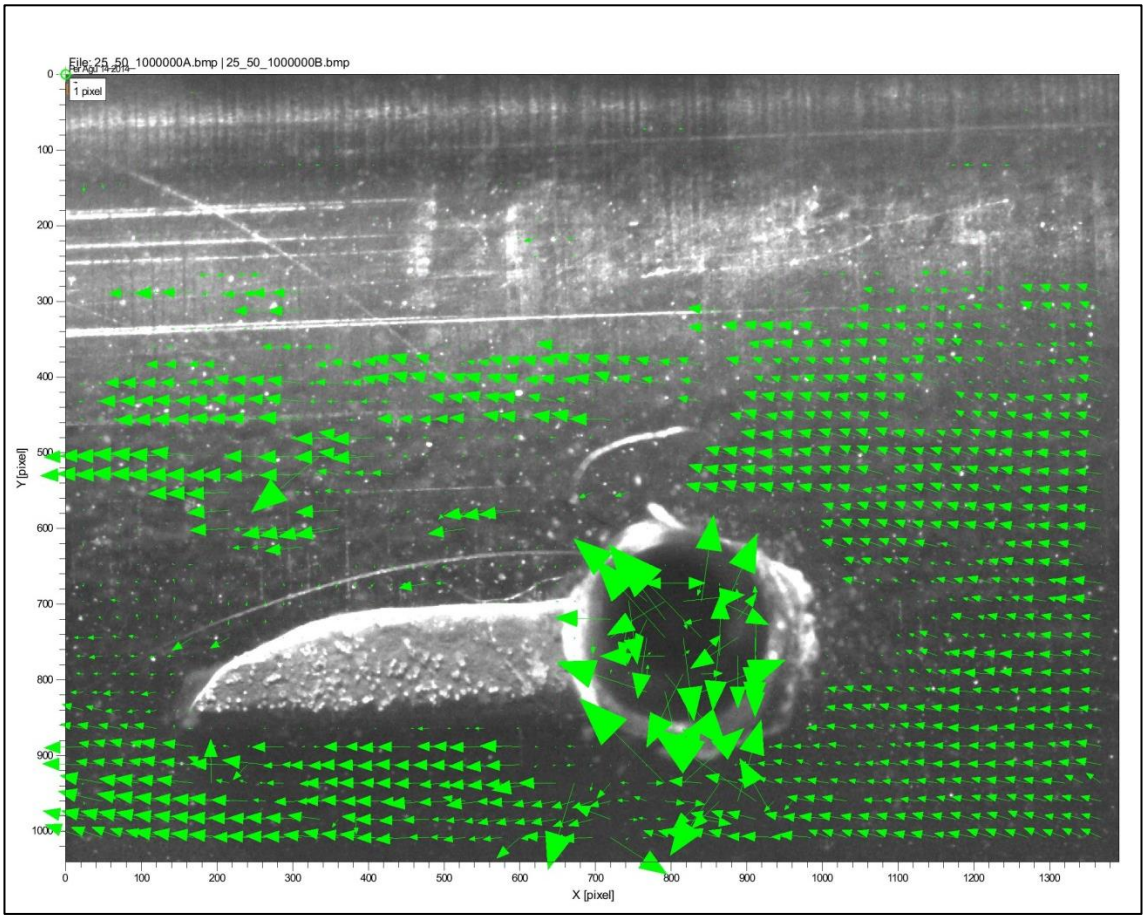


***Source:*** **Made by I.B. Aka**

## 3.2 BEARING WASHING CHANNEL RESULTS

Bearing washing channels cause no significant decrease of efficiency or head pressure. Streamlines inside the inducer channel follows the direction of the general flow. However, flow in the diffuser channel is in the opposite direction of the regular flow due to the higher pressure at pump exit (Fig 3.11). Therefore, approximately 2.5% of the total flow turns back into the inducer channel to wash the bearings. Ratio of the flow passing through the inducer channel to total flow is much lower, 0.5% due to lower pressure difference at the inlet of the pump. Flow directions and patterns are observed by streamlines in Fluent (ANSYS, USA).

**Figure 3.11: Flow directions inside the channels(Red)**

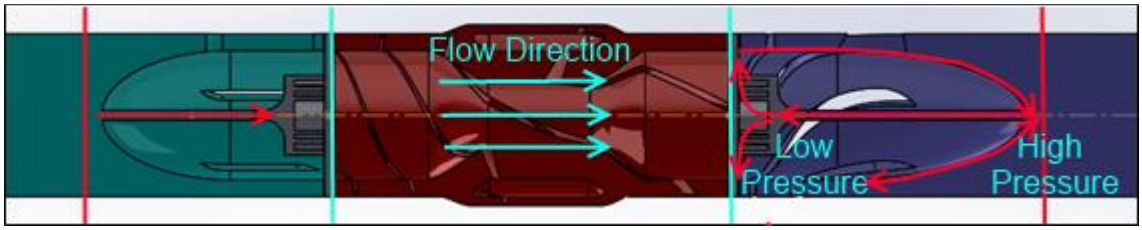


***Source:*** **Made by I.B. Aka**

**Table 4: EDM results at 1060 rad/s impeller speed and 5lt/min flow rate**

| Pump Prototype | FP1 | FP1 Washing Channel |
|---|---|---|
| **Pressure Head** | 148.2778 mmHg | 144.7369 mmHg |
| **Efficiency** | 28.85% | 28.37% |
| **Back Flow(Inducer-Rotor)** | 0.0017% | 0.75% |
| **Back Flow(Rotor-Diffuser)** | 16.66% | 7.82% |
| **Inducer Channel Flow** | - | 0.59% |
| **Inducer Channel Flow** | - | 2.50% |

**Figure 3.12: Streamlines in the washing channels of inducer(left), diffuser (right)**

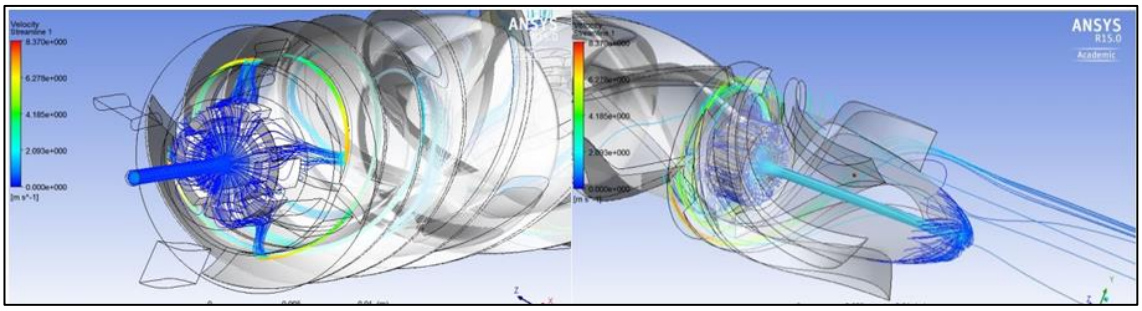


***Source:*** **Made by I.B. Aka**

**Figure 3.13: Streamlines passing through the washing channels**

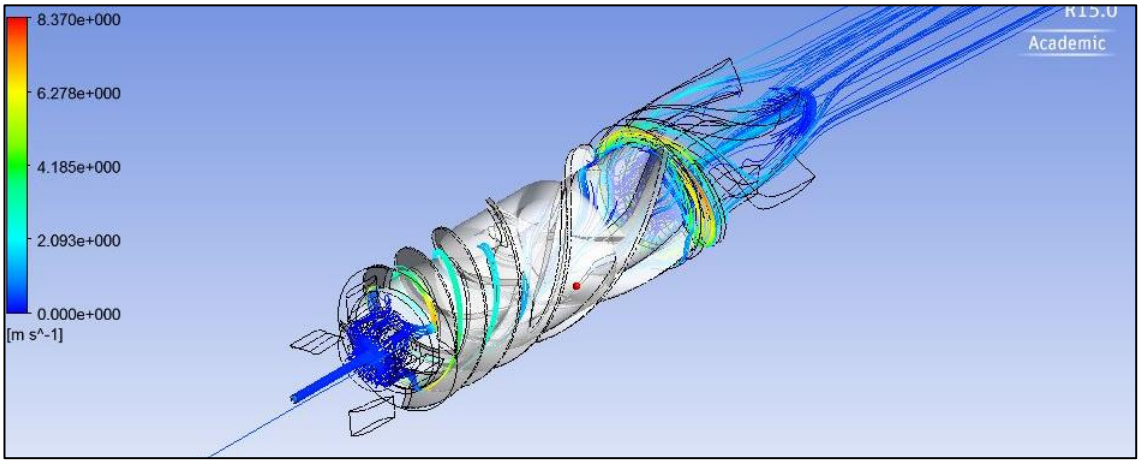


***Source:*** **Made by I.B. Aka**

**Figure 3.14: Complete streamline profile of FP1 with bearings and washing channels**

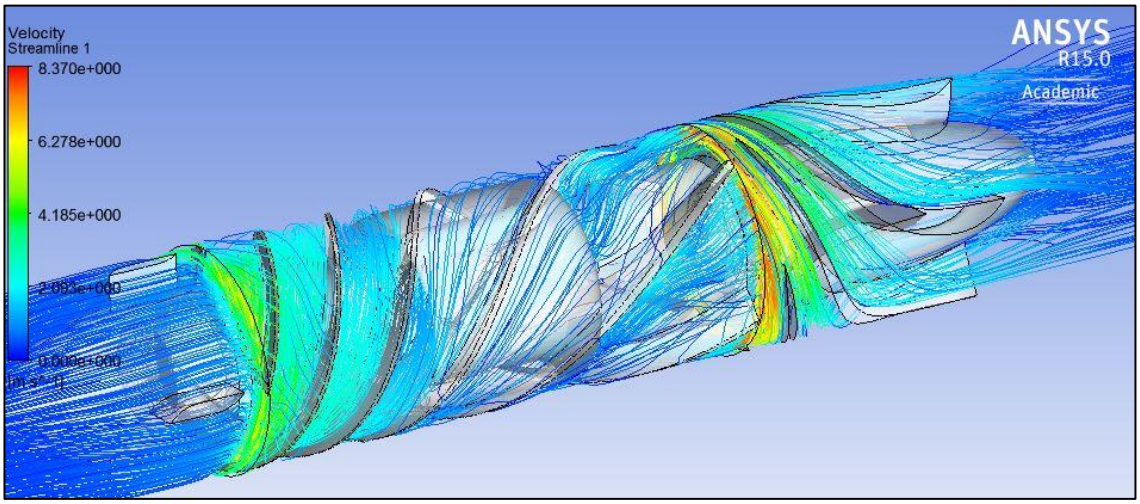


***Source:*** **Made by I.B. Aka**

# 4. CONCLUSION

## 4.1 EDM

EDM functions without leakage and without major vibration up to 10 krpm impeller speed and 9 lt/min flow rate. EDM tested over 10 hours without a problem. PID controller is achieved but requires software modifications. Initial PIV testing is completed on stationary parts of current setup without a problem. Titanium pump parts are removed, painted and placed again, that shows modularity of the setup. Ceramic bearings were visually investigated befor painting and no serious wear is observed. Transparency is superior than machined acrylic. Real time DAQ from torque sensor shows the vibration in acceptable limits.

## 4.2 WASHING CHANNELS

CFD results show that washing channels for mechanical bearings is a promising idea. Overall pump performance had minor decrease due to washing channels. Continuous flow over all surfaces contacting blood was achieved in CFD model. Channel dimensions can be adjusted with respect to the pump characteristics to control channel flow rate.

# 5. DISCUSSION

## 5.1 EDM

EDM tests are conducted with water. Water is less viscous than blood. Therefore, glycerin-water mixture must be used to understand hemodynamics of the pump. Moreover, ratio of glycerin to water must be adjusted to have same refractive index of the shroud[24]. EDM base should have a presicion-sliding rail system for controlling layer position of PIV light sheet.

FP1 to EDM comparison in this work is a physical water to virtual blood test. Therefore, comparison must be repeated after water-glycerin tests for realistic evaluation of virtual FP1 in terms of hemodynamics. Moreover, In-vitro blood test must be conducted to observe possible hemolysis and thrombosis formation. Surface finish of the titanium parts should be improved. Electromechanic and hydromechanic efficiencies must be measured and calculated. Motor power rating at various conditions must be evaluated.

Vibration measurement is necessary for evaluating true vibration. Vibration of the EDM must be minimized for accurate estimation of pump endurance which can be evaluated with rapid testing analogue to 10 years of function[29]. Laser alignment couldn't accomplished due to lack of equipment which is required to eliminate vibration.

EDM velocitiy is measured in dSPACE by counting number of encoder increments between two samplings. However, this method cause high errors at high speeds which causes steady-state errors in PID response. Therefore, capturing the time between two increments is necessary for precise velocity readings. Calibration of pressure transducers and flow meters are necessary for accurate measurements of all parameters. Error rates of all sensors must be evaluated. Digital filtering of data must be optimized. PID controller must be optimized for CVMC testing which mimics human cardiologic physiology. Pump speed must be adjusted with respect to the patients' physiological needs (pressure and flow readings of CVMC).

## 5.2 WASHING CHANNELS

Bearing washing channel concept only tested virtually in CFD. Moreover, only one physical condition is tested (1060 rad/sec, 5lt/min). Complete spectrum of physiologic pressures and flow rates must be investigated. Additionally, only 2 different channel diameter is tested. Channel diamater must be optimized by furter iterations.

Bearing model is simplified for CFD testing. A detailed micro model of the bearings and washing channels must be tested in CFD for observing possible stasis in bearings.

Titanium parts with washing channels are manufactured with current channel diameter (1mm). These parts must be assembled in EDM for hemodynamic evaluation. PIV testing of washing channels are necessary along with hemodynamic evaluation to observe flow profile around the inlet and outlet of the washing channels.

Titanium parts are opaque. Therefore PIV testing can not be conducted inside the parts. Therefore, transparent diffuser and inducer can be manufactured for conducting PIV tests inside the channels.

## REFERENCES


[1] J. E. Hall, *Guyton and Hall Textbook of Medical Physiology: Enhanced E-book*: Elsevier Health Sciences, 2010.

[2] A. Cassar, D. R. Holmes Jr, C. S. Rihal, and B. J. Gersh, "Chronic coronary artery disease: diagnosis and management," in *Mayo Clinic Proceedings*, 2009, pp. 1130-1146.

[3] A. S. Go, D. Mozaffarian, V. L. Roger, E. J. Benjamin, J. D. Berry, W. B. Borden, *et al.*, "Heart disease and stroke statistics--2013 update: a report from the American Heart Association," *Circulation*, vol. 127, p. e6, 2013.

[4] P. A. Heidenreich, J. G. Trogdon, O. A. Khavjou, J. Butler, K. Dracup, M. D. Ezekowitz, *et al.*, "Forecasting the future of cardiovascular disease in the United States a policy statement from the American heart association," *Circulation*, vol. 123, pp. 933-944, 2011.

[5] S. BAKANLIĞI and T. S. H. G. MÜDÜRLÜĞÜ, "Türkiye'de Bulaşıcı Olmayan Hastalıklar ve Risk Faktörleri ile Mücadele Politikaları."

[6] R. C. Starling, "Advanced heart failure: Transplantation, LVADs, and beyond," *Cleveland Clinic journal of medicine*, vol. 80, pp. 33-40, 2013.

[7] S. Bakanlığı and İ. Yıllığı, "Sağlık Araştırmaları Genel Müdürlüğü," *Sağlık İstatistikleri Yıllığı,* 2013.

[8] D. Liotta, D. W. Wieting, C. W. Hall, J. Chidoni, and M. E. DeBakey, "In vitro and in vivo flow studies in blood pumps," *ASAIO Journal*, vol. 13, pp. 280-287, 1967.

[9] J. K. Kirklin, D. C. Naftel, R. L. Kormos, L. W. Stevenson, F. D. Pagani, M. A. Miller, *et al.*, "The fourth INTERMACS annual report: 4,000 implants and counting," *The Journal of Heart and Lung Transplantation*, vol. 31, pp. 117-126, 2012.

[10] F. D. Pagani, L. W. Miller, S. D. Russell, K. D. Aaronson, R. John, A. J. Boyle, *et al.*, "Extended mechanical circulatory support with a continuous-flow rotary left ventricular assist device," *Journal of the American College of Cardiology*, vol. 54, pp. 312-321, 2009.

[11] L. H. Lund, L. B. Edwards, A. Y. Kucheryavaya, A. I. Dipchand, C. Benden, J. D. Christie, *et al.*, "The Registry of the International Society for Heart and Lung Transplantation: thirtieth official adult heart transplant report–2013; focus theme: age," *J Heart Lung Transplant*, vol. 32, pp. 951-64, 2013.

[12] H. AKALIN, E. T. ÇORAPÇIOĞLU, K. UÇANOK, N. T. EREN, A. Atilla, Ü. ÖZYURDA, *et al.*, "Ülkemizde İlk Yapay Kalp (Symbion J-7) Uygulaması," *Turkiye Klinikleri Journal of Medical Sciences*, vol. 9, pp. 294-296, 1989.

[13] D. S. Kucukaksu, E. Sener, A. Undar, G. P. Noon, and O. Tasdemir, "First turkish experience with the MicroMed DeBakey VAD®," *Texas Heart Institute Journal*, vol. 30, p. 114, 2003.

[14] O. Erbasan, " Total Yapay Kalp ve Ventrikül Destek Cihazları," *http://dalyatur.com/akdenizhemsireliksunu/ozan_erbasan.pdf*, 2014.

[15] H. G. Wood, A. L. Throckmorton, A. Untaroiu, and X. Song, "The medical physics of ventricular assist devices," *Reports on Progress in Physics*, vol. 68, p. 545, 2005.

[16] K. Toptop, "Computational Fluid Dynamic Analysis Of Axial-Flow Left-Ventricular Assist Device," *Bahcesehir University*, 2013.
[17] H. M. Reul and M. Akdis, "Blood pumps for circulatory support," *PERFUSION-SEVENOAKS-*, vol. 15, pp. 295-312, 2000.
[18] O. Demir, E. Biyikli, I. Lazoglu, and S. Kucukaksu, "Design of a centrifugal blood pump: Heart Turcica Centrifugal," *Artificial organs,* vol. 35, pp. 720-725, 2011.
[19] J. Garbade, H. B. Bittner, M. J. Barten, and F.-W. Mohr, "Current trends in implantable left ventricular assist devices," *Cardiology research and practice,* vol. 2011, 2011.
[20] T. Nakazawa, K. Makinouchi, Y. Ohara, S. Ohtsubo, K. Kawahito, K. Tasai, *et al.*, "Development of a pivot bearing supported sealless centrifugal pump for ventricular assist," *Artificial organs,* vol. 20, pp. 485-490, 1996.
[21] K. Toptop and K. A. Kadipasaoglu, "Design and Numeric Evaluation of a Novel Axial-Flow Left Ventricular Assist Device," *ASAIO Journal,* vol. 59, pp. 230-239, 2013.
[22] I. o. A. a. F. T. (IAS) and Braunschweig/Göttingen, "http://www.dlr.de/as/en/DesktopDefault.aspx/tabid-183/251_read-12796/gallery-1/gallery_read-Image.5.1574/."
[23] E. G. Eken, "Design Of Left Ventricle For Cardiovascular System Mock Circuit," *Bahçeşehir Üniversitesi,* 2014.
[24] T. Yagi, W. Yang, D. Ishikawa, H. Sudo, K. Iwasaki, and M. Umezu, "Multiplane scanning Stereo-PIV measurements of flow inside a spiral vortex pulsatile blood pump," in *13th international symposium on applications of laser techniques to fluid mechanics, Lisbon, Portugal*, 2006.
[25] S. W. Day, J. C. McDaniel, H. G. Wood, P. E. Allaire, N. Landrot, and A. Curtas, "Particle image velocimetry measurements of blood velocity in a continuous flow ventricular assist device," *ASAIO journal,* vol. 47, pp. 406-411, 2001.
[26] A. Untaroiu, H. G. Wood, P. E. Allaire, A. L. Throckmorton, S. Day, S. M. Patel, *et al.*, "Computational design and experimental testing of a novel axial flow LVAD," *ASAIO journal,* vol. 51, pp. 702-710, 2005.
[27] B. Su, L. P. Chua, and X. Wang, "Validation of an axial flow blood pump: computational fluid dynamics results using particle image velocimetry," *Artificial organs,* vol. 36, pp. 359-367, 2012.
[28] N. Moazami, R. J. Steffen, Y. Naka, U. Jorde, S. Bailey, S. Murali, *et al.*, "Lessons Learned From the First Fully Magnetically Levitated Centrifugal LVAD Trial in the United States: The DuraHeart Trial," *The Annals of thoracic surgery,* vol. 98, pp. 541-547, 2014.
[29] M. P. Siegenthaler, O. Frazier, F. Beyersdorf, J. Martin, H. Laks, J. Elefteriades, *et al.*, "Mechanical reliability of the Jarvik 2000 Heart," *The Annals of thoracic surgery,* vol. 81, pp. 1752-1759, 2006.
[30] K. Makinouchi, T. Nakazawa, Y. Takami, S. Takatani, and Y. Nosé, "Evaluation of the wear of the pivot bearing in the Gyro C1E3 pump," *Artificial organs,* vol. 20, pp. 523-528, 1996.
[31] E. G. P. Bock, A. J. P. de Andrade, E. A. E. Wada, J. W. G. da Fonseca, J. Leme, D. E. C. Nicolosi, *et al.*, "A new concept of centrifugal blood pump using

pivot bearing system: the conversion of the spiral pump inlet port," *Technology Meets Surgery International, São Paulo, SP, 4p,* 2005.
[32] A. B. M. Association, "Instrument Ball Bearings—Metric Design," *ANSI/ABMA*, vol. 12, 1992.
[33] P. Aarts, P. A. Bolhuis, K. S. Sakariassen, R. M. Heethaar, and J. J. Sixma, "Red blood cell size is important for adherence of blood platelets to artery subendothelium," *Blood*, vol. 62, pp. 214-217, 1983.
[34] J. E. Shigley, R. G. Budynas, and C. R. Mischke, "Mechanical engineering design," 2004.
[35] S. GmbH, "http://www.sick.com/instruments/EN/home/products/pressure_sensors/Pages/PBT.aspx."
[36] A. Technology, "http://www.artisantg.com/79961."
[37] B. GmbH, "Data sheet 8661," *http://www.burster.com/fileadmin/Documents/Products/Data_Sheets/Section_8/8661_EN.pdf*, 2014.
[38] M. Behbahani, M. Behr, M. Hormes, U. Steinseifer, D. Arora, O. Coronado, *et al.*, "A review of computational fluid dynamics analysis of blood pumps," *European Journal of Applied Mathematics,* vol. 20, pp. 363-397, 2009.
[39] X. Song, A. L. Throckmorton, H. G. Wood, J. F. Antaki, and D. B. Olsen, "Quantitative evaluation of blood damage in a centrifugal VAD by computational fluid dynamics," *Journal of fluids engineering,* vol. 126, pp. 410-418, 2004.
[40] I. Roberts, C. Wang, R. Esterlein, M. Stanford, and D. Mynors, "A three-dimensional finite element analysis of the temperature field during laser melting of metal powders in additive layer manufacturing," *International Journal of Machine Tools and Manufacture,* vol. 49, pp. 916-923, 2009.
[41] I. World, "IRFZ48N Data Sheet," *http://www.irf.com/product-info/datasheets/data/irfz48n.pdf*.